SAINT PETERSBURG STATE UNIVERSITY

PETERSBURG NUCLEAR PHYSICS INSTITUTE
NAMED BY B.P. KONSTANTINOV
OF NATIONAL RESEARCH CENTRE "KURCHATOV INSTITUTE"

Popov Roman Vladimirovich

Positron spectra in low-energy heavy-nuclei collisions as a tool for observing spontaneous vacuum decay in a supercritical Coulomb field

Scientific specialisation 1.3.3. Theoretical physics

Dissertation is submitted for the degree
of Candidate of Physical and Mathematical Sciences

Thesis supervisor:
Vladimir M. Shabaev
Dr. Sci. (Phys.-Math), Prof.

Saint Petersburg
2024

Contents

Introduction

The present thesis concerns the phenomenon of spontaneous reconstruction of the quantum electrodynamical (QED) vacuum state, also referred to as the spontaneous vacuum decay, in supercritical Coulomb fields. During this reconstruction the initially neutral vacuum state acquires a non-zero charge and one or two positrons are emitted. According to QED, this effect can occur in collisions of heavy nuclei with the total charge number $Z_{\rm t} = Z_{\rm A} + Z_{\rm B}$ exceeding the critical value $Z_{\rm cr} \approx 173$. For this, the nuclei have to approach each other at a distance less than the critical value $R_{\rm cr}$, which depends on $Z_{\rm B}$ and $Z_{\rm B}$. Experimental observation of the vacuum decay in such collisions is greatly complicated by prevailing dynamical (induced) pair production due to time dependence of the nuclear potential. The goal of this work is the search for an experimental scenario that would allow one to observe signatures of the transition to the supercritical regime and the spontaneous vacuum decay. To this end we developed an efficient numerical technique for calculations of the electron-positron pair-creation probabilities and energy spectra of the positrons emitted in low-energy collisions of heavy nuclei. By utilizing this technique we investigated collisions of heavy nuclei within a wide range of collision parameters. The calculations were performed both within the monopole approximation, where only spherically symmetric part of the two-center nuclear potential is taken into account, and beyond. The results of the calculations show qualitative changes of both the pair-creation probabilities and the positron spectra when the collision parameters enter deeply enough into the supercritical domain.

Relevance of the topic

Spontaneous vacuum decay in supercritical Coulomb fields represents a fundamental nonperturbative quantum electrodynamical phenomena predicted to take place in strong electromagnetic fields. Its existence was suggested more than 50 years ago in 1969. Since then it had been intensively studied both theoretically and experimentally. But all the attempts to observe any manifestations of this phenomenon were not successful. As a result, after more than 20 years it was concluded that the spontaneous pair creation can only be observed if the nuclei would stick one to another for some time during the collision due to nuclear forces. Not so long ago interest to this process raised again in view of several new experimental facilities

such as GSI/FAIR in Germany, HIAF in China and NICA in Russia that are currently being built. Concerning observation of the spontaneous pair creation, a major improvement of these new facilities compared to the ones utilized before is twofold. Firstly, they will provide the possibility to work with ions in substantially higher charge states and potentially even with bare nuclei. Secondly, they can make available experiments using crossed beams instead of fixed-target collisions used earlier. Both of these factors lead to the decrease in the population of the quasimolecular $1s\sigma$ state. This plays a crucial role for observation of the spontaneous vacuum decay, since the latter can only occur when the $1s\sigma$ state has a vacancy before it enters the lower continuum. The less the population of this state, the bigger the contribution of the spontaneous mechanism to the pair creation.

Elaboration of the topic

Quantum electrodynamics in the presence of superstrong electromagnetic fields predicts a number of nonlinear and nonperturbative effects such as light-by-light scattering, vacuum birefringence and production of electron-positron pairs (see, e.g., reviews [1–4]). Experimental observation of these effects is complicated by extremely high requirements on the field strength needed for their manifestation. One of the ways to attain such fields relies on ever evolving laser technologies. Although laser facilities in the near future might meet requirements for some of the effects, vacuum pair production is still far from being experimentally accessible. An alternative approach suggests to use heavy nuclei as a source of a strong electric field.

In a pioneering work [5] it was shown that the $1s$ level of a hydrogen-like ion with an extended nucleus continuously goes down with increasing nuclear charge until at a certain value $Z_{\rm cr}$ it reaches the border of the negative-energy continuum. It raised the question of what happens to a bound state when it joins the positron continuum. In works of Soviet and German physicists [6, 7] it was conjectured that the diving of an initially empty bound state into the negative-energy continuum can result in spontaneous reconstruction of the QED vacuum accompanied with creation of electron-positron pairs (for details see, e.g., Refs. [8–21]). Such reconstruction of the vacuum state happens every time a new empty bound state enters the negative-energy continuum. The new vacuum state attains a charge Ne, where N is is the number of submerged bound states and e is the electron charge.

The heaviest element synthesized to date is oganesson, which has a nuclear

charge $Z = 118$. This is well below the minimum required nuclear charge $Z_{\rm cr}$, which is evaluated to be approximately equal to 173. Nonetheless, a realistic scenario for observation of this process can be realized in low-energy collision of two heavy nuclei with the total charge exceeding the critical value $Z_{\rm A} + Z_{\rm B} > Z_{\rm cr}$ [6]. When during such collisions the nuclei get sufficiently close to each other, $1s\sigma$ state of the quasimolecule, transiently formed by them, enters the negative-energy continuum as a resonance. As a result, if $1s\sigma$ state was unoccupied, additional two (due to spin degeneracy) holes enter the lower continuum. Initially localized near the nuclei, these holes can escape to infinity as free positrons, and the initially neutral vacuum becomes charged with the charge $2e$. This process is known as the spontaneous decay of the neutral QED vacuum.

Spontaneous vacuum decay in heavy-ion collisions was a subject of intense theoretical and experimental investigations (see, e.g., reviews [22–27] and references therein). The first theoretical calculations of pair creation in the supercritical collisions were carried out in the quasistatic approximation, according to which the pair-creation probability is proportional to the time integral of the resonance width $\Gamma(R)$ taken along the nuclear trajectory $R(t)$ [28–30]. Within this approximation, the total probability of spontaneous pair creation, associated with the resonance decay, energy spectra of the emitted positrons as well as their angular distributions were obtained. In Ref. [30], a correction for the nonadiabaticity of the tunneling process was also considered. However, the quasistatic approach does not take into account the dynamical pair creation induced by the time-dependent potential of the moving nuclei. It turns out that the supercritical resonance has a rather long lifetime, compared to the duration of the supercritical regime $\tau_{\rm cr}$. For example, in collisions of uranium nuclei at the energies near the Coulomb barrier (when the nuclei touch each other) the resonance lifetime is about two orders of magnitude larger than $\tau_{\rm cr}$. This makes the probability of spontaneous pair creation quite small. Moreover, an additional width $\Gamma_{\rm dyn} \sim \hbar/\tau_{\rm cr}$, caused by the uncertainty principle, prevents appearance of narrow resonance structures in the energy distribution of the emitted positrons, predicted in the quasistatic approximation. Therefore, in order to verify the possibility to observe the signal from the vacuum decay, one needs to take into account the dynamical pair production.

Both the spontaneous and the dynamical mechanisms of pair creation were investigated by the Frankfurt group. The first attempts to take into account induced

pair creation were based on the time-dependent perturbation theory [31, 32]. Later, a nonperturbative procedure was realized for solution of the time-dependent Dirac equation. It employed the coupled-channel technique in the basis of adiabatic quasimolecular wave functions calculated in the monopole approximation. Nonperturbative calculations showed the importance of multistep processes for various aspects of the ion-atom collision such as pair-creation, electron excitations and $1s\sigma$ vacancy formation, which plays a crucial role for the spontaneous pair-creation mechanism (see, e.g., [33–36]). From the obtained results it was eventually concluded that experimental observation of spontaneous vacuum decay is possible only if the colliding nuclei would stick to each other for some time due to nuclear forces [26, 27]. However, since no evidence of such sticking have been registered to date for the nuclei of the interest, this scenario also does not seem promising.

In view of the upcoming experimental facilities in Germany (GSI/FAIR) [37, 38], China (HIAF) [39], and Russia (NICA) [40] the interest to this problem was renewed. New investigations concerned both static and dynamic aspects of spontaneous positron emission. The properties of the supercritical resonance were addressed for spherically symmetric [41–44] and two-center [45–47] field configurations. The behavior of the vacuum polarization energy for supercritical Coulomb fields was examined in a series of papers (see, e.g., [48–50] and references therein). Dynamic consideration of pair creation in heavy-nuclei collisions was targeted in the framework of the monopole approximation [51–53] and beyond [54–56]. First nonperturbative calculations of the angular resolved positron spectra can be found in Ref. [57]. Relativistic semiclassical approach to the vacuum instability problem was considered in detail in Ref. [58].

Recently there was proposed a new way to see the signatures indicating the transition to the supercritical regime, where spontaneous electron-positron pair creation becomes possible [59, 60]. The method suggests to consider collisions along trajectories corresponding to different energies but having the same distance of the closest approach, $R_{\min}$. As the parameters that define the specific trajectory, it is convenient to use $R_{\min}$ and the ratio $\eta = E/E_0 \in [1, \infty)$ of the collision energy E to the energy of the head-on collision with the same $R_{\min}$. The idea behind this is the opposite dependence of the dynamic and spontaneous contributions to the pair-creation probability on the nuclear velocity, characterized here by the parameter η. Indeed, it is clear that the contribution of the spontaneous mechanism is determined

by the duration of the supercritical regime $\tau_{\rm cr}$. This time monotonically decreases with the increase of collision energy, i.e., η, and so does the contribution of the spontaneous mechanism. On the contrary, the dynamical pair production should increase with the increase of η. Therefore, the raise of the pair-creation probability with $\eta \to 1$ is to be attributed to the transition to the supercritical regime and activation of the spontaneous mechanism. More details are to be found in Ref. [60].

By employing the aforementioned approach, we carried out a detailed investigation of the η-dependence of the pair-production probabilities and positron energy spectra (see Ref. [60]). The calculations were conducted within the monopole approximation, where only spherically symmetric part of the two-center nuclear potential is taken into account. The evidence of the transition to the supercritical regime have been found in both the pair-creation probabilities and the positron spectra. These findings were later independently confirmed in Ref. [61]. As it was quantitatively shown in works [54–56], the monopole approximation works rather well for description of the pair-creation process. Nonetheless it is important to study how consideration of the full two-center potential would affect the signs of the transition to the supercritical regime mentioned above. Also, calculations beyond the monopole approximations are necessary to get access to other important aspects of nuclei collisions, e.g., the angular resolved positron spectra. To this end, in Ref. [62] we extended our numerical technique beyond the monopole approximation and performed the calculations of the pair-creation probabilities and positron energy spectra taking into account higher-order terms in the decomposition of the nuclear potential over spherical harmonics. The results demonstrated that all the signatures of the transition to the supercritical regime remain and some of them even get enhanced. The calculations were performed in the rotating coordinate system with z-axis directed along the internuclear line and the origin located at the center of mass. The rotational-coupling term that appears in the time-dependent Dirac equation due to the transition to this noninertial reference frame (see, e.g., Ref. [63, 64]) as well as the magnetic field of the moving nuclei were not taken into account in that work. As it was argued in Refs. [33, 65–67], the influence of these effects on the total probability and positron energy spectra should be small. To quantitatively assess the role of the rotational coupling on the pair-creation we developed two methods of incorporating it into our code. By using these methods we quantitatively demonstrated that the rotational coupling can be safely neglected when considering pair-creation

probabilities for low-energy near head-on collisions. Investigation of its impact on the positron energy and angular distributions is currently under way.

Purpose

The main goal of the present study is the search for an experimental scenario that would allow one to observe signatures of the transition to the supercritical regime in low-energy collisions of heavy nuclei. This requires development of an effective numerical technique allowing one to nonperturbatively examine the process of the electron-positron pair-creation occurring in such collisions. To achieve the stated goal, the following **objectives** have to be accomplished:

1. Derivation of the calculation formulas.

2. Development of the numerical code for nonperturbative solution of the time-dependent Dirac equation in the monopole approximation and its testing by comparison with the available data.

3. Carrying out extensive calculations of the pair-creation probabilities and the positron energy spectra for a wide range of collision parameters, i.e. charge numbers, collision energies, and impact parameters.

4. Analysis of the obtained data looking for signatures of the transition to the supercritical regime.

5. Extension of the numerical code beyond the scope of the monopole approximation.

6. Investigation of the impact the higher-order terms of the multipole expansion of the time-dependent nuclear potential has on the results obtained earlier in the monopole approximation.

Scientific novelty

The main results of this research concerning the qualitative changes of both the pair-creation probabilities and the positron energy spectra following the transition to the supercritical regime in collisions of heavy nuclei have not been demonstrated before, and thus are novel. The developed technique of nonperturbative numerical calculations of the probabilities and the spectra within and beyond the monopole

approximation which allowed us to reveal these changes is novel as well. This is confirmed by the fact of publication of our findings in high-impact scientific journals and their presentation at national and international conferences.

Theoretical and practical significance

The found qualitative changes in the behavior of the pair-creation probabilities and the positron energy spectra represent the first indications of the supercritical transition occurring in heavy-nuclei collisions. They do not require a transient formation of a bound nuclear compound, also referred to as the nuclear sticking, as it was thought to be necessary before. These signatures of the supercritical transition can be experimentally observed in impact parameter sensitive measurements of the positron yield.

Methodology and research methods

The calculation method numerically implemented in the present research is based on the formalism of quantum electrodynamics in the Furry picture. Within this formalism the physical quantities of interest to us are expressed in terms of one-electron transition amplitudes. The one-electron wave functions are found by numerically solving of the time-dependent Dirac equation within a finite one-center static basis set. The radial part of the basis functions are described with B-splines, for the angular part the spherical spinors are used.

Approbation of the research

The findings of the investigation were reported and discussed at the following conferences:

- 18th Topical Workshop of the Stored Particles Atomic Physics Research Collaboration (SPARC 2021), September 6–9, 2021.
- 56th Winter School of Petersburg Nuclear Physics Institute NRC KI, March 17-22, 2024.

The results obtained within this study were published in 3 articles (the journals are recommended by the Higher Attestation Commission of the Russian Federation and included in the RSCI, Web of Science and Scopus databases):

- R. V. Popov, A. I. Bondarev, Y. S. Kozhedub, I. A. Maltsev, V. M. Shabaev, I. I. Tupitsyn, X. Ma, G. Plunien, and T. Stöhlker, *One-center calculations of the electron-positron pair creation in low-energy collisions of heavy bare nuclei*, Eur. Phys. J. D **72**, 115 (2018).

- R. V. Popov, V. M. Shabaev, D. A. Telnov, I. I. Tupitsyn, I. A. Maltsev, Y. S. Kozhedub, A. I. Bondarev, N. V. Kozin, X. Ma, G. Plunien, T. Stöhlker, D. A. Tumakov, and V. A. Zaytsev, *How to access QED at a supercritical Coulomb field*, Phys. Rev. D **102**, 076005 (2020).

- R. V. Popov, V. M. Shabaev, I. A. Maltsev, D. A. Telnov, N. K. Dulaev, and D. A. Tumakov, *Spontaneous vacuum decay in low-energy collisions of heavy nuclei beyond the monopole approximation*, Phys. Rev. D **107**, 116014 (2023).

Personal contribution of the author

All of the main findings were obtained personally by the applicant or in work of joint authorship.

Thesis structure

The thesis consists of Introduction, five Chapters, Conclusion, and a list of references. The thesis contains 84 pages, 25 figures, and 4 tables. The list of references includes 82 items.

- In **Introduction** we describe the relevance of the topic, its elaboration, the purpose and main objectives of this investigation, its novelty, significance and methods. Finally, we formulate the main statements to defend and discuss the approbation of the research conducted.

- In **Chapter 1** we make a short overview of the supercritical resonance and the process of spontaneous vacuum decay.

- In **Chapter 2** we briefly outline the formalism of quantum electrodynamics with unstable vacuum in the Furry picture and elucidate the main steps in derivation of the formulae that underlie the calculation technique.

- In **Chapter 3** we elaborate on the set of collision trajectories used to observe the transition to the supercritical regime.

- In **Chapter 4** we describe the core components of the numerical calculation technique and discuss the results obtained in the monopole approximation.
- In **Chapter 5** the numerical algorithm is extended beyond the monopole approximation and the influence of the higher-order multipole terms of the two-center nuclear potential is examined.
- In **Conclusion** we recapitulate the major findings of the present research.

Main scientific results

1. A program has been developed for one-center nonperturbative calculations of the electron-positron pair-creation probabilities in low-energy collisions of heavy nuclei beyond the monopole approximation. Calculations of the electron-positron pair-creation probabilities in head-on collisions of uranium nuclei have been carried out, see Ref. [56] (personal contribution is 80%).
2. Investigation of the pair-creation probability and the positron energy spectra have been performed within the framework of the monopole approximation for a wide range of nuclear charge numbers, collision energies and impact parameters, including both subcritical and supercritical values. Qualitative changes have been found in the energy spectra of positrons during the transition to the supercritical regime in collisions of heavy nuclei with a fixed distance of the closest approach, see Ref. [60] (personal contribution is 75%).
3. The behavior of the electron-positron pair-creation probability and the positron energy spectra at the transition to the supercritical regime in collisions of heavy nuclei has been studied beyond the monopole approximation. It is shown that taking into account higher-order terms in the multipole decomposition of the two-center potential of nuclei preserves all the signatures of the transition to the supercritical regime found within the monopole approximation, see Ref. [62] (personal contribution is 90%).

Thesis statements to be defended

The statements read:

1. A numerical method for nonperturbative calculations beyond the monopole approximation of the electron-positron pair-creation probabilities and the positron energy spectra in low energy-collisions of heavy nuclei was developed.

2. The pair-creation probabilities and the energy spectra of emitted positrons near the supercritical transition were investigated for a wide range of the collision energies, impact parameters, and the nuclei charge numbers.

3. A qualitative changes of the positron energy spectra were revealed at the transition from the subcritical to the supercritical regime in collisions of heavy nuclei with fixed distance of the closest approach.

4. Taking into account higher-order terms in the multipole expansion of the two-center nuclear potential retains the signatures of the supercritical transition found in the monopole approximation.

Chapter 1. Supercritical resonance. Short overview

In this section, we will dwell a little more on the nature of the supercritical resonance and its connection with the decay of the QED vacuum. We will start by considering the behavior of the bound-state energies of hydrogen-like ions with the nuclear charge number growing beyond the point-charge limit $Z = 137$. The energy of a bound state in the case of one-electron ion with a point-like nucleus can be found analytically with the help of the well known Zommerfeld fine-structure formula

$$E_{n\kappa} = \frac{mc^2}{\sqrt{1 + \left(\frac{\alpha Z}{n - |\kappa| + \sqrt{\kappa^2 - (\alpha Z)^2}}\right)^2}}. \tag{1.1}$$

Here n is the principal quantum number, $\kappa = (-1)^{j+l+1/2}(j+1/2)$ is the relativistic angular-momentum–parity quantum number, $\alpha \approx 1/137$ is the fine structure constant, m is the electron mass, and c is the speed of light. It is readily seen that the formula (1.1) is valid only when the square root $\sqrt{\kappa^2 - (\alpha Z)^2}$ is real, i.e. for $Z \leq |\kappa|/\alpha$. The lowest energy $1s$ state has $\kappa = -1$. Therefore, one can use (1.1) only for $Z \leq 137$. For $Z > 137$ the standard procedure for construction of the relativistic self-adjoint Hamilton operator with the pure Coulomb potential fails and one has to turn to special methods to overcome this problem (see, e.g., Refs. [68–70]). This issue can be avoided by employing a more realistic model of the nuclear charge distribution, e.g. homogeneously charged shell, sphere or the Fermi model. In a pioneering work [5] Pomeranchuk and Smorodinsky examined the dependence of the bound state energies of one-electron ions on the nuclear charge utilizing the shell model of the nuclear charge distribution. They found out that the energy of the $1s$ state continuously goes down with increasing Z, becomes negative and at some critical value $Z_{\rm cr}$ reaches the border of the lower continuum. Although $Z_{\rm cr}$ turned out to be overestimated, this work opened the question of what happens when a bound energy level dives into the lower continuum with the increase of the nuclear charge beyond the critical value. The dependence of a few low-lying bound states on Z, obtained in our calculations with the nuclear model of homogeneously charged

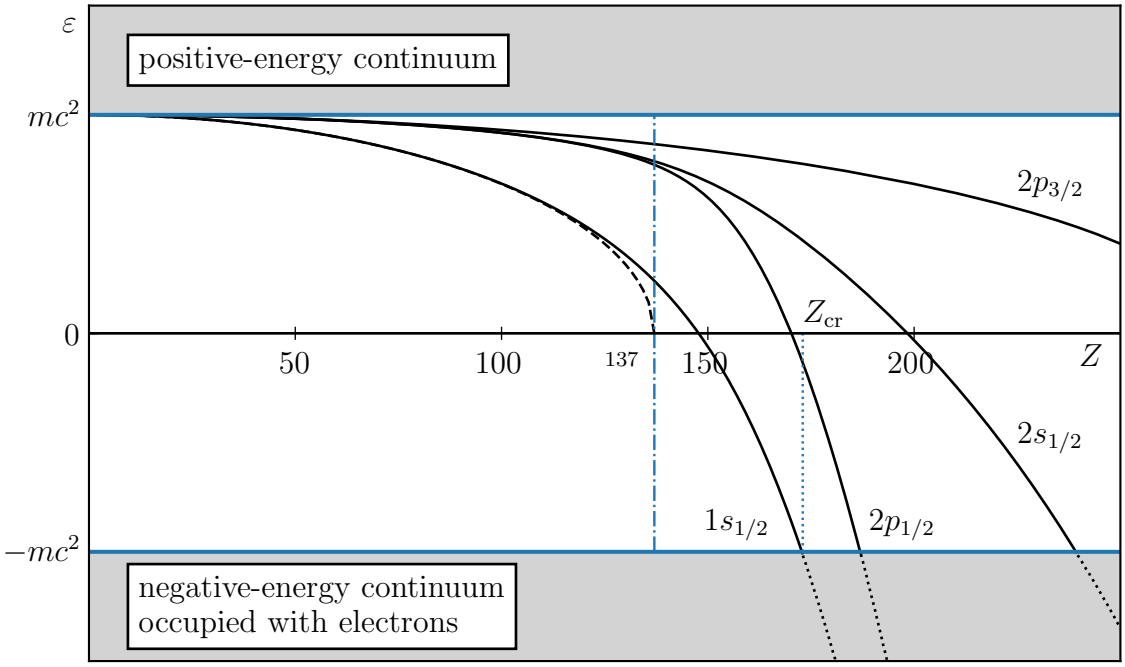

Figure 1: Dependence of the lowest bound state energies of hydrogen-like ions on the nuclear charge Z.

sphere, is illustrated in the Fig. 1. For comparison, we plotted also the dashed line corresponding to the $1s$ level of H-like ions with point-like nucleus.

Despite the fact that atoms with charge numbers close to $Z_{\rm cr}$ do not exist, the question stated above retains its significance. This is because the scenario of a bound state entering the negative-energy continuum can be experimentally realized in low-energy collision of two heavy ions, given that the total charge $Z_{\rm A}+Z_{\rm B}$ exceeds the critical value $Z_{\rm cr}$. In this case, instead of atomic, one deals with quasimolecular energy levels, which are temporarily formed when the relatively slow moving ions get close to each other. The behavior of the lowest-lying quasimolecular levels during a collision is demonstrated in Fig. 2. It is seen from the picture that for a short period of time denoted as $\tau_{\rm cr}$, when the internuclear distance $R(t)$ becomes less than a certain value, the $1s\sigma$ state ceases to exist diving in the negative-energy continuum. The internuclear distance $R_{\rm cr}$ at which this occurs is referred to as critical. During this time, the corresponding bound energy level transforms into a resonance. For illustration purposes, a nonlinear time scale is used in Fig. 2, the real duration of $\tau_{\rm cr}$ is significantly smaller. The emergence of the resonance is related to appearance of a barrier in the effective potential of the electron for ions with for $Z > Z_{\rm cr}$ and $\varepsilon \lesssim -mc^2$ (see eg. Refs. [12, 43]). As it is well known, the variables in the Dirac equation for a spherically symmetric potential $V(r)$ can be separated. The

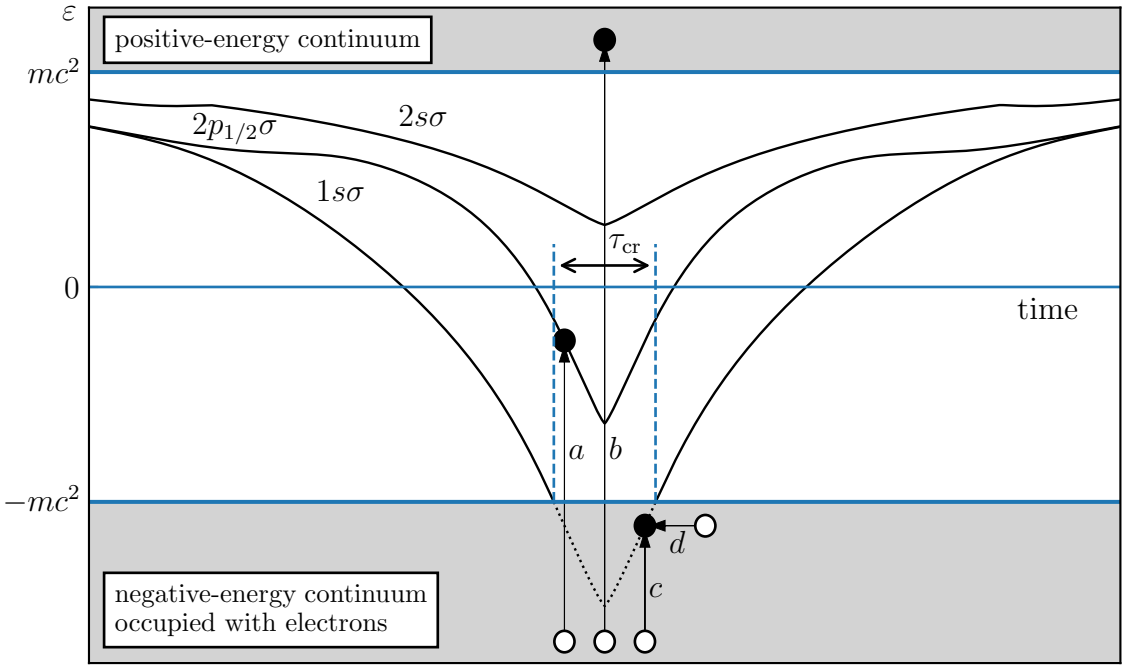

Figure 2: Lowest-lying energy levels of U_2^{183+} quasimolecule formed in a low-energy collision as functions of time.

stationary Dirac equation in this case reads

$$\left(\boldsymbol{\alpha}\cdot\boldsymbol{p}+\beta m+V(r)\right)\psi(\boldsymbol{r})=\varepsilon\psi(\boldsymbol{r}) \tag{1.2}$$

where $\boldsymbol{\alpha}$, β — are the Dirac matrices. Here and further we use the relativistic units ($\hbar = c = 1$), but sometimes we explicitly write the light speed c for clarity. The solution of the equation (1.2) can be expressed as a bispinor

$$\psi(\boldsymbol{r})=\frac{1}{r}\begin{pmatrix} G(r)\boldsymbol{\Omega}_{\kappa\mu}(\boldsymbol{n}) \\ iF(r)\boldsymbol{\Omega}_{-\kappa\mu}(\boldsymbol{n}) \end{pmatrix}, \tag{1.3}$$

where $\boldsymbol{\Omega}_{\kappa\mu}(\boldsymbol{n})$ — is a spherical spinor [71]. Substituting the wave function in this form into the equation (1.2), one obtains the system of two first order differential equations on the radial components [72]:

$$\left(\frac{d}{dr}+\frac{\kappa}{r}\right)G-(m+\varepsilon-V)F=0, \tag{1.4}$$

$$\left(\frac{d}{dr}-\frac{\kappa}{r}\right)F-(m-\varepsilon+V)G=0. \tag{1.5}$$

Using the first equation one can express the small component of the wave function,

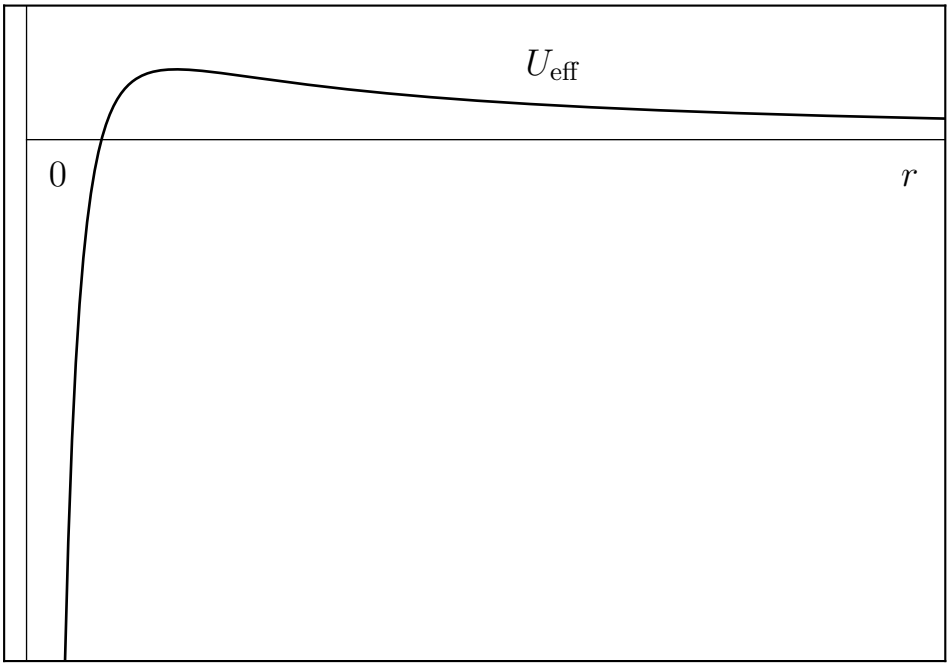

Figure 3: Effective potential for electron with $\kappa = -1$ and $\varepsilon = -mc^2$

F, through a large component, G. Then, substituting it into the second equation, one obtains the equivalent differential equation of the second order:

$$G'' + \frac{V'}{m + \varepsilon - V}\left(G' + \frac{\kappa}{r}G\right) + \left[(\varepsilon - V)^2 - m^2 - \frac{\kappa(\kappa+1)}{r^2}\right]G = 0. \qquad (1.6)$$

Utilizing the substitution $G = \chi\sqrt{m + \varepsilon - V}$, Eq. (1.6) can be written as

$$\chi'' + k^2\chi = 0, \qquad (1.7)$$

where $k^2 = 2(E - U_{\text{eff}})$, $E = \frac{1}{2}(\varepsilon^2 - m^2)$, and U_{eff} is an effective potential, which depends on ε. In a particular case of the Coulomb potential $V = -\alpha Z/r$, $\kappa = -1$ and $\varepsilon = -m$ the potential U_{eff} has the form

$$U_{\text{eff}} = \frac{m\alpha Z}{r} - \frac{4(\alpha Z)^2 - 3}{8r^2}. \qquad (1.8)$$

As can be seen from the Fig. 3, the effective potential has a wide barrier.

In order to understand what happens with the Coulomb system when its bound state dives into a negative-energy continuum we need to recall the definition

of the relativistic current operator. We use the following definition

$$\hat{j}^{\mu}(x) = \frac{e}{2}\left[\hat{\overline{\psi}}(x), \gamma^{\mu}\hat{\psi}(x)\right], \tag{1.9}$$

where e is the electron charge, $[\hat{A}, \hat{B}] = \hat{A}\hat{B} - \hat{B}\hat{A}$ stands for the commutator of operators $\hat{A}$ and $\hat{B}$, γ^{μ} is the 4-vector of the Dirac matrices, $\hat{\psi}$ is the electron-positron field operator, and $\hat{\overline{\psi}} = \hat{\psi}^{\dagger}\gamma^{0}$. In particular, we are interested in the zeroth component of the current, which represents the electron charge density operator

$$\hat{\rho}(x) = \frac{e}{2}\left[\hat{\psi}^{\dagger}(x), \hat{\psi}(x)\right]. \tag{1.10}$$

The mean value of $\hat{\rho}$ evaluated for the vacuum state gives the well known vacuum-polarisation charge density

$$\rho_{\rm vac}(x) = \langle 0 \left|\hat{\rho}(x)\right| 0\rangle = \frac{e}{2}\left[\sum_{\varepsilon_n \le -mc^2} \left|\psi_n(x)\right|^2 - \sum_{\varepsilon_n > -mc^2} \left|\psi_n(x)\right|^2\right]. \tag{1.11}$$

Suppose that the two nuclei have a total charge $Z_{\rm A} + Z_{\rm B} > Z_{\rm cr}$. In the subcritical case, i.e. when $R > R_{\rm cr}$, the total charge of the system evaluated as the spatial integration of $\rho_{\rm vac}(x)$ yields zero:

$$Q_{\rm vac} = \int d\boldsymbol{x}\, \rho_{\rm vac}(x) = 0. \tag{1.12}$$

Thus, the vacuum is said to be electrically neutral. Now, let us look at what happens at the verge of supercriticality. To this end, it is convenient to separate the contribution of the lowest-energy bound state to the total charge density. For $R = R_{\rm cr} + \delta R$, where δR is infinitesimally small, we have

$$\rho_{\rm vac}(x) = \frac{e}{2}\left[\sum_{\varepsilon_n \le -mc^2} \left|\psi_n(x)\right|^2 - 2\left|\psi_{1s\sigma}(x)\right|^2 - \sum_{\varepsilon_n > -mc^2;\, \varepsilon_n \ne \varepsilon_{1s\sigma}} \left|\psi_n(x)\right|^2\right]. \tag{1.13}$$

The factor of two in front of the $1s\sigma$ contribution stems from the two projections of the total angular momentum on the internuclear axis. Since the density $\rho(x)$ continuously depends on R, when R is slowly decreased to the point $R = R_{\rm cr} - \delta R$,

$\rho_{\rm vac}$ will approximately stay unchanged

$$\rho'_{\rm vac}(x) \approx \frac{e}{2}\left[\sum_{\varepsilon_n \le -mc^2} \big|\psi_n(x)\big|^2 - 2\big|\psi_{1s\sigma}(x)\big|^2 - \sum_{\varepsilon_n > -mc^2;\, \varepsilon_n \ne \varepsilon_{1s\sigma}} \big|\psi_n(x)\big|^2\right]. \quad (1.14)$$

This is the charge density of the subcritical vacuum state in the supercritical potential. The supercritical vacuum state is defined in a regular way as a state in which all the energy levels with energies $\varepsilon_n \le -mc^2$ are occupied with electrons, and the ones with $\varepsilon_n > -mc^2$ are empty. The only difference with the subcritical case is is the absence of the $1s\sigma$ state in the energy spectrum. But the contribution of this state to the charge density does not disappear. When the $1s\sigma$ state joins the negative energy-continuum, the continuum wave functions get distorted in such a way that the charge density associated with the $1s\sigma$ state becomes distributed over a range of them in a resonant manner. The supercritical vacuum can be obtained from the subcritical state with occupied $1s\sigma$ shell by adiabatically slow decrease of the internuclear separation R over the critical value. Due to continuity of ρ with respect to R, one can approximately express the supercritical vacuum charge density $\rho^{\rm cr}_{\rm vac}(x)$ as

$$\rho^{\rm cr}_{\rm vac}(x) \approx \frac{e}{2}\left[\sum_{\varepsilon_n \le -mc^2} \big|\psi_n(x)\big|^2 + 2\big|\psi_{1s\sigma}(x)\big|^2 - \sum_{\varepsilon_n > -mc^2;\, \varepsilon_n \ne \varepsilon_{1s\sigma}} \big|\psi_n(x)\big|^2\right]. \quad (1.15)$$

Comparing Eqs. (1.14) and (1.15), it is readily seen that $\rho^{\rm cr}_{\rm vac}(x)$ differs from the $\rho'_{\rm vac}(x)$ by the density of the submerged $1s\sigma$ shell $2\big|\psi_{1s\sigma}(x)\big|^2$. Although, the approximate expression (1.14) of the charge density in the supercritical regime is valid only for $R(t) \approx R_{\rm cr}$, the qualitative picture remains the same until the next bound state joins the lower continuum. Thus, for $R(t) \le R_{\rm cr}$ we have a system in state with two vacancies spread over the lower continuum. Initially these vacancies are localised near the nuclei. But within a certain period of time they can go through the potential barrier, like the one depicted in Figure 3, and escape to infinity as positrons. This process is called spontaneous electron-positron pair creation.

However, the actual nuclear collisions are not adiabatically slow but happen at finite speeds. In this case there exists an additional pair-creation mechanism referred to as dynamic or induced. Due to time-dependence of the nuclear potential the electrons in the negative-energy continuum can be exited to bound states or

positive-energy continuum. The energy required for this transition is taken from the kinetic energy of the nuclei. Figure 2 illustrates all possible ways an electron-positron pair can be created during a collision. Channels a, b and c correspond to the dynamic mechanism. The remaining channel d demonstrates the spontaneous mechanism. It is seen from the figure that in contrast to the spontaneous pair creation, which can happen only for a short period of time $\tau_{\rm cr}$, the dynamic mechanism is active during the whole collision process.

Chapter 2. General formalism

For nonperturbative description of the pair-creation process we employ the formalism of quantum electrodynamics in the presence of a strong external field [23,73]. In our case, this field is induced by two colliding heavy nuclei, which are considered as classical finite-size particles moving along the hyperbolic Rutherford trajectories. Within the zeroth order of perturbation theory with respect to interaction with the quantized electromagnetic field, the Lagrangian density is given as

$$\mathcal{L} = \hat{\bar{\psi}} \left(i\partial_\mu - e\mathcal{A}^{\rm ext}_\mu \right) \gamma^\mu \hat{\psi} - m\hat{\bar{\psi}}\hat{\psi}. \tag{2.1}$$

Here $\hat{\psi}$ represents the operator of the electron-positron field, $\hat{\bar{\psi}} = \hat{\psi}^\dagger \gamma^0$ is the Dirac adjoint operator, m is the electron mass, γ^μ are the Dirac matrices, and $\mathcal{A}^{\rm ext}_\mu$ denotes the classical external field. Since we consider collisions with energies near the Coulomb barrier, the internuclear velocity appears to be relatively small. Therefore, the 4-potential $\mathcal{A}^{\rm ext}_\mu$ can be approximated with a good accuracy by its scalar part, neglecting the vector component

$$\mathcal{A}^{\rm ext}_0 = V(\boldsymbol{r}, t), \tag{2.2}$$

$$\mathcal{A}^{\rm ext}_i = 0, \quad i = 1, 2, 3. \tag{2.3}$$

Here $V(\boldsymbol{r}, t)$ is the time-dependent Coulomb potential of the colliding nuclei

$$V(\boldsymbol{r}, t) = V_{\rm A}\left(|\boldsymbol{r} - \boldsymbol{R}_{\rm A}(t)|\right) + V_{\rm B}\left(|\boldsymbol{r} - \boldsymbol{R}_{\rm B}(t)|\right), \tag{2.4}$$

$$V_{\rm A,B}(r) = \frac{e}{4\pi} \int d\boldsymbol{r}' \frac{\rho_{\rm A,B}(r')}{|\boldsymbol{r} - \boldsymbol{r}'|}, \tag{2.5}$$

where $\boldsymbol{R}_{\rm A,B}(t)$ are the nuclear coordinates and $\rho_{\rm A,B}(r)$ are the nuclear charge densities. The latter are described by the model of homogeneously charged sphere.

According to the canonical quantization procedure, the momenta conjugate

to the electron-positron field read

$$p_\psi = \frac{\partial \mathcal{L}}{\partial \dot{\hat{\psi}}} = i\hat{\bar{\psi}}\gamma^0, \tag{2.6}$$

$$p_{\bar{\psi}} = \frac{\partial \mathcal{L}}{\partial \dot{\hat{\bar{\psi}}}} = 0. \tag{2.7}$$

This leads to the Hamiltonian

$$\hat{H}(t) = \int d\boldsymbol{x}\hat{\bar{\psi}}(x)\left(-i\boldsymbol{\gamma}\cdot\boldsymbol{\nabla} + m + e\gamma^\mu \mathcal{A}^{\text{ext}}_\mu(x)\right)\hat{\psi}(x) = \int d\boldsymbol{x}\hat{\psi}^\dagger(x)H(t)\hat{\psi}(x), \tag{2.8}$$

where $H(t) = \boldsymbol{\alpha}\cdot\boldsymbol{p} + m\beta + V(\boldsymbol{r},t)$ is the Dirac Hamiltonian. To ensure that the Dirac field, describing spin-$\frac{1}{2}$ particles, complies with the Pauli exclusion principle, the following anticommutation relations, taken at the same time $x_0 = y_0$, are imposed onto the operators $\hat{\psi}$ and $\hat{\bar{\psi}}$:

$$\begin{aligned} \left\{\hat{\psi}(x), \hat{\psi}(y)\right\} &= \left\{\hat{\bar{\psi}}(x), \hat{\bar{\psi}}(y)\right\} = 0, \\ \left\{\hat{\psi}(x), \hat{\bar{\psi}}(y)\right\} &= \gamma^0\delta(\boldsymbol{x}-\boldsymbol{y}), \quad x_0 = y_0. \end{aligned} \tag{2.9}$$

The time dependence of an arbitrary operator $\hat{A}$ in the Heisenberg representation is governed by equation

$$\partial_t \hat{A}(\boldsymbol{r},t) = i\left[\hat{H}(t), \hat{A}(\boldsymbol{r},t)\right]. \tag{2.10}$$

Therefore, combining expressions (2.8)–(2.10), one arrives at the following equation describing the time evolution of the electron-positron field operator $\hat{\psi}$:

$$i\partial_{x_0}\hat{\psi}(x) = H(x_0)\hat{\psi}(x). \tag{2.11}$$

Let us now introduce two sets of solutions of the time-dependent Dirac equation

$$i\partial_{x_0}\varphi(x) = H(x_0)\varphi(x), \tag{2.12}$$

namely the so called in- and out-solutions. In-solutions will be denoted as ${}_\zeta\varphi_n(x)$,

and out-solutions as ${}^{\zeta}\varphi_n(x)$, where $\zeta = \pm$ is used to specify if the corresponding solution is of the positive-energy $(+)$ or the negative-energy $(-)$ type. The difference between these two sets is that the in-solutions are subject to the initial conditions

$$\begin{cases} (i\partial_{x_0} - H(x_0))_{\zeta}\varphi_n(x) = 0, \\ {}_{\zeta}\varphi_n(x)\big|_{x_0=t_{\rm in}} = {}_{\zeta}\phi_n(\boldsymbol{x}), \end{cases} \tag{2.13}$$

whereas the out-solutions obey the final conditions

$$\begin{cases} (i\partial_{x_0} - H(x_0))^{\zeta}\varphi_n(x) = 0, \\ {}^{\zeta}\varphi_n(x)\big|_{x_0=t_{\rm out}} = {}_{\zeta}\phi_n(\boldsymbol{x}). \end{cases} \tag{2.14}$$

Here ${}_{\zeta}\phi(\boldsymbol{x})$ and ${}^{\zeta}\phi(\boldsymbol{x})$ are the eigenstates of the Dirac Hamiltonian taken at the time $t_{\rm in}$ and $t_{\rm out}$, respectively:

$$H(t_{\rm in})_{\zeta}\phi_n = {}_{\zeta}\varepsilon_n\, {}_{\zeta}\phi_n, \tag{2.15}$$

$$H(t_{\rm out})^{\zeta}\phi_n = {}^{\zeta}\varepsilon_n\, {}^{\zeta}\phi_n. \tag{2.16}$$

The sets $\{{}_{\zeta}\varphi_n(x)\}$, $\{{}^{\zeta}\varphi_n(x)\}$ are complete and orthonormal at any instant of time

$$({}_{\zeta}\varphi_n, {}_{\zeta'}\varphi_m) = ({}^{\zeta}\varphi_n, {}^{\zeta'}\varphi_m) = \delta_{\zeta\zeta'}\delta_{nm}, \quad \zeta, \zeta' = \pm, \tag{2.17}$$

$$\sum_{\zeta,n} {}_{\zeta}\varphi_n(x)\,{}_{\zeta}\varphi_n^{\dagger}(y) = \sum_{\zeta,n} {}^{\zeta}\varphi_n(x)\,{}^{\zeta}\varphi_n^{\dagger}(y) = \delta(\boldsymbol{x}-\boldsymbol{y}), \quad x_0 = y_0, \tag{2.18}$$

$$(f, g) = \int d\boldsymbol{x}\; f^{\dagger}(\boldsymbol{x}) g(\boldsymbol{x}). \tag{2.19}$$

Therefore, the electron-positron field operator $\hat{\psi}(x)$ can be expanded over either of them

$$\hat{\psi}(x) = \sum_n \left[\hat{a}_n({\rm in})_{+}\varphi_n(x) + \hat{b}_n^{\dagger}({\rm in})_{-}\varphi_n(x)\right], \tag{2.20}$$

$$\hat{\psi}(x) = \sum_n \left[\hat{a}_n({\rm out})^{+}\varphi_n(x) + \hat{b}_n^{\dagger}({\rm out})^{-}\varphi_n(x)\right]. \tag{2.21}$$

The corresponding expansion of the conjugate field $\hat{\bar{\psi}}(x)$ reads

$$\hat{\bar{\psi}}(x) = \sum_n \left[\hat{a}_n^\dagger(\mathrm{in})_+\bar{\varphi}_n(x) + \hat{b}_n(\mathrm{in})_-\bar{\varphi}_n(x)\right], \tag{2.22}$$

$$\hat{\bar{\psi}}(x) = \sum_n \left[\hat{a}_n^\dagger(\mathrm{out})^+\bar{\varphi}_n(x) + \hat{b}_n(\mathrm{out})^-\bar{\varphi}_n(x)\right]. \tag{2.23}$$

The operators $\hat{a}^\dagger(\mathrm{in/out})$ and $\hat{a}(\mathrm{in/out})$ are referred to as the operators of creation and annihilation of an electron in an in-/out-state. The operators $\hat{b}^\dagger(\mathrm{in/out})$ and $\hat{b}(\mathrm{in/out})$ represent the corresponding operators of creation and annihilation of a positron in an in-/out-state. Using the equal-time anti-commutation relations (2.9) for $\hat{\psi}$ and $\hat{\bar{\psi}}$, one readily obtains the following relations for the just introduced creation/annihilation operators:

$$\left\{\hat{a}_n(\mathrm{in}), \hat{a}_m(\mathrm{in})\right\} = \left\{\hat{a}_n^\dagger(\mathrm{in}), \hat{a}_m^\dagger(\mathrm{in})\right\} = \left\{\hat{b}_n(\mathrm{out}), \hat{b}_m(\mathrm{out})\right\} = \left\{\hat{b}_n^\dagger(\mathrm{out}), \hat{b}_m^\dagger(\mathrm{out})\right\} = 0, \tag{2.24}$$

$$\left\{\hat{a}_n(\mathrm{in}), \hat{a}_m^\dagger(\mathrm{in})\right\} = \left\{\hat{b}_n(\mathrm{in}), \hat{b}_m^\dagger(\mathrm{in})\right\} = \left\{\hat{a}_n(\mathrm{out}), \hat{a}_m^\dagger(\mathrm{out})\right\} = \left\{\hat{b}_n(\mathrm{out}), \hat{b}_m^\dagger(\mathrm{out})\right\} = \delta_{nm}. \tag{2.25}$$

Since the functions ${}_\zeta\varphi_n(x)$ and ${}^\zeta\varphi_n(x)$ satisfy the same time-dependent Dirac equation as $\hat{\psi}(x)$, the creation and annihilation operators appear to be independent of time. However, it should be noted that they relate to physical particles only at certain moments of time, namely, in-operators — at t_{in} and out-operators — at t_{out}. Only at these time instants the Hamiltonian (2.8) acquires a diagonal form in terms of in-/out-operators:

$$\hat{H}(t_{\mathrm{in}}) = \sum_n \left[{}_+\varepsilon_n(t_{\mathrm{in}})\hat{a}_n^\dagger(\mathrm{in})\hat{a}_n(\mathrm{in}) + \left|{}_-\varepsilon_n(t_{\mathrm{in}})\right|\hat{b}_n^\dagger(\mathrm{in})\hat{b}_n(\mathrm{in})\right], \tag{2.26}$$

$$\hat{H}(t_{\mathrm{out}}) = \sum_n \left[{}^+\varepsilon_n(t_{\mathrm{out}})\hat{a}_n^\dagger(\mathrm{out})\hat{a}_n(\mathrm{out}) + \left|{}^-\varepsilon_n(t_{\mathrm{out}})\right|\hat{b}_n^\dagger(\mathrm{out})\hat{b}_n(\mathrm{out})\right]. \tag{2.27}$$

The vacuum states are defined in a regular manner:

$$\hat{a}_n(\mathrm{in})|0,\mathrm{in}\rangle = \hat{b}_n(\mathrm{in})|0,\mathrm{in}\rangle = \hat{a}_n(\mathrm{out})|0,\mathrm{out}\rangle = \hat{b}_n(\mathrm{out})|0,\mathrm{out}\rangle = 0. \tag{2.28}$$

The generic form of the in-/out-states with specific occupation numbers reads

$$|\text{in}\rangle = \hat{a}_k^\dagger(\text{in})\ldots\hat{b}_l^\dagger(\text{in})\ldots|0,\text{in}\rangle, \tag{2.29}$$

$$|\text{out}\rangle = \hat{a}_k^\dagger(\text{out})\ldots\hat{b}_l^\dagger(\text{out})\ldots|0,\text{out}\rangle. \tag{2.30}$$

The quantities of interest to us are the mean numbers electrons n_m and positrons $\bar{n}_m$ produced from the vacuum in a certain state m. They are defined as

$$n_m = \langle 0,\text{in}|\hat{a}_m^\dagger(\text{out})\hat{a}_m(\text{out})|0,\text{in}\rangle, \tag{2.31}$$

$$\bar{n}_m = \langle 0,\text{in}|\hat{b}_m^\dagger(\text{out})\hat{b}_m(\text{out})|0,\text{in}\rangle. \tag{2.32}$$

In order to calculate these matrix elements, the in-operators are to be written in terms of out-operators. The following expressions come in helpful for this:

$$\hat{a}_m(\text{out}) = \int d\boldsymbol{x}\ {}^+\varphi_m^\dagger(x)\hat{\psi}(x), \tag{2.33}$$

$$\hat{a}_m^\dagger(\text{out}) = \int d\boldsymbol{x}\ \hat{\psi}^\dagger(x){}^+\varphi_m(x), \tag{2.34}$$

$$\hat{b}_m(\text{out}) = \int d\boldsymbol{x}\ \hat{\psi}^\dagger(x){}^-\varphi_m(x), \tag{2.35}$$

$$\hat{b}_m^\dagger(\text{out}) = \int d\boldsymbol{x}\ {}^-\varphi_m^\dagger(x)\hat{\psi}(x). \tag{2.36}$$

Substituting here $\hat{\psi}(x)$, $\hat{\psi}^\dagger(x)$, written in terms of in-operators, one arrives at

$$\hat{a}_m(\text{out}) = \sum_n \left[G({}^+|_+)_{mn}\hat{a}_n(\text{in}) + G({}^+|_-)_{mn}\hat{b}_n^\dagger(\text{in})\right], \tag{2.37}$$

$$\hat{a}_m^\dagger(\text{out}) = \sum_n \left[G({}_+|^+)_{nm}\hat{a}_n^\dagger(\text{in}) + G({}_-|^+)_{nm}\hat{b}_n(\text{in})\right], \tag{2.38}$$

$$\hat{b}_m(\text{out}) = \sum_n \left[G({}_+|^-)_{nm}\hat{a}_n^\dagger(\text{in}) + G({}_-|^-)_{nm}\hat{b}_n(\text{in})\right], \tag{2.39}$$

$$\hat{b}_m^\dagger(\text{out}) = \sum_n \left[G({}^-|_+)_{mn}\hat{a}_n(\text{in}) + G({}^-|_-)_{mn}\hat{b}_n^\dagger(\text{in})\right], \tag{2.40}$$

where

$$G({}_{\xi}|^{\zeta})_{mn} = \int d\boldsymbol{x}\ {}_{\xi}\varphi_m^{\dagger}(x)^{\zeta}\varphi_n(x), \tag{2.41}$$

$$G({}^{\zeta}|_{\xi}) = G({}_{\xi}|^{\zeta})^{\dagger}, \quad \xi,\zeta = \pm. \tag{2.42}$$

Because of orthonormality and completeness of the sets $\{{}_{\pm}\varphi(x)\}$ and $\{{}^{\pm}\varphi(x)\}$, the matrices $G({}_{\pm}|^{\pm})$, $G({}^{\pm}|_{\pm})$ possess a number of properties:

$$\sum_{\xi=\pm} G({}_{\pm}|^{\xi})G({}^{\xi}|_{\pm}) = \sum_{\xi=\pm} G({}^{\pm}|_{\xi})G({}_{\xi}|^{\pm}) = I, \tag{2.43}$$

$$\sum_{\xi=\pm} G({}_{\pm}|^{\xi})G({}^{\xi}|_{\mp}) = \sum_{\xi=\pm} G({}^{\pm}|_{\xi})G({}_{\xi}|^{\mp}) = 0. \tag{2.44}$$

Substituting (2.37), (2.38) into (2.31) and using the permutation relations (2.24), (2.25) and the definition of the vacuum state (2.28), one obtains the mean number of produced electrons in a particular state m equal to [73]

$$n_m = \left(G({}^{+}|_{-})G({}_{-}|^{+})\right)_{mm}. \tag{2.45}$$

Analogously, the mean number of positrons is given by

$$\bar{n}_m = \left(G({}^{-}|_{+})G({}_{+}|^{-})\right)_{mm}. \tag{2.46}$$

The quantity $n_m/\bar{n}_m$ can also be interpreted as the mean number of the produced electron-positron pairs with electron/positron in a state m, while the positron/electron can occupy any of possible state. The total numbers of the created electrons, n, and positrons, $\bar{n}$, are given as

$$n = \sum_m n_m, \tag{2.47}$$

$$\bar{n} = \sum_m \bar{n}_m. \tag{2.48}$$

It can be readily shown that the total numbers of electrons and positrons coincide, i.e., $n = \bar{n}$. Due to the fact that the probability of creation of $k+1$ electron-positron pairs from the vacuum is several orders of magnitude smaller than the probability production of k pairs, the mean values of created particles n_m and $\bar{n}_m$

are predominately determined by the probability of a single pair production. For this reason in the thesis we use the words "pair-creation probability" and "mean number of created pairs" interchangeably, but the actual values are always calculated according to the formulae (2.45)–(2.48).

It should be noted that the indices in the sums and matrices above are not exclusively discrete but run over a continuous set of values as well. However, since in the numerical calculations we employ the finite-size basis approach, effectively we deal with a pure discrete spectrum. Thus, direct evaluation of the energy spectra of emitted particles according to Eqs. (2.45) and (2.46) is not possible. Therefore, the differential probabilities $dP/d\varepsilon$ are calculated using a modified version of the Stiltjes procedure [55]

$$\frac{dP}{d\varepsilon}\Big(\frac{\varepsilon_p + \varepsilon_{p+s-1}}{2}\Big) = \frac{1}{\varepsilon_{p+s-1} - \varepsilon_p}\left(\frac{\overline{n}_p + \overline{n}_{p+s-1}}{2} + \sum_{i=1}^{s-2} \overline{n}_{p+i}\right) . \tag{2.49}$$

Here s determines the number of energy eigenvalues ε_i involved in the calculation of one point in the positron energy spectrum. With $s = 2$ the equation (2.49) turns into the regular Stieltjes formula [52, 53, 74].

Chapter 3. Collision trajectories

Within the scope of our calculation method the nuclei are treated classically as uniformly charged balls. The nuclear motion is determined by the nonrelativistic classical mechanics which prescribes them to follow the hyperbolic Rutherford trajectories. Conventionally, the scattering trajectories are parameterized with a collision energy E and an impact parameter b. In our study we focus on the behavior of the electron-positron pair-creation probability and the positron energy spectra obtained in collisions with different energies E but corresponding to the same distance of the closest approach $R_{\min}$. Hence, it turns out to be convenient to characterize a specific trajectory with $R_{\min}$ and a parameter $\eta = E/E_0$, which is the ratio of the collision energy E to the energy E_0 of the head-on collision with the same $R_{\min}$. With $R_{\min}$ being fixed, the impact parameter b is related to the collision energy E in the center-of-mass reference frame via the equation

$$b^2 = R_{\min}^2 - \frac{\alpha Z_{\mathrm{A}} Z_{\mathrm{B}}}{E} R_{\min}, \tag{3.1}$$

where $\alpha \approx 1/137$ is the fine structure constant and Z_{A}, Z_{B} are the colliding nuclei charge numbers. Keeping in mind that for head-on collisions $E_0 = \alpha Z_{\mathrm{A}} Z_{\mathrm{B}}/R_{\min}$ and using the definition of the parameter $\eta = E/E_0$, one obtains the following unique correspondence between the conventional trajectory parameters (E, b) and our new ones $(R_{\min}, \eta)$

$$E = \eta E_0, \tag{3.2}$$

$$b = R_{\min}\sqrt{1 - 1/\eta}. \tag{3.3}$$

The scattering angle θ turns out to be a function of η only and is expressed as

$$\theta = \pi - 2\arccos\left(1/(2\eta - 1)\right). \tag{3.4}$$

Solving Eq. (3.1) for $R_{\min}$, one arrives at the inverse transformation from (E, b) to $(R_{\min}, \eta)$

$$R_{\min} = \frac{\alpha Z_{\mathrm{A}} Z_{\mathrm{B}}}{E} \eta, \tag{3.5}$$

$$\eta = \frac{1}{2} \left(1 + \sqrt{1 + \left(\frac{2bE}{\alpha Z_{\mathrm{A}} Z_{\mathrm{B}}} \right)^2} \right). \tag{3.6}$$

Using Eq. (3.4), η can be expressed as a function of the scattering angle θ as

$$\eta = \frac{1}{2} \left(1 + \left[\cos \left(\frac{\pi - \theta}{2} \right) \right]^{-1} \right). \tag{3.7}$$

An examples of trajectories corresponding to U^{92+}-U^{92+} collisions with various energies, E, and impact parameters, b, but having the same distance of the closest approach $R_{\min} = 17.5$ fm are presented in Fig. 4. All trajectories of this sort are tangent to a circle with a diameter $d = R_{\min}$. In Fig. 4 this circle is depicted with a solid blue line. The second circle drawn with a dashed orange line outlines the region

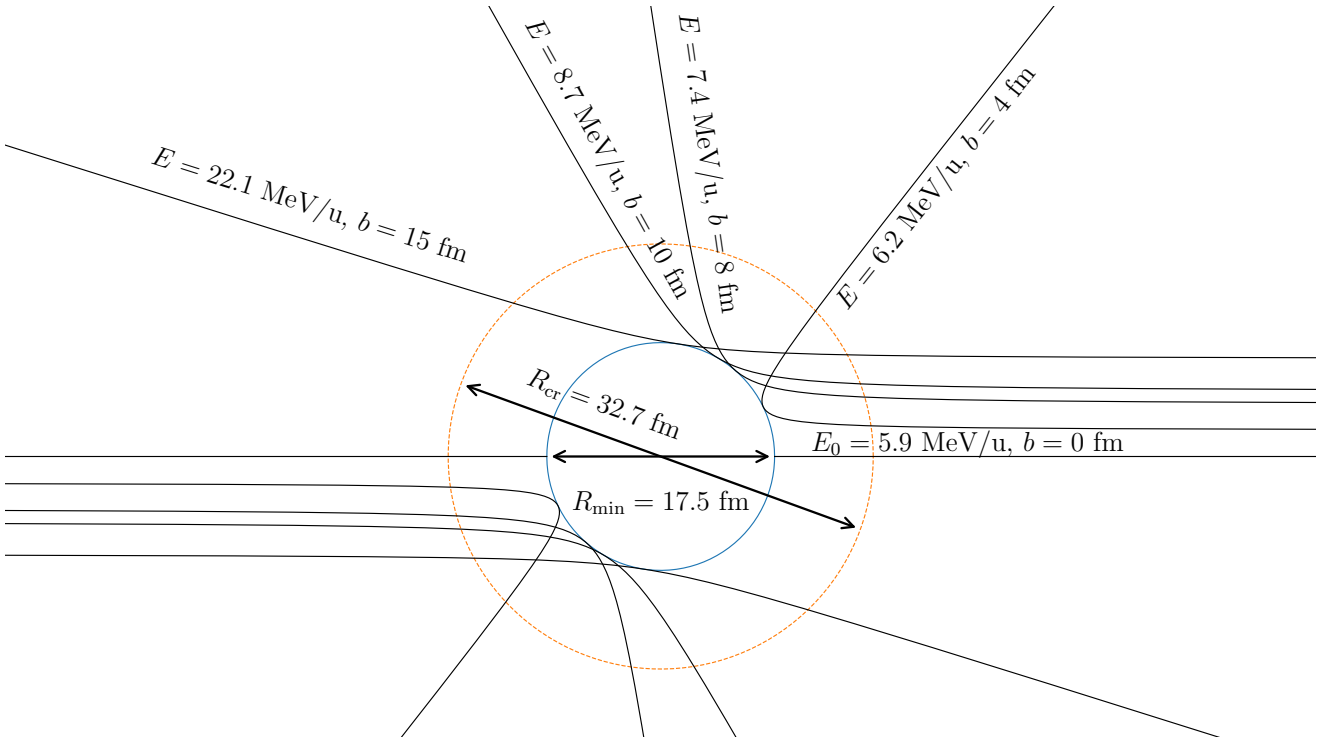

Figure 4: Example of considered U^{92+}-U^{92+} collision trajectories corresponding to $R_{\min} = 17.5$ fm. The circle $R = 32.7$ fm delineates the boundary of the supercritical region.

of supercritical internuclear separations. This means that when the nuclei are inside the region $R(t) \leq R_{\rm cr}$, the lower continuum acquires a resonance originating from the lowest-energy quasimolecular bound state reaching the energy $\varepsilon_{1s\sigma}(Z_{\rm A}, Z_{\rm B}, R_{\rm cr}) = -mc^2$. For collisions of uranium nuclei considered in the monopole approximation the critical internuclear distance $R_{\rm cr} = 32.7$ fm.

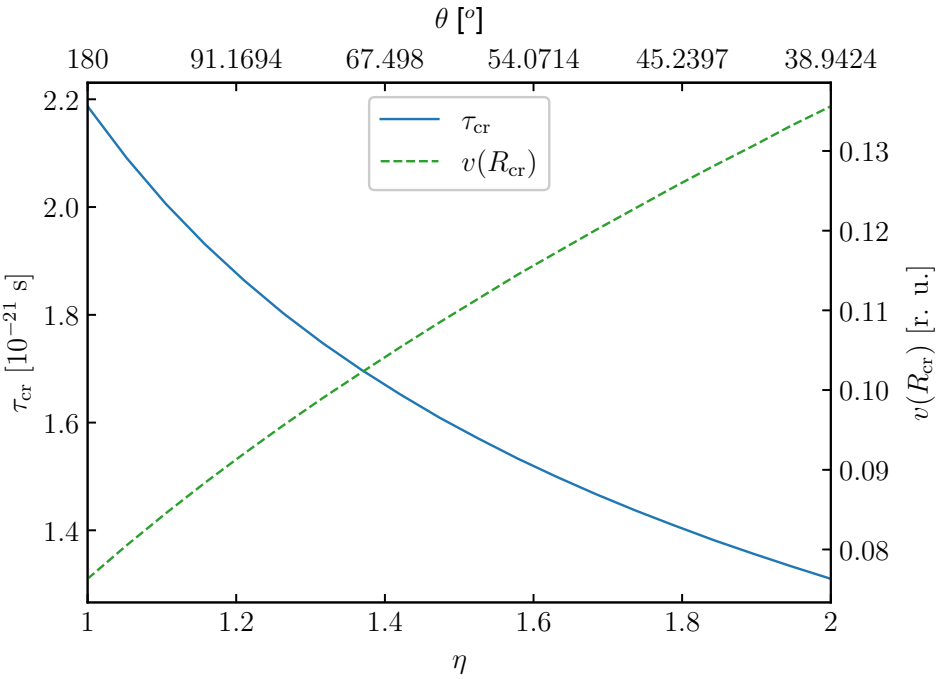

Figure 5: Duration of the supercritical regime and nuclear velocity at $R = R_{\rm cr}$ in U^{92+}-U^{92+} collisions with $R_{\rm min} = 17.5$ fm as functions of $\eta = E/E_0$ and the corresponding scattering angle θ.

The duration of the supercritical regime is determined by the time $\tau_{\rm cr}$ the nuclei spend in the ring $R_{\rm min} \leq R(t) < R_{\rm cr}$ (see also Fig. 2). This time monotonously decreases with increasing η. Actual dependence of $\tau_{\rm cr}$ on η for the case of U^{92+}-U^{92+} collisions with $R_{\rm min} = 17.5$ fm is displayed in Fig. 5. The figure also presents the relative nuclear velocity at the border of the supercritical region, i.e. when $R(t) = R_{\rm cr}$, as a function of η. In contrast to the duration $\tau_{\rm cr}$, this velocity monotonously rises with $\eta = E/E_0$. From general considerations it is clear that when $R_{\rm min}$ is fixed, the regular dynamic pair creation should intensify with growing nuclear velocity, characterized here by the parameter η, and diminish with its decrease. On the other hand, the reduction of the velocity positively affects the spontaneous mechanism by extending the time interval when it is active. Therefore, keeping aside the subject of interplay between the two mechanisms, an increase in the pair-creation probability as $\eta \to 1$ is to be considered as a signature of supercritical regime, where spontaneous

vacuum decay becomes possible.

Chapter 4. Calculations within the monopole approximation

In this section we will consider the process of electron-positron creation in low-energy collisions of heavy nuclei within the framework of the monopole approximation, which takes into account only spherically symmetric part of the two-center nuclear potential. Firstly, the procedure is described that is used for solving the stationary Dirac equation necessary for specifying the initial conditions of the time-dependent wave functions. After that we proceed to outlining the main points of the technique developed to solve the time-dependent Dirac equation. And finally, we present and discuss the results of calculations of the pair-creation probabilities and the positron energy spectra for collisions of heavy nuclei for a wide range of the collision parameters. The results of the research described in this chapter have been published in the paper [60].

4.1 Stationary Dirac equation

To set the starting point for integration of the time-dependent Dirac equation for the sets of the in-/out-solutions introduced above, the eigenstates of the Dirac Hamiltonian taken at the time instant $t_{\rm in}/t_{\rm out}$ have to be found. The time-dependence of the Hamiltonian is completely contained within the potential term. In the monopole approximation, the nuclear potential is given as

$$V^{\rm mon}(r,t) = \frac{1}{4\pi}\int d\boldsymbol{n} V(\boldsymbol{r},t), \tag{4.1}$$

$$V(\boldsymbol{r},t) = V_{\rm A}\left(|\boldsymbol{r}-\boldsymbol{R}_{\rm A}(t)|\right) + V_{\rm B}\left(|\boldsymbol{r}-\boldsymbol{R}_{\rm B}(t)|\right), \tag{4.2}$$

$$V_{\rm A,B}(r) = \frac{e}{4\pi}\int d\boldsymbol{r}' \frac{\rho_{\rm A,B}(r')}{|\boldsymbol{r}-\boldsymbol{r}'|}, \tag{4.3}$$

where $V(\boldsymbol{r},t)$ is the total two-center potential of the nuclei positioned at $\boldsymbol{R}_{\rm A,B}(t)$, $\boldsymbol{n} = \boldsymbol{r}/|\boldsymbol{r}|$ is the unit vector directed along $\boldsymbol{r}$. The charge density of the nuclei, $\rho_{\rm A,B}(r)$, was described with the model of homogeneously charged sphere, which

yields

$$V(r) = \begin{cases} -\dfrac{\alpha Z}{R_{\rm nucl}} \left(\dfrac{3}{2} - \dfrac{1}{2} \left(\dfrac{r}{R_{\rm nucl}} \right)^2 \right), & \text{if } r \le R_{\rm nucl}, \\ -\dfrac{\alpha Z}{r}, & \text{if } r > R_{\rm nucl}, \end{cases} \tag{4.4}$$

where $\alpha \approx 1/137$ is the fine structure constant, Z is the nuclear charge number, and $R_{\rm nucl}$ is its charge radius. The nuclear radii were calculated by the approximate formula $R_{\rm nucl} = 1.2 \times A^{1/3}$ fm, with $A = 2.5Z$ being the atomic mass number. Situated at the distance d from the origin a homogeneously charged spherically symmetric nucleus induces the potential with the following monopole part

$$V^{\rm mon}(r;d) = \begin{cases} -\dfrac{\alpha Z}{d}, & \text{for } r \le r_-, \\ -\dfrac{\alpha Z}{R_{\rm nucl}^3 d} \left[\dfrac{1}{16r}(d - R_{\rm nucl})^3 (d + 3R_{\rm nucl}) \right. & \\ \qquad -\frac{1}{4} r_+^2 (d - 2R_{\rm nucl}) + \frac{3}{8}(d^2 - R_{\rm nucl}^2) & \text{for } r_- < r < r_+, \\ \left. \qquad -\frac{1}{4} d r^2 + \frac{1}{16} r^3 \right], & \\ -\dfrac{\alpha Z}{r}, & \text{for } r \ge r_+, \end{cases} \tag{4.5}$$

where

$$r_+ = d + R_{\rm nucl}, \tag{4.6}$$

$$r_- = d - R_{\rm nucl}. \tag{4.7}$$

For symmetric collisions considered in the center-of-mass reference frame the parameter d is equal to the half of the internuclear distance $R(t)$. If the colliding nuclei are of different sorts, then each of them will have its own value of the distance d given by

$$d_{\rm A} = \frac{M_{\rm B}}{M_{\rm A} + M_{\rm B}} R(t), \tag{4.8}$$

$$d_{\rm B} = \frac{M_{\rm A}}{M_{\rm A} + M_{\rm B}} R(t), \tag{4.9}$$

where $M_{\rm A}$ and $M_{\rm B}$ denote the corresponding nuclear masses.

Since the monopole potential (4.1) depends on time only via the internuclear distance $R(t)$, which has the same values at $t_{\rm in}$ and $t_{\rm out}$, we have

$$H(t_{\rm in}) = H(t_{\rm out}). \tag{4.10}$$

Therefore, only one set of eigenstates needs to be evaluated. As it was stated above, the process of nuclear collision is treated within the finite-basis-set approach. The radial part of the basis functions is described with B-splines [75], while the angular part is represented by spherical spinors $\mathbf{\Omega}_{\kappa\mu}(\boldsymbol{n})$ [71]. To get rid of the spurious states, we employed the dual kinetic balance method (DKB) [76].

The stationary Dirac equation for a spherically symmetric potential $V(r)$ reads

$$H_0\varphi_i(\boldsymbol{r}) = \varepsilon_i\varphi_i(\boldsymbol{r}), \tag{4.11}$$

$$H_0 = \boldsymbol{\alpha}\cdot\boldsymbol{p} + m\beta + V(r), \tag{4.12}$$

where $\boldsymbol{\alpha}$, β are the Dirac matrices. It is well known that for spherically symmetric fields the stationary wave function φ can be written in the form of a single bispinor

$$\varphi_{n\kappa\mu}(\boldsymbol{r}) = \frac{1}{r}\begin{pmatrix} G_{n\kappa}(r)\mathbf{\Omega}_{\kappa\mu}(\boldsymbol{n}) \\ iF_{n\kappa}(r)\mathbf{\Omega}_{-\kappa\mu}(\boldsymbol{n}) \end{pmatrix}, \tag{4.13}$$

where n is the principal quantum number, $\mathbf{\Omega}_{\kappa\mu}(\boldsymbol{n})$ is the spherical spinor with the relativistic angular-momentum–parity quantum number $\kappa = (-1)^{j+l+\frac{1}{2}}(j+\frac{1}{2})$ and z-projection of the total angular momentum μ. This form of the wave function allows one to exclude angular variables from the equation (4.11). Then, introducing a two-component array of the functions $G(r)$ and $F(r)$ as

$$\phi(r) = \begin{pmatrix} G(r) \\ F(r) \end{pmatrix}, \tag{4.14}$$

the resulting radial Dirac equation can be expressed as

$$H_\kappa\phi = \varepsilon\phi, \tag{4.15}$$

where

$$H_\kappa = \begin{pmatrix} m + V(r) & -\frac{d}{dr} + \frac{\kappa}{r} \\ \frac{d}{dr} + \frac{\kappa}{r} & -m + V(r) \end{pmatrix}. \tag{4.16}$$

In a finite basis approach the function $\phi(r)$ is approximately expressed as a finite sum

$$\phi(r) = \sum_{i=1}^{2n} c_i u_i(r) \tag{4.17}$$

of linearly independent and square integrable two-component functions $u_i(r)$. Consequently, the radial Dirac equation (4.15) transforms into a generalised eigenvalue problem

$$H_\kappa \boldsymbol{c} = \varepsilon S_\kappa \boldsymbol{c}, \tag{4.18}$$

where $\boldsymbol{c} = \{c_1, \ldots, c_{2n}\}$ denotes the array of the expansion coefficients, $H_{\kappa;\,ij} = \langle u_i | H_\kappa | u_j \rangle$ is the Hamiltonian matrix, and $S_{\kappa;\,ij} = \langle u_i | u_j \rangle$ is the overlap matrix. Solving the problem (4.18) yields a set of eigenvalues ε_i and eigenvectors $\boldsymbol{c}_i$ ($i = 1, \ldots, 2n$) which represent a discretized version of the H_0 operator spectrum.

The gist of the DKB method is in a special choice of the basis functions $u_i(r)$, incorporating the connection between the upper and lower components of the Dirac bispinors, namely,

$$u_i(r) = \begin{pmatrix} \pi_i(r) \\ \frac{1}{2m}\left(\frac{d}{dr} + \frac{\kappa}{r}\right)\pi_i(r) \end{pmatrix}, \quad i \le n, \tag{4.19}$$

$$u_i(r) = \begin{pmatrix} \frac{1}{2m}\left(\frac{d}{dr} - \frac{\kappa}{r}\right)\pi_{i-n}(r) \\ \pi_{i-n}(r) \end{pmatrix}, \quad i > n. \tag{4.20}$$

The use of basis functions of this form ensures that the matrices H_κ and $H_{-\kappa}$ have in general different sets of eigenvalues, retaining the symmetries inherent in the Dirac equation, e.g., charge conjugation symmetry. It should be noted that DKB approach is applicable only for potentials that do not have singularities at the origin. The

Coulomb potential of a point-like charge does not belong to this category due to the singularity as $r \to 0$. Though, this does not cause any complications to us, since the total potential of the nuclei is finite at any point. In actual computations the functions $\pi_i(r)$ were the B-splines.

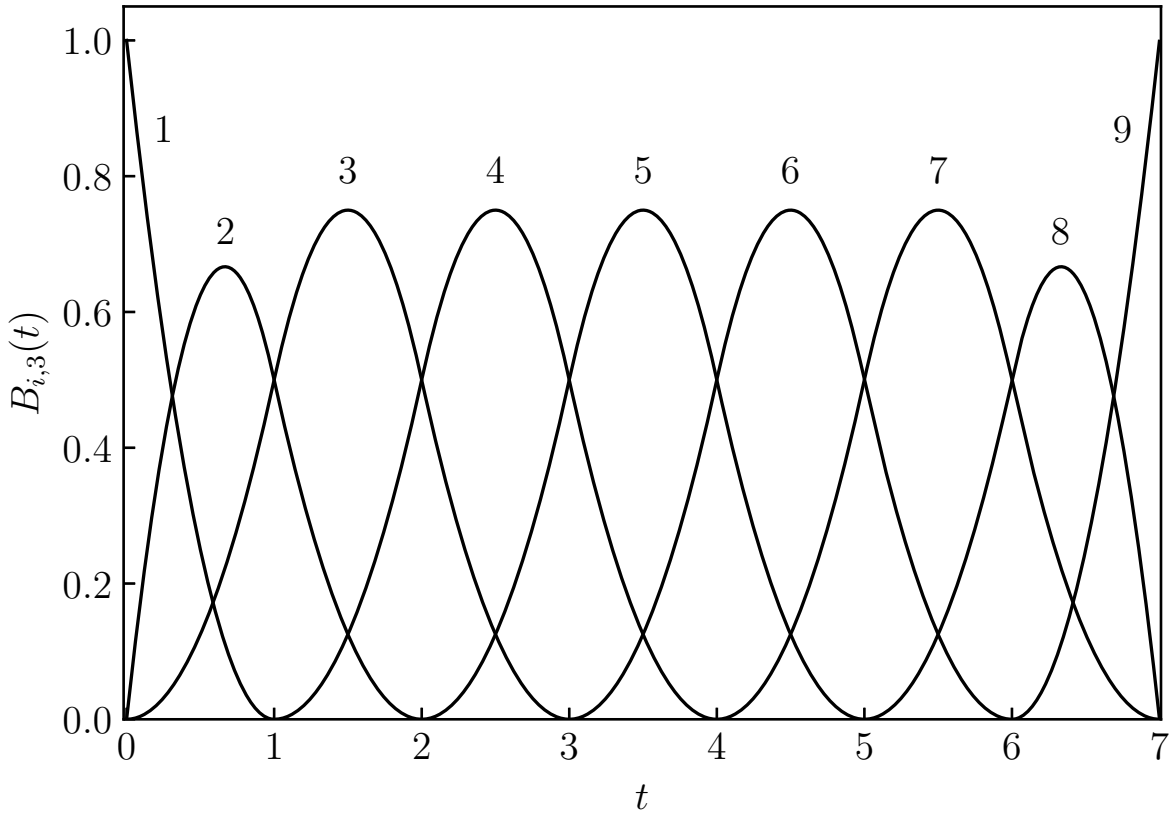

Figure 6: Example of a set of B-splines of the 3rd order constructed on the grid $t_i = [0, 0, 0, 1, 2, 3, 4, 5, 6, 7, 7, 7]$

The term B-splines is a short for basis splines, which means that an arbitrary spline function can be uniquely represented as a linear combination of B-splines with the same order. A spline function of the nth order in turn is a piecewise polynomial function defined on a given grid of knots. On each interval of the grid this function has a form of a polynomial of the nth degree. For a given grid of knots $\{t_i\}_{i=0}^{N}$ the B-spline of order p is represents a set of piecewise polynomial functions $B_{i,p}(t)$ of the degree p, which have a very compact support. Namely, $B_{i,p}(t)$ is zero everywhere except for the region $t_i \leq t \leq t_{i+p+1}$. This strong localisation of the B-splines comes in quite advantageous especially for calculations beyond the monopole approximation. The reason for this is that the work with large but sparse matrices, appearing in such calculations, can be optimised by employing numerical algorithm designed to efficiently deal with this sort of matrices.

The functions $B_{i,p}(t)$ can be defined recursively by relations

$$B_{i,0}(t) = \begin{cases} 1, & \text{if } t_i \le t < t_{i+1}, \\ 0, & \text{otherwise,} \end{cases} \tag{4.21}$$

and

$$B_{i,k}(t) = \frac{t - t_i}{t_{i+k} - t_i} B_{i,k-1}(t) + \frac{t_{i+k+1} - t}{t_{i+k+1} - t_{i+1}} B_{i+1,k-1}(t). \tag{4.22}$$

An example of the 3rd order B-splines constructed on the grid t_i = [0, 0, 0, 1, 2, 3, 4, 5, 6, 7, 7, 7] is depicted in Fig. 6. A uniform grid here is chosen for the sake of simplicity. From the figure one can see that the first spline is equal to 1 at the beginning of the first interval. The same holds for the last spline at the end of the last interval of the grid. The second and the second last splines at these points have nonzero derivatives. Other B-splines have zero values and first derivatives at the start and end of the their intervals. The sum of all B-splines of a given degree is unity

$$\sum_i B_{i,k}(t) = 1. \tag{4.23}$$

B-splines can be used for approximation of functions with different smoothness at the knots. The number of continuous derivatives is naturally set by appropriate number of repetitive knots in the grid. The more knots coincide the less smooth function is obtained. To satisfy the zero boundary conditions imposed on wave functions we exclude the first and the last B-splines from the basis set.

4.2 Time-dependent Dirac equation

Having examined the stationary states, which determine the initial and final conditions, let us proceed to description of their time evolution during a collision. To calculate the electron-positron pair-creation probability according to the formulae (2.45)–(2.46), one needs to know the wave function at the time instant $t_{\rm out}$. For this, the time-dependent Dirac equation subject to certain initial conditions needs

to be solved

$$\begin{cases} \left(i\partial_t - H(t)\right)\varphi_i(\boldsymbol{r},t) = 0 \\ \varphi_i(\boldsymbol{r},t_{\rm in}) = \phi_i(\boldsymbol{r}), \end{cases} \tag{4.24}$$

where

$$H(t) = \boldsymbol{\alpha}\cdot\boldsymbol{p} + m\beta + V^{\rm mon}(r,t), \tag{4.25}$$

$$H(t_{\rm in})\phi_i(\boldsymbol{r}) = \varepsilon_i\phi_i(\boldsymbol{r}), \tag{4.26}$$

and $V^{\rm mon}(r,t)$ stands for the monopole part of the total two-center potential of the nuclei, defined by Eq. (4.1).

The time-dependent wave function $\varphi_i(\boldsymbol{r},t)$ is decomposed over the basis set consisting of the eigenstates of the Hamiltonian $H(t_{\rm in})$,

$$\varphi_i(\boldsymbol{r},t) = \sum_j a_{ji}(t)e^{-i\varepsilon_j t}\phi_j(\boldsymbol{r}). \tag{4.27}$$

Substituting this decomposition into Eq. (4.24), multiplying it from the left by $e^{i\varepsilon_k t}\phi_k^\dagger(\boldsymbol{r})$ and performing spatial integration, we arrive at the following set of equations on the expansion coefficients $a_{ki}(t)$:

$$i\partial_t a_{ki}(t) = \sum_j V_{kj}(t)a_{ji}(t)e^{i(\varepsilon_k-\varepsilon_j)t}, \tag{4.28}$$

$$V_{kj}(t) = \langle\phi_k|V^{\rm mon}(r,t) - V^{\rm mon}(r,t_{\rm in})|\phi_j\rangle. \tag{4.29}$$

Since the monopole potential is spherically symmetric, the angular integration in Eq. (4.29) leads to the Kronecker deltas for angular symmetry related quantum numbers κ and μ of the corresponding bra- and ket- states:

$$V_{kj}(t) = \delta_{\kappa_k\kappa_j}\delta_{\mu_k\mu_j}\int dr\rho_{kj}(r)\left[V^{\rm mon}(r,t) - V^{\rm mon}(r,t_{\rm in})\right], \tag{4.30}$$

with

$$\rho_{kj}(r) = F_k(r)F_j(r) + G_k(r)G_j(r). \tag{4.31}$$

The remaining radial part of the matrix element $V_{kj}(t)$ is evaluated numerically

using Gauss-Legendre quadratures.

As a result, the partial differential equation (4.24) is replaced with the equivalent system of ordinary differential equations:

$$\begin{cases} i\partial_t \boldsymbol{a}_i(t) = M(t)\boldsymbol{a}_i(t), \\ a_{ji}(t_{\rm in}) = \delta_{ji}, \end{cases} \tag{4.32}$$

where $\boldsymbol{a}_i(t) = \{a_{1i}(t), \ldots, a_{Ni}(t)\}$ and

$$M_{kj}(t) = V_{kj}(t)e^{i(\varepsilon_k - \varepsilon_j)}. \tag{4.33}$$

To solve this system we employ the Crank-Nicolson scheme [77], which imposes the following relation on the expansion coefficients taken at adjacent time steps separated by an interval Δt:

$$\boldsymbol{a}_i(t + \Delta t) \approx U(t + \Delta t, t)\boldsymbol{a}_i(t), \tag{4.34}$$

where the matrix U is defined as

$$U(t + \Delta t, t) = \left[I + i\frac{\Delta t}{2}M\left(t + \frac{\Delta t}{2}\right)\right]^{-1}\left[I - i\frac{\Delta t}{2}M\left(t + \frac{\Delta t}{2}\right)\right], \tag{4.35}$$

and I is the identity matrix. The advantages of this scheme is that it conserves the normalisation of the wave function, does not require diagonalisation of the matrix $M(t)$ and provides the error of the expression (4.34) on the level of $O(\Delta t^3)$. In actual calculations, instead of evaluating the matrix $U(t + \Delta t, t)$ we solve the system of linear equations

$$\left[I + \frac{i\Delta t}{2}M(t + \Delta t/2)\right]\boldsymbol{a}_i(t + \Delta t) = \left[I - \frac{i\Delta t}{2}M(t + \Delta t/2)\right]\boldsymbol{a}_i(t). \tag{4.36}$$

Finally, the matrices $G(^{\zeta}|_{\xi})$ in Eqs. (2.45) and (2.46) for mean numbers of created electrons end positron are related to the expansion coefficients $\boldsymbol{a}(t)$ as

$$G(^{\zeta}|_{\xi})_{ij} = a_{ij}(t_{\rm out}), \tag{4.37}$$

where $\zeta = +$ if the ith out-state has a positive energy and $\zeta = -$ otherwise. The

same rule applies for ξ and in-states.

4.3 Results

Using the technique described above we performed a detailed investigation of the electron-positron pair-creation probabilities and the positron energy spectra for low-energy collisions of heavy nuclei in a broad range of collision parameters. The energy of a quasimolecular bound state and the parameters of the corresponding supercritical resonance are mostly determined by three parameters: the charge numbers of the nuclei $Z_{A,B}$ and the internuclear distance R. In order to enter the supercritical region, all these parameters should have appropriate values. The border of the supercritical domain of collision parameters is given by the equation $\varepsilon_{1s\sigma}(Z_{\rm A}, Z_{\rm B}, R_{\rm min}) = -mc^2$. With this in mind, we studied the behavior with respect to the parameter $\eta = E/E_0$ of the pair-creation probabilities and the positron energy spectra when the supercritical regime is activated by increasing the total nuclear charge $Z_{\rm tot}$ beyond $Z_{\rm cr}$ and by decreasing the minimal internuclear distance $R_{\rm min}$ below $R_{\rm cr}$. The basis set included functions with $|\kappa| = 1$, that were shown to give the dominant contribution to the process under consideration. Since the states with different values of κ or μ do not get mixed by a spherically symmetric potential, we assembled the basis sets from functions with $\mu = -\frac{1}{2}$ only and carried out the calculations for $\kappa = -1$ and $\kappa = 1$ independently. The obtained results were then summed and doubled. For calculations of the probabilities we used B-splines of the 9th order constructed on a radial grid with 200 nodes distributed exponentially. In calculations of the positron spectra we utilised B-splines of the same order constructed on a polynomial grid with 400 nodes.

4.3.1 Pair-creation probabilities

Figure 7 represents the pair-creation probability as a function of $\eta = E/E_0$ and $Z = Z_{\rm A} = Z_{\rm B}$ for symmetric collisions with the distance of the closest approach $R_{\rm min} = 17.5$, 25, 35, 50 fm. For the largest charge number considered in Fig. 7, i.e., $Z = 96$, the critical value of the internuclear distance is approximately equal to 48 fm. This means that the pair-creation in collisions with $R_{\rm min} = 50$ fm is of pure dynamical origin. The top left pane of Fig. 7 shows that in this case the pair-creation probability monotonically decreases as $\eta \to 1$ for each Z. As the distance of the

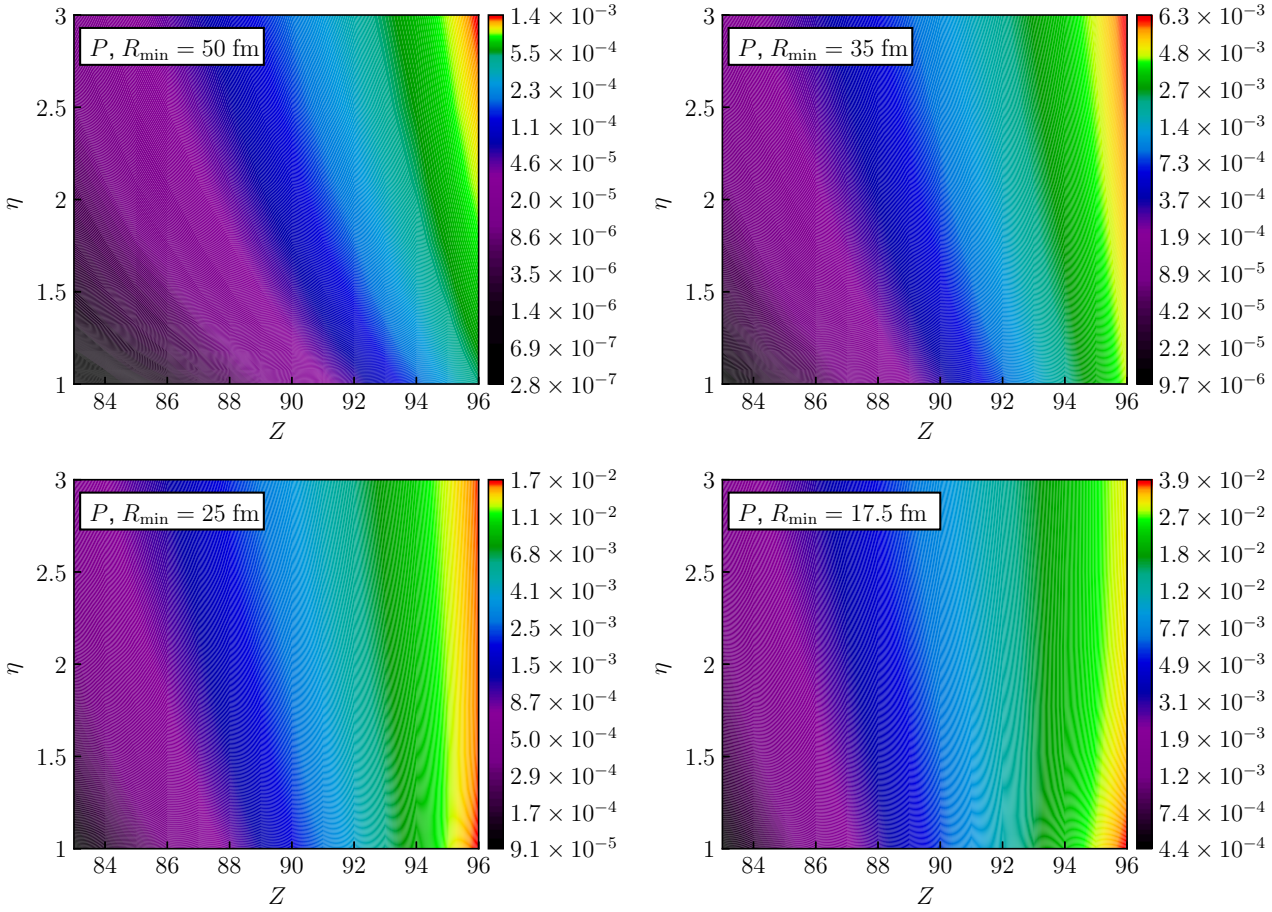

Figure 7: Probability of e^-e^+ pair creation in symmetric collisions as a function of the nuclear charge Z and the parameter $\eta = E/E_0$, obtained for various distances of the closest approach $R_{\rm min}$.

closest approach gets smaller, the systems of colliding nuclei with large enough Z begin to spend some time in the supercritical regime, i.e., with the resonance in the negative-energy continuum. This entails a significant change in the behavior of the pair-creation probability as a function of η. The change is most pronounced for the smallest regarded $R_{\rm min} = 17.5$ fm with the critical charge $Z_{\rm cr} \approx 87.5$. As it is illustrated on the bottom right pane of Fig. 7, the monotonous decrease of the pair-creation probability as $\eta \to 1$, taking place for $Z < Z_{\rm cr}$, gradually transforms to the increase for sufficiently large charge numbers.

This transition from decrease to increase can be traced in more detail in Fig. 8, which depicts the contribution of the s ($\kappa = -1$) and $p_{1/2}$ ($\kappa = 1$) states to the pair-creation probability as functions of η for a number of charge numbers and $R_{\rm min} = 17.5$ fm. Figure 8 reveals that already for $Z = 92$ the contribution of s states exhibits an increase as $\eta \to 1$, which gets compensated in the total probability by the decrease of the $p_{1/2}$ contribution. The difference in η-dependence of the contributions

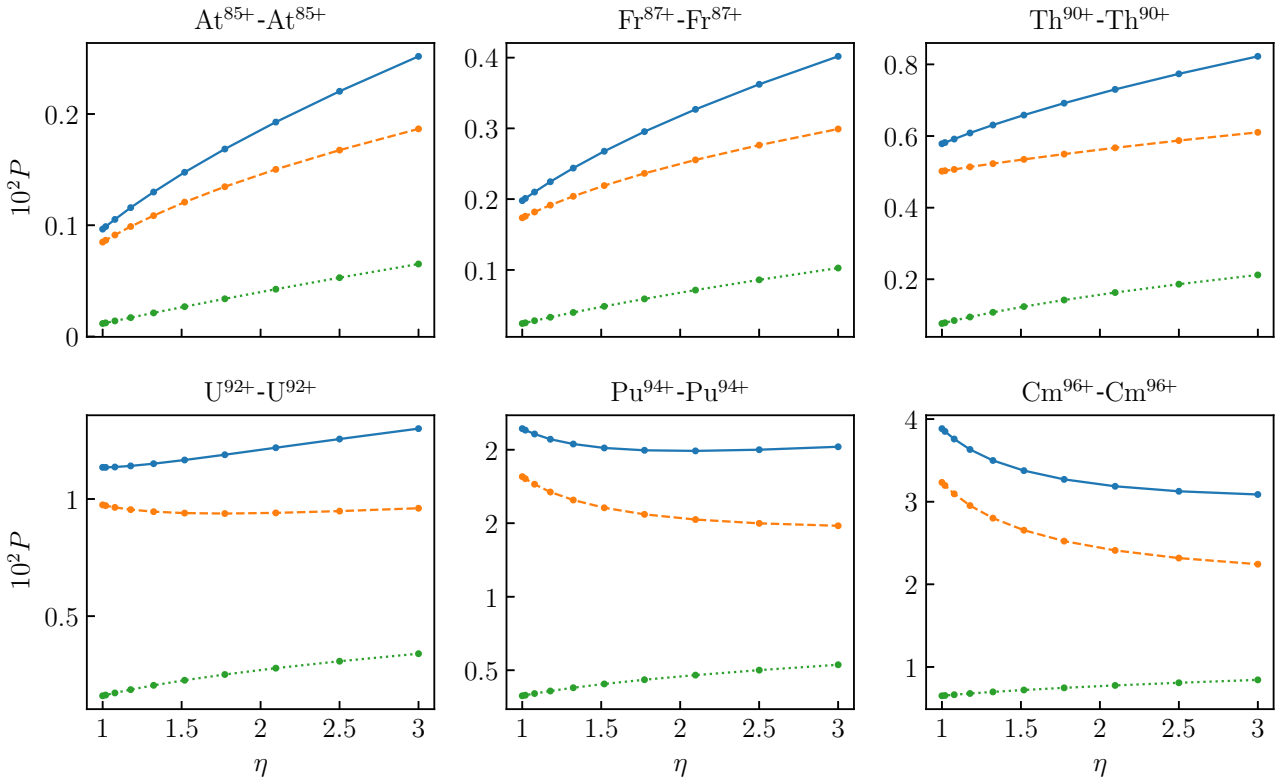

Figure 8: Probability of e^-e^+ pair creation in symmetric collisions as a function of $\eta = E/E_0$ obtained for $R_{\min} = 17.5$ fm. The green dotted line represents the contribution of $p_{1/2}$ states, the orange dashed line corresponds to s states, and the solid blue line is the sum of s and $p_{1/2}$ contributions.

of s and $p_{1/2}$ channels is due to different values of the critical charge at which $1s$ and $2p_{1/2}$ states reach the border of the negative-energy continuum. For instance, for $R_{\min} = 17.5$ fm, it happens at $Z_{\rm cr}^{1s}/2 \approx 87.5$ for $1s$ state and at $Z_{\rm cr}^{2p_{1/2}}/2 \approx 95$ for $2p_{1/2}$ state.

Figure 9 displays the dependence of the pair-creation probability on $R_{\min}$ and η for symmetric collisions with $Z_{\rm A} = Z_{\rm B} = 96$. As in Fig. 7, where the distance of the closest approach was fixed, here we see that the decrease of the probability as $\eta \to 1$, typical for the dynamic mechanism, gives place to the increase when $R_{\min}$ gets sufficiently smaller than the critical distance $R_{\rm cr} \approx 48$ fm.

An important characteristic, which makes the tendency of the pair-creation probability to change its behavior in the supercritical region more lucid is the derivative $dP/d\eta$ of the probability with respect to the parameter η. Figure 10 represents the derivative $dP/d\eta$ as a function of the nuclear charge $Z = Z_{\rm A} = Z_{\rm B}$ and the distance of the closest approach $R_{\min}$. There is an unambiguous correspondence between the parameter η and the scattering angle θ expressed in Eqs. (3.4) and (3.7).

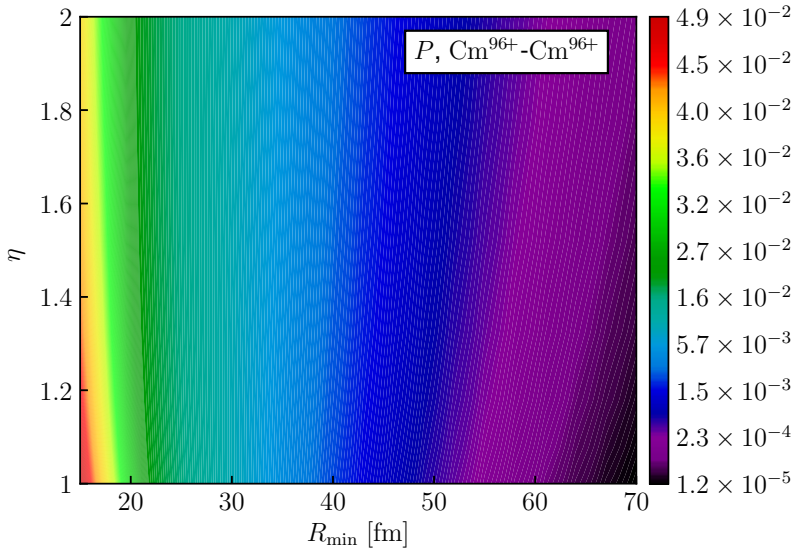

Figure 9: Probability of e^-e^+ pair creation in symmetric collisions with $Z_A = Z_B = 96$ as a function of R_{min} and $\eta = E/E_0$.

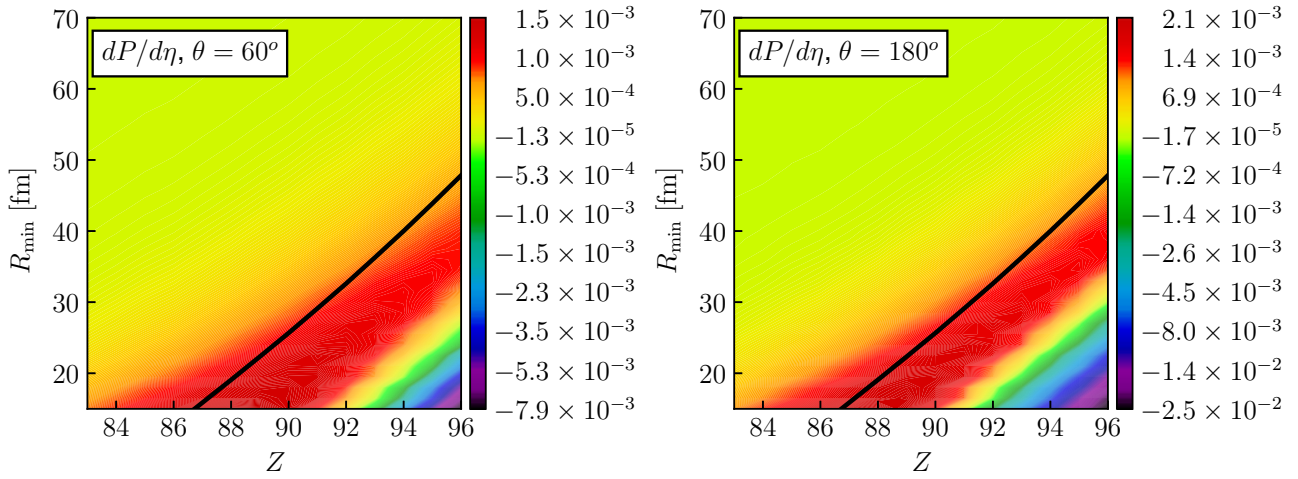

Figure 10: Derivative of the e^-e^+ pair-creation probability $dP/d\eta$ as a function of $Z = Z_A = Z_B$ and R_{min}. Black solid curve outlines the border of the supercritical domain of collision parameters.

The data plotted in Fig. 10 corresponds to the scattering angles $\theta = 60^\circ, 180^\circ$. The black solid line delineates the border of the supercritical domain of collision parameters located in the bottom right corner. In accordance with the above said, in the subcritical domain the derivative $dP/d\eta$ is positive and furthermore increases when moving in the direction of larger Z and smaller R_{min}. However, after crossing the border of the supercritical region, the increase of $dP/d\eta$ gives way to the decrease and when the point (Z, R_{min}) is deep enough in this region the derivative becomes negative.

Individual contributions of s ($\kappa = -1$) and $p_{1/2}$ ($\kappa = 1$) states to $dP/d\eta$ are

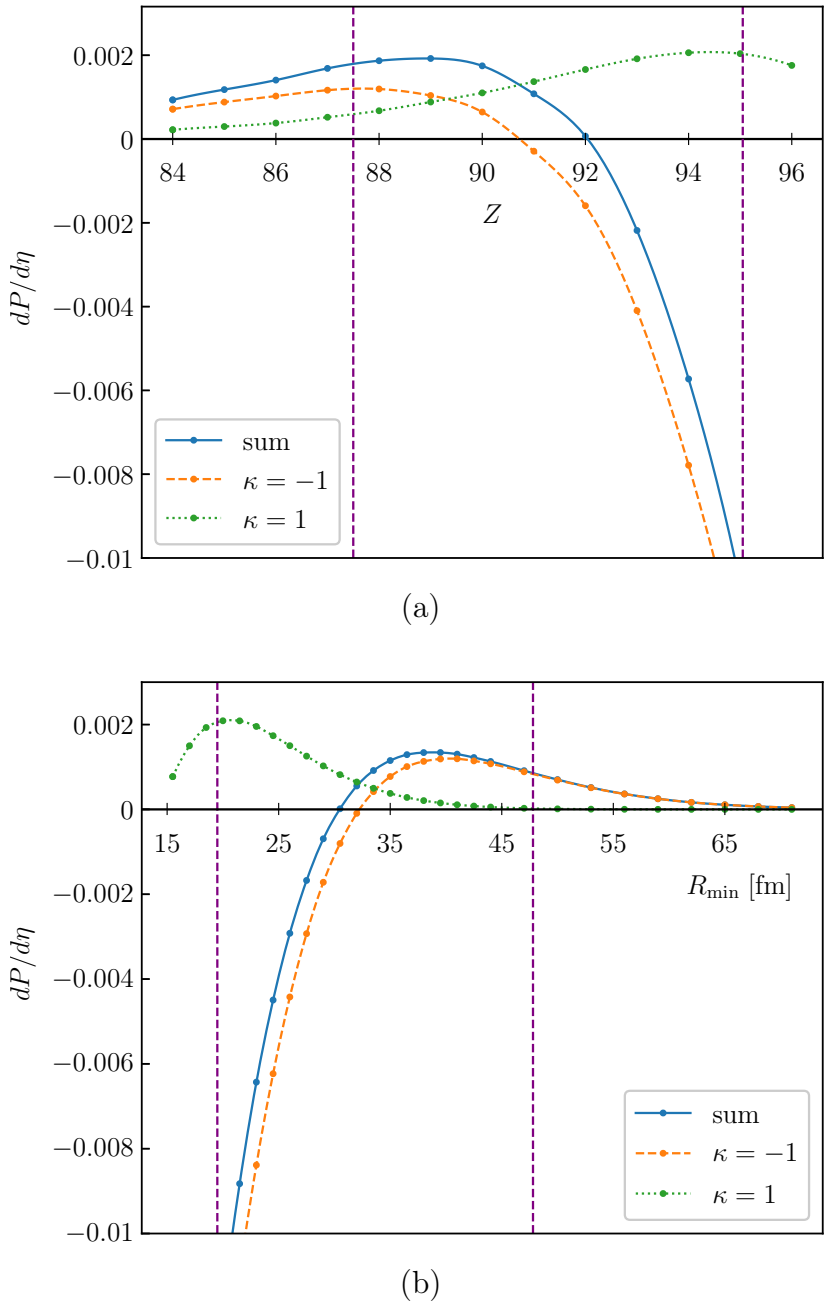

Figure 11: Derivative of the e^-e^+ pair-creation probability $dP/d\eta$ at $\eta = 1$ ($\theta = 180^\circ$) as a function of: a) Z with $R_{\rm min} = 17.5$ fm, b) $R_{\rm min}$ for $Z = 96$. Vertical lines mark the values of the abscissa at which the energies of $1s$ and $2p_{1/2}$ states are equal to $-mc^2$. On the upper pane the left line corresponds to $1s$ state, right — to $2p_{1/2}$. On the lower pane the left line corresponds to $2p_{1/2}$ state, right — to $1s$.

depicted in Fig. 11. Figure 11a represents these contributions as functions of the charge number $Z = Z_{\rm A} = Z_{\rm B}$ with $R_{\rm min} = 17.5$ fm, and Fig. 11b depicts them as functions of the distance of the closest approach $R_{\rm min}$ for $Z_{\rm A} = Z_{\rm B} = 96$. Both plots clearly show that the behavior of a contribution undergoes a substantial change once the corresponding lowest-energy bound state reaches the border of the negative energy continuum.

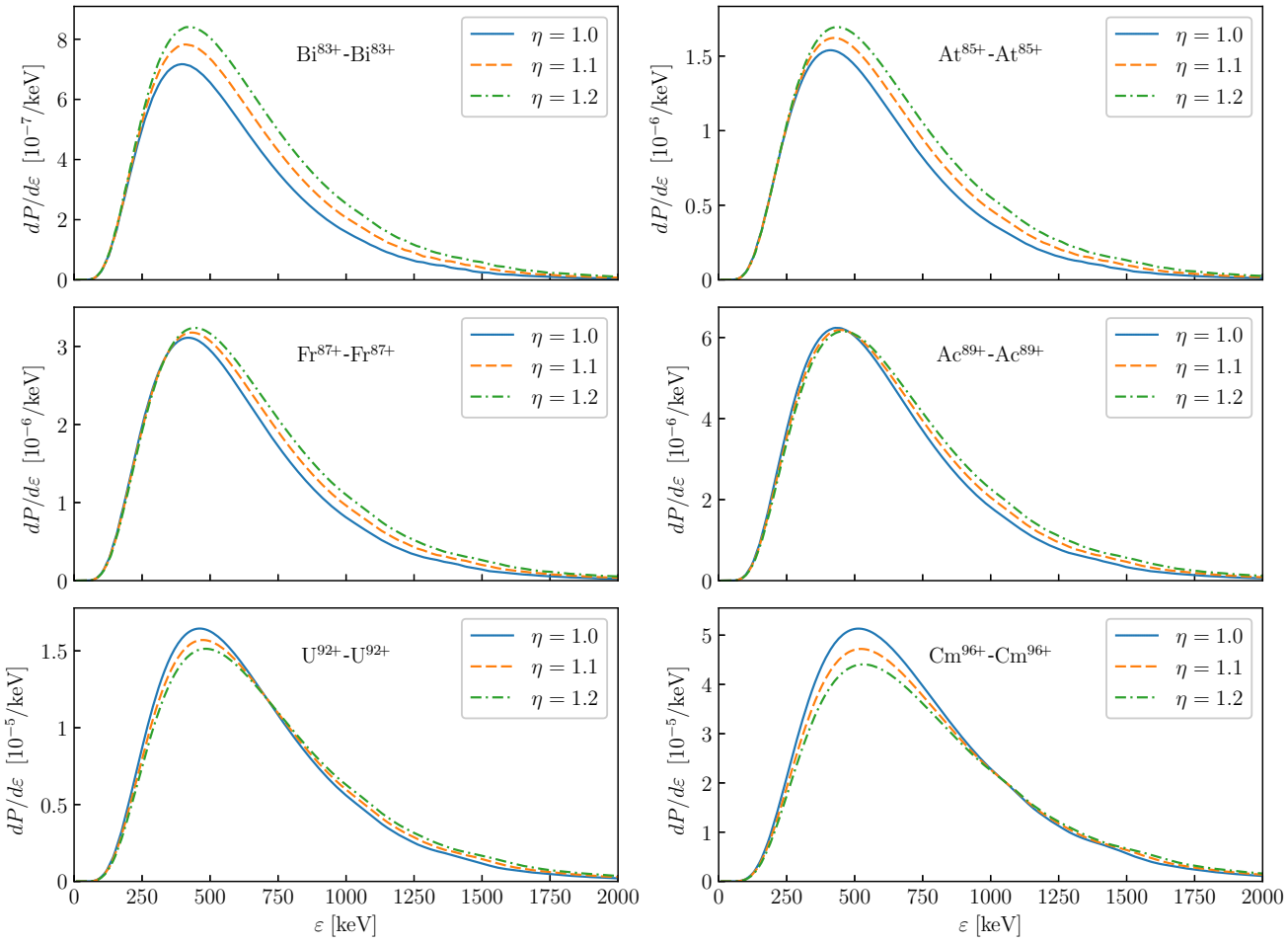

Figure 12: Energy-spectra of the positrons produced in symmetric collisions with $R_{\min} = 17.5$ fm. Here $\eta = E/E_0$ is the ratio of the collision energy E to the energy of the head-on collision with the same $R_{\min}$.

4.3.2 Positrons energy spectra

Having studied the dependence of the pair-creation probability on the parameter $\eta = E/E_0$, which demonstrated a significant change in the supercritical region of collision parameters, we investigated η-dependence of energy spectra of the positrons produced in low-energy collisions of heavy nuclei. Figure 12 represents the positron energy spectra obtained for symmetric collisions with $Z = Z_A = Z_B = 83 - 96$, $R_{\min} = 17.5$ fm and $\eta = 1, 1.1, 1.2$. Individual contributions of s ($\kappa = -1$) and $p_{1/2}$ ($\kappa = 1$) states to the positron spectra are given in Figs. 13 and 14, correspondingly. As it was already stated above, these channels almost completely determine the total pair-creation probability. In the case of $R_{\min} = 17.5$ fm, the supercritical regime starts at $Z \approx 87.5$ for the $1s$ state and at $Z \approx 95$ for the $2p_{1/2}$ state. Figures 13 and 14 display a substantial transformation of η-dependence of the positron spectra, once the respective channel becomes supercritical. Namely, for subcritical charge

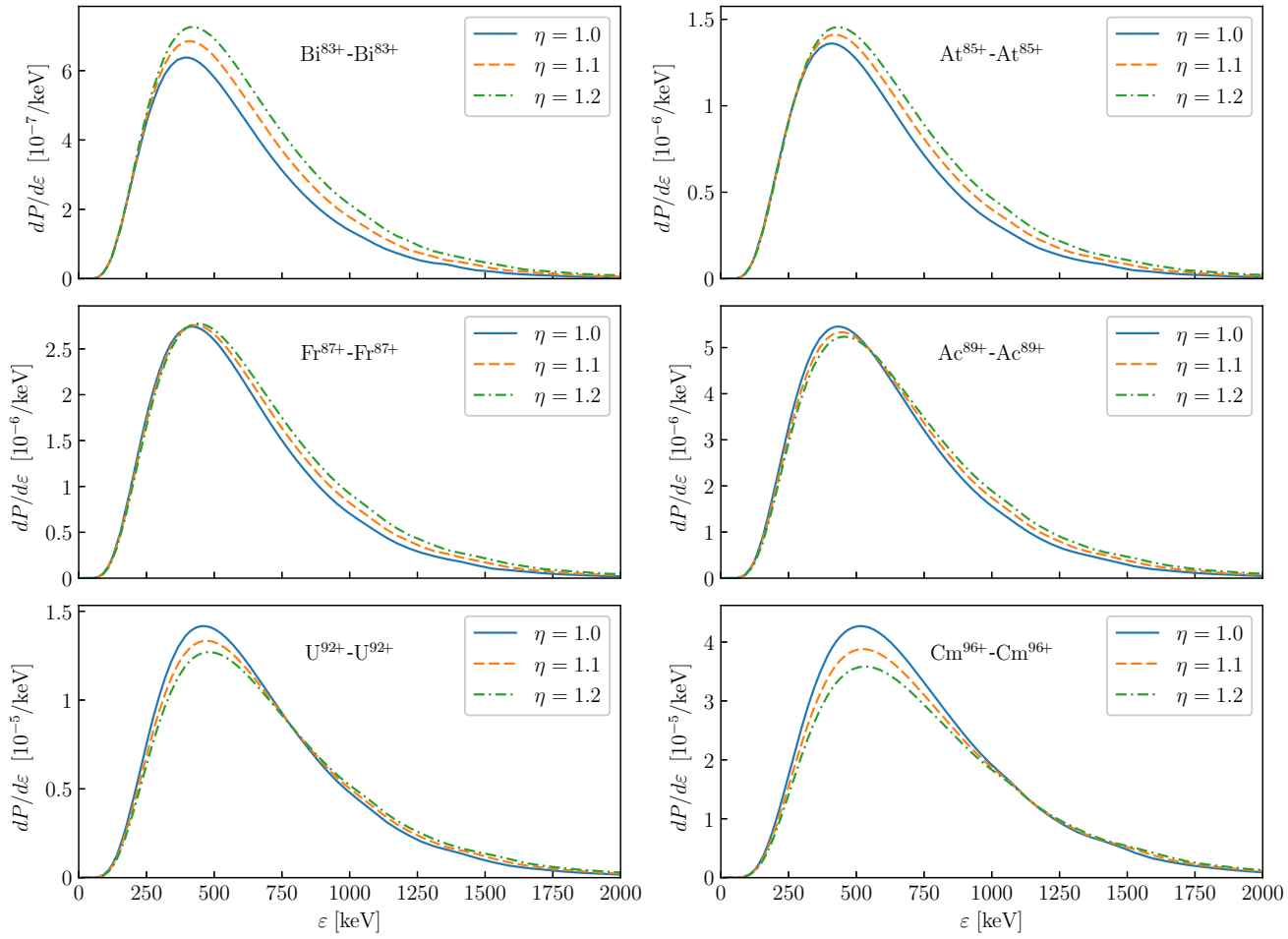

Figure 13: Contribution of s ($\kappa = -1$) states to the positron spectra for symmetric collisions with $R_{\min} = 17.5$ fm. Here $\eta = E/E_0$ is the ratio of the collision energy E to the energy of the head-on collision with the same $R_{\min}$.

numbers, the curves obtained for larger values of η are located above the ones corresponding to smaller η. However, once the charge number passes the critical value, the relative position of the curves near the peak gets inverted and the spectra calculated for larger η lie under the ones for smaller η. Though, the positioning of the tails remains unchanged. The total spectra depicted in Fig. 12, with the main contribution provided by s states, rather closely follow the behavior illustrated in Fig. 13. A possible explanation of this change might be the following. The spontaneous pair creation, active in the supercritical regime, monotonously depends on the time $\tau_{\rm cr}$ the bound state spends in the negative-energy continuum as a resonance. Therefore it is more pronounced for smaller η (see Fig. 5). Besides, the energies of the positrons originating from the supercritical resonance decay are confined within a certain region. For instance, in the case of U^{92+}-U^{92+} collisions, the energy of the spontaneous positrons should mostly be below the bound of 600 keV. Indeed, let us first consider a hypothetical adiabatically slow collision, when transitions in-

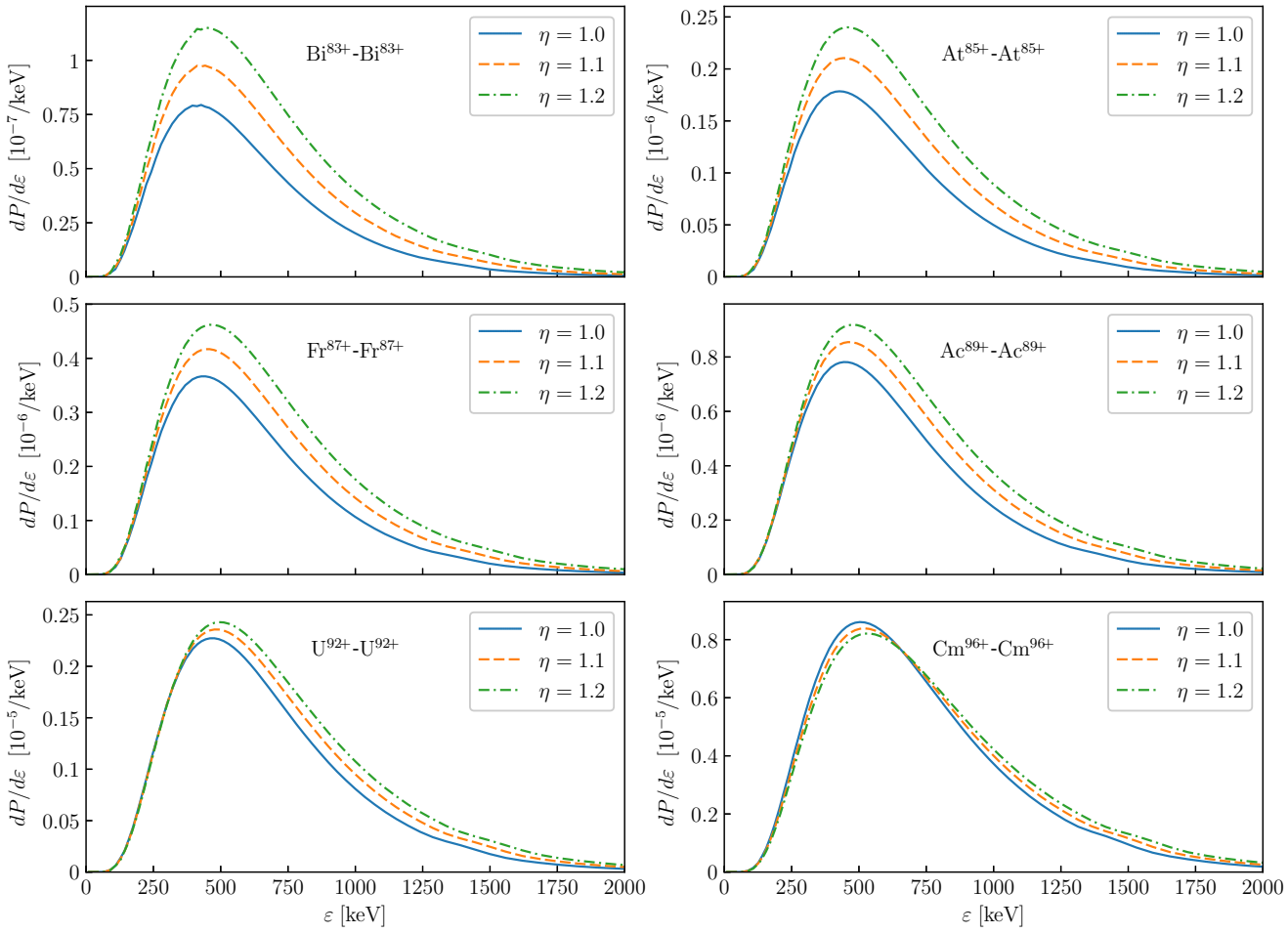

Figure 14: Contribution of $p_{1/2}$ ($\kappa = 1$) states to the positron spectra for symmetric collisions with $R_{\min} = 17.5$ fm. Here $\eta = E/E_0$ is the ratio of the collision energy E to the energy of the head-on collision with the same $R_{\min}$.

duced by the time-dependence of the total nuclear potential can be neglected. In this scenario, positrons are created exclusively due to the spontaneous mechanism and their energy distribution is determined by the position $\varepsilon^{\rm res}\left(R(t)\right)$ and width $\Gamma^{\rm res}\left(R(t)\right)$ of the supercritical resonance as composite functions of time, $R(t)$ is the internuclear distance. A qualitative behavior of the positron spectrum for this case is depicted, for example, in Fig. (4) of Ref. [15]. Both the energy and the width of a supercritical resonance monotonously increase with decreasing R. According to Refs. [46, 47], the position of the resonance for two uranium nuclei with $R = 16$ fm corresponds to the peak energy of the emitted positrons of about 300 keV with the natural width of less than 2 keV. In real collisions, finite duration of the supercritical regime, $\tau_{\rm cr}$, leads to appearance of an additional width, which greatly exceeds the value of the natural one. This additional width can be roughly estimated by the uncertainty principle $\Gamma_{\rm dyn} \sim \hbar/\tau_{\rm cr}$ and with $\tau_{\rm cr} \sim 2\times10^{-21}$ s (see Fig. 5) one obtains $\Gamma_{\rm dyn} \sim 300$ keV. Thus, the energy of spontaneous positrons gets distributed over

the interval from 0 to 600 keV. A major consequence of such a large value of the dynamical width is that it prevents the emergence of sharp resonance structures in the spectra. Together with the interference between the spontaneous and dynamic mechanisms, this make the transition to the supercritical regime smooth. Despite this fact, the qualitative changes in the positron spectra, especially when comparing the subcritical Bi^{83+}-Bi^{83+} and supercritical Cm^{96+}-Cm^{96+} collisions, should be regarded as an unambiguous proof of the access to the supercritical regime. This claim is also corroborated by the positron spectra obtained for head-on U^{92+}-U^{92+} collisions with various $R_{\min}$ demonstrated in Fig. 15. As in the case of fixed $R_{\min}$ and varying Z, the same change of the positron spectra layout takes place when $R_{\min}$ drops past the critical value $R_{\mathrm{cr}} = 32.7$ fm.

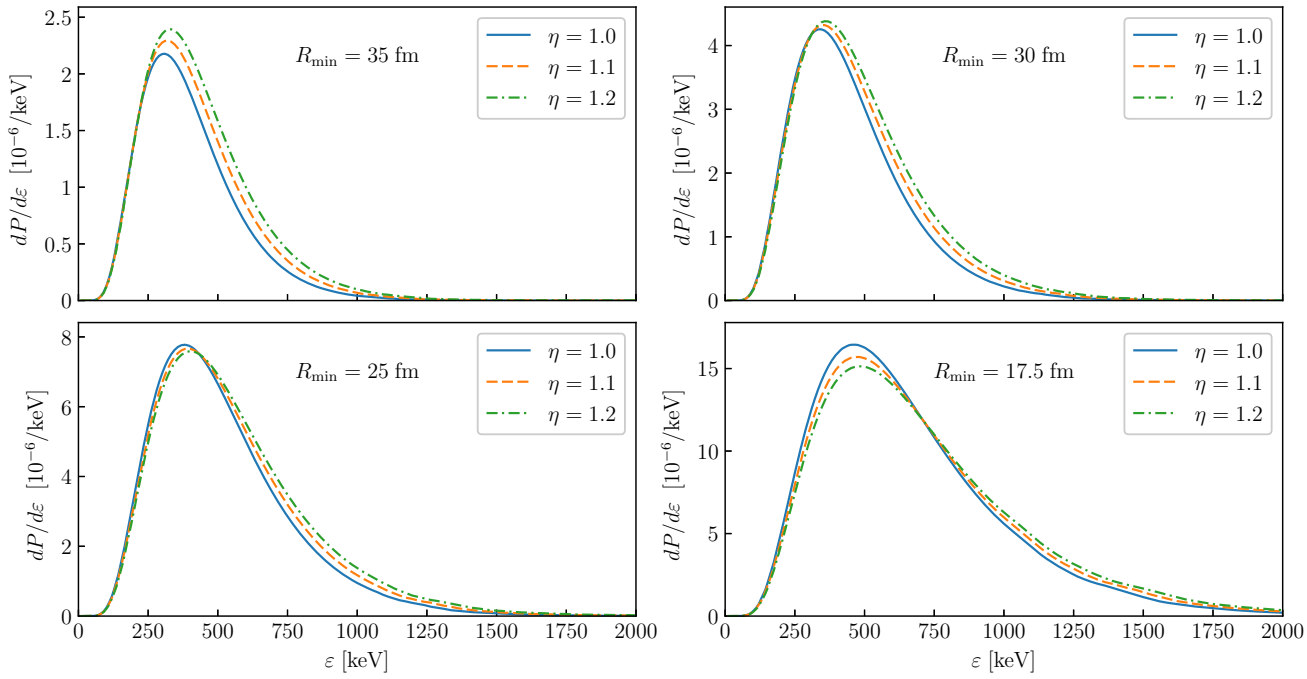

Figure 15: Energy spectra of the positron created in symmetric collisions with $Z = Z_{\mathrm{A}} = Z_{\mathrm{B}} = 92$. Here $\eta = E/E_0$ is the ratio of the collision energy E to the energy of the head-on collision with the same $R_{\min}$.

Looking closely at Figs. 12–15, one can notice that the changes in the positron spectra associated with the transition to the supercritical regime are mostly concentrated at the area near the maximum and on the left from it. This area matches the energy region where the spontaneous pair-creation takes place. This circumstance can be taken advantage of to improve the quantitative characteristic of the transition to the supercritical regime. The probability P in $dP/d\eta$ represents the integral

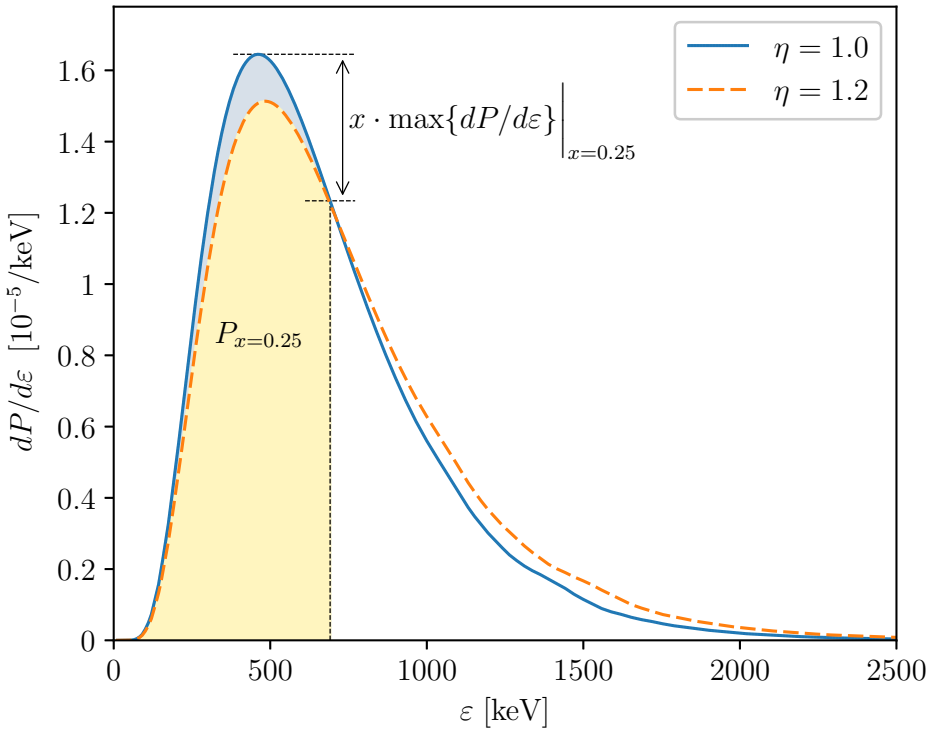

Figure 16: Definition of the partial pair-creation probability P_x.

of the differential probability $dP/d\varepsilon$ over the whole range of the positron energies

$$P = \int_0^\infty \frac{dP}{d\varepsilon} d\varepsilon. \tag{4.38}$$

By focusing only on the energy interval where the spontaneous mechanism can contribute, it is possible to construct a characteristic, which is more sensitive to the supercritical transition compared to $dP/d\eta$. To this end, we introduce a partial probability P_x defined as the probability of creating an electron-positron pair with the positron energy in the interval $0 \leq \varepsilon \leq \varepsilon(x)$,

$$P_x = \int_0^{\varepsilon(x)} \frac{dP}{d\varepsilon} d\varepsilon, \quad x \in [0, 1]. \tag{4.39}$$

Here $\varepsilon(x)$ is the bigger one of the two positron energies for which the differential probability calculated for head-on collision ($\eta = 1$) amounts to $(1 - x)$ part of its peak value, i.e. $dP/d\varepsilon\big|_{\varepsilon=\varepsilon(x)} = (1 - x) \max\{dP/d\varepsilon\}$. The visualisation of this definition of P_x can be found in Fig. 16. According to the definition, when $x = 0$ the cutoff energy $\varepsilon(x)$ coincides with the position of the peak in the spectra for the head-on collisions. The case $x = 1$ corresponds to the energy $\varepsilon(x)$ for which the differential probability is equal to zero. This happens at infinity, which means that

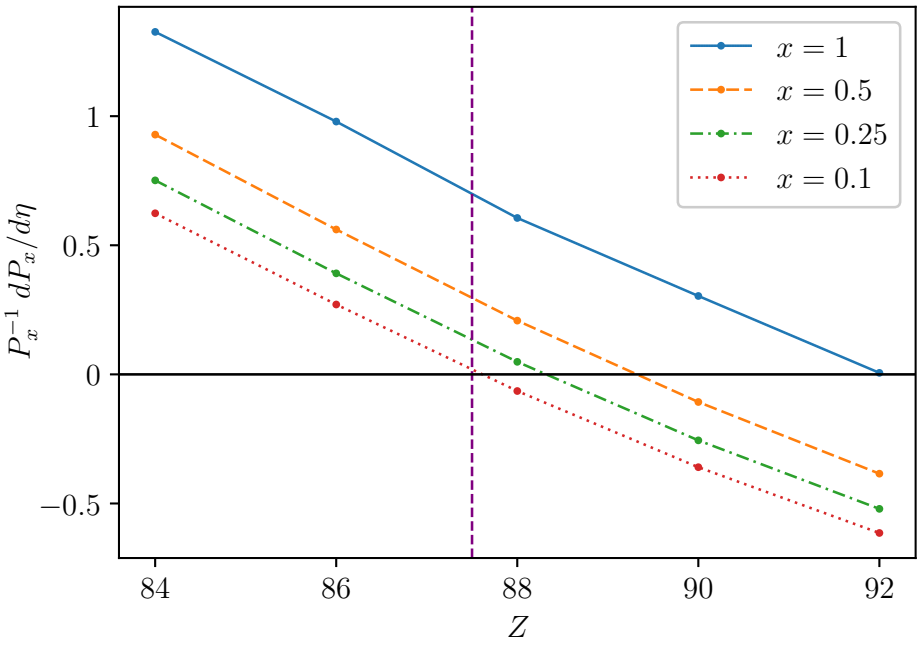

Figure 17: Derivative $d \ln P_x/d\eta$ at $\eta = 1$, obtained for various x in symmetric collisions with $R_{\min} = 17.5$ fm. The vertical line at $Z \approx 87.5$ marks the border of the supercritical region.

with $x = 1$ we return to the total probability, i.e. $P_1 = P$. The parameter x should be chosen in such a way as to cover the area of width $\Gamma_{\rm dyn}$ around the position of the supercritical resonance. As it was discussed above, for U^{92+}-U^{92+} collisions this area spans from 0 to 600 keV. Therefore, it is reasonable to consider $x \gtrsim 0.1$, taking into account at least around 50% of the total pair-creation probability.

In Fig. 17 we present the derivative $d \ln P_x/d\eta$ with $x = 0.1$, 0.25, 0.5, 1.0 calculated for symmetric head-on collisions ($\eta = 1$). The figure demonstrates that the use of P_x noticeably enhances the signature of the transition to the supercritical regime, namely the sign change of the derivative $dP_x/d\eta$ (and hence $d \ln P_x/d\eta$) from positive to negative. For example, in the case of U^{92+}-U^{92+} collisions $d \ln P_x/d\eta\big|_{\eta=1}$ is approximately equal to -0.6 at $x = 0.1$, -0.5 at $x = 0.25$, and -0.4 at $x = 0.5$, whereas the derivative of the total probability ($x = 1$) is almost zero. The enhancement is also visible in Fig. 18, where the ratio $P_x(\eta)/P_x(1)$ is depicted as a function of the charge number Z for fixed $R_{\min}$ (Fig. 18a) and the distance of the closest approach $R_{\min}$ for U^{92+}-U^{92+} (Fig. 18b). Here, the transition to the supercritical mode is manifested in the passing through the unity of the ratio $P_x(\eta)/P_x(1)$ towards smaller values. As it can be seen in the figure, for $x = 0.5$, 0.25, and 0.1, this transition takes place at successively smaller values of the charge number Z, when $R_{\min}$ is fixed, and larger $R_{\min}$, when Z is fixed.

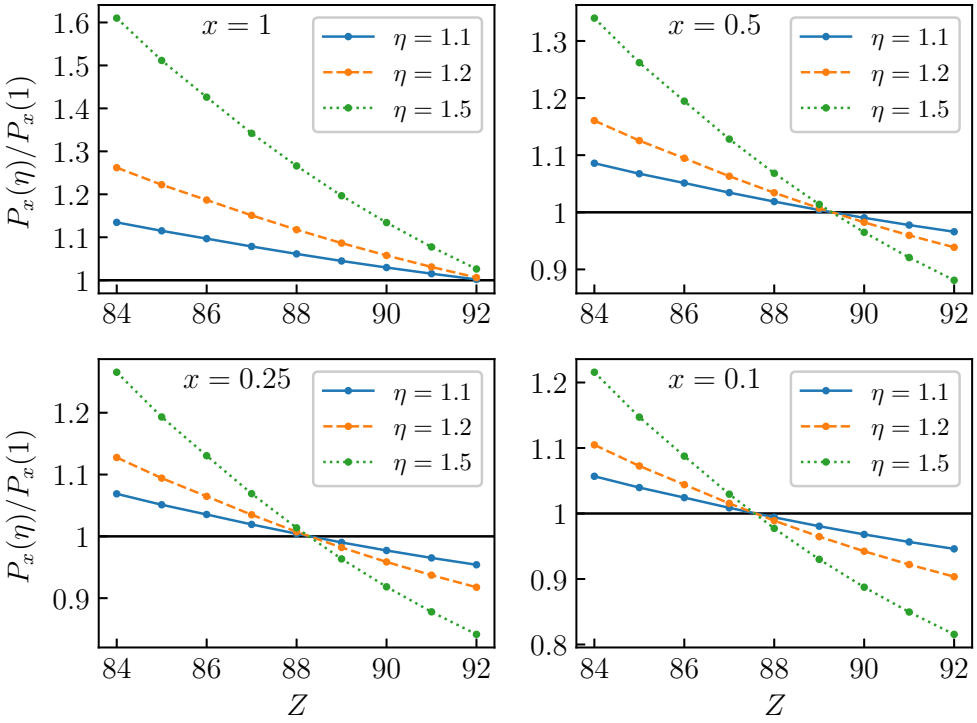

(a)

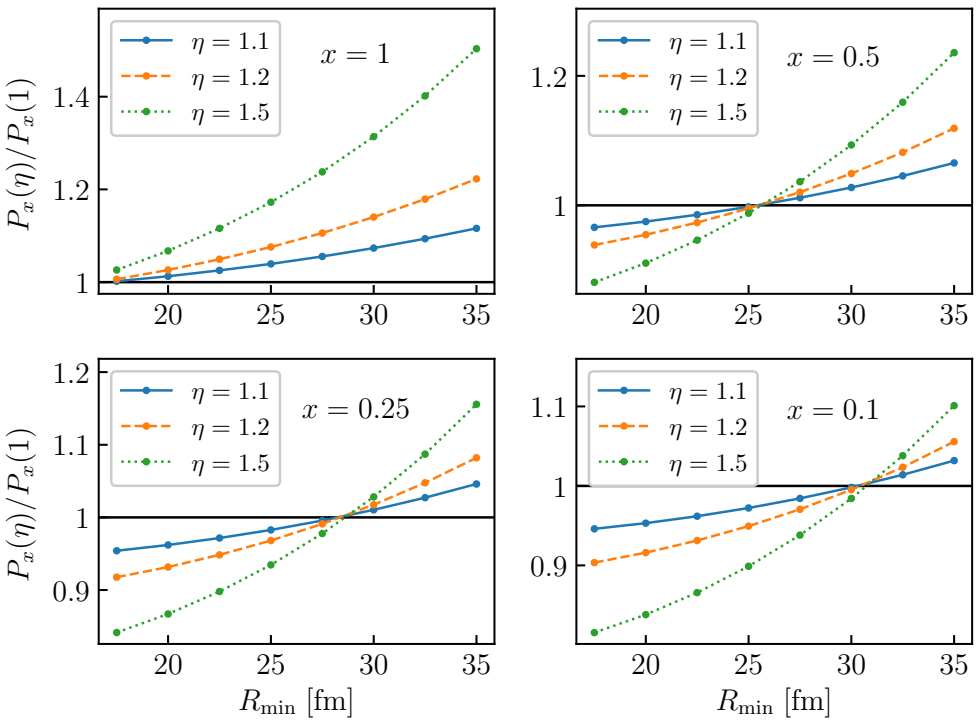

(b)

Figure 18: Ratio $P_x(\eta)/P_x(1)$ for $\eta = 1.1$, 1.2 and 1.5 as a function of: a) Z with $R_{\mathrm{min}} = 17.5$ fm, b) R_{min} for $Z = 92$.

Chapter 5. Calculations beyond the monopole approximation

In this section we will consider the process of electron-positron creation in low-energy collisions of heavy nuclei beyond the scope of the monopole approximation. To this end, we employ the multipole expansion of the two-center potential over the spherical harmonics in the center-of-mass reference frame. We begin with description of the procedure used to solve the stationary Dirac equation for axially symmetric potentials. This procedure is necessary for specifying the initial/final conditions for the time-dependent problem. After that we turn to outlining the algorithm of solving the time-dependent Dirac equation. Finally, we present the results of calculations of the pair-creation probabilities and the positron energy spectra. We study their convergence with respect to the number of terms in the multipole expansion of the two-center potential and examine the influence of the $L > 0$ terms on the signatures of the transition to the supercritical regime found in the monopole approximation. The results of the research described in this chapter have been published in the papers [56, 62].

5.1 Stationary Dirac equation

Going beyond the monopole approximation means the loss of the spherical symmetry, which substantially simplified the calculations described in the previous chapter. Now, if one is to proceed the calculation working with a single-center basis, the latter has to contain functions that transforms differently under three-dimensional rotations. This entails a drastic augmentation of the basis set, which can make the computations resource-heavy and substantially time-consuming. Especially, it affects the time evolution procedure, where a system of linear equations is to be solved at every time step, of which there may be dozens of thousands. Fortunately, the complexity of the problem can be reduces to a large extent by transitioning to a reference frame with z-axis directed along the internuclear line and rotating together with it. This transition does not in itself introduce any approximations but brings into the Hamiltonian a new coupling term referred to as the rotational coupling. However, if we disregard the rotational coupling, then we will gain the symmetry with respect to rotations around the z-axis. Thus, functions

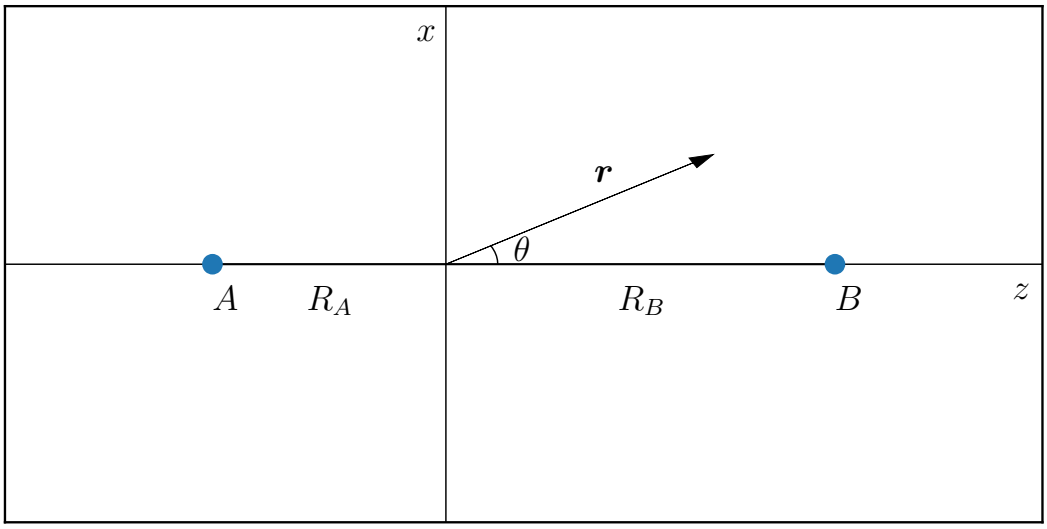

Figure 19: Quasimolecular reference frame for the general case of nuclei with different masses.

with different z-projections of the total angular momentum, denoted by the symbol μ, get decoupled and their contributions to the process under consideration can be computed independently. Restriction of the basis set to a single value of μ allows one to noticeably reduce its size and therefore significantly facilitate the computations.

The stationary Dirac equation written in the reference frame with z-axis directed along the internuclear line reads

$$H_0\varphi_i(\boldsymbol{r}) = \varepsilon_i\varphi_i(\boldsymbol{r}), \tag{5.1}$$

$$H_0 = \boldsymbol{\alpha}\cdot\boldsymbol{p} + m\beta + V(r,\theta). \tag{5.2}$$

Here $\boldsymbol{\alpha}$, β are the Dirac matrices, m is the electron mass, $V(r,\theta)$ is the potential function, $r = |\boldsymbol{r}|$, and θ is the polar angle, i.e. the angle between $\boldsymbol{r}$ and z-axis (see Fig. 19). In the monopole approximation the potential V possessed spherical symmetry and was a function of a single argument r (see Eq. (4.12)). Now the symmetry is reduced to cylindrical and the potential acquires an additional dependence on the polar angle θ. Using a complete set of orthogonal Legendre polynomials $\left\{P_L(x)\right\}_{L=0}^{\infty}$ the two-center nuclear potential can be expressed as an infinite sum

$$V(r,\theta) = \sum_{\alpha=A,B}\sum_{L=0}^{\infty} V_L^{\alpha}\left(r, R_\alpha(t_{\text{in}})\right)\sqrt{\frac{2L+1}{4\pi}}P_L(\cos\theta), \tag{5.3}$$

where

$$V_L^{\alpha}\left(r, R_{\alpha}(t)\right) = \int_0^{\pi} d\theta \ \sin\theta P_L(\cos\theta) V_{\alpha}\left(|\boldsymbol{r} - \boldsymbol{R}_{\alpha}(t)|\right). \tag{5.4}$$

For practical calculations it is convenient to rewrite (5.3) in terms of spherical harmonics $Y_{LM}(\hat{\boldsymbol{r}})$ ($\hat{\boldsymbol{r}} = \boldsymbol{r}/|\boldsymbol{r}|$):

$$V(r,\theta) = \sum_{L=0}^{\infty} V_L(r, t_{\rm in}) Y_{L0}(\hat{\boldsymbol{r}}), \tag{5.5}$$

$$V_L(r,t) = V_L^A\left(r, R_{\rm A}(t)\right) + V_L^B\left(r, R_{\rm B}(t)\right). \tag{5.6}$$

This expression can be readily derived from (5.3) by employing the following properties of the spherical functions (see, e.g., [71]):

$$\sum_{M=-L}^{L} Y_{LM}(\boldsymbol{n}_1) Y_{LM}^*(\boldsymbol{n}_2) = \frac{2L+1}{4\pi} P_L(\cos\theta_{12}), \tag{5.7}$$

$$Y_{LM}^*(\boldsymbol{n}) = \delta_{M0}\sqrt{\frac{2L+1}{4\pi}} \text{ for } \boldsymbol{n} \text{ parallel to } z\text{-axis}, \tag{5.8}$$

where θ_{12} is the angle between the vectors $\boldsymbol{n}_1$ and $\boldsymbol{n}_2$. In our case $\boldsymbol{n}_1 = \hat{\boldsymbol{r}}$, $\boldsymbol{n}_2 = \boldsymbol{e}_z$ is the unit vector along z-axis, and $\theta_{12} = \theta$.

As before, the wave function with a certain angular momentum projection μ is approximated as a finite sum

$$\varphi(\boldsymbol{r}) = \sum_{\kappa} \sum_{j=1}^{2n} c_j^{\kappa\mu} u_j^{\kappa\mu}(\boldsymbol{r}). \tag{5.9}$$

In contrast to the monopole expression (4.17) this sum is twofold, since κ is no longer a good quantum number. The basis functions $u_j^{\kappa\mu}(\boldsymbol{r})$ are bispinors with the radial part represented by B-splines in accordance with the dual kinetic balance (DKB) approach [76]. The angular part is described by spherical spinors. Each subset of $u_j^{\kappa\mu}$, pertaining to certain κ, is split into two parts. The first part with $1 \le j \le n$

is defined as

$$u_j^{\kappa\mu}(\boldsymbol{r}) = \frac{1}{r}\begin{pmatrix} B_j(r)\boldsymbol{\Omega}_{\kappa\mu}(\hat{\boldsymbol{r}}) \\ \frac{1}{2m}\left(\frac{d}{dr}+\frac{\kappa}{r}\right)B_j(r)\boldsymbol{\Omega}_{-\kappa\mu}(\hat{\boldsymbol{r}}) \end{pmatrix} \tag{5.10}$$

and the second one with $n < j \leq 2n$ reads

$$u_j^{\kappa\mu}(\boldsymbol{r}) = \frac{1}{r}\begin{pmatrix} \frac{1}{2m}\left(\frac{d}{dr}-\frac{\kappa}{r}\right)B_{j-n}(r)\boldsymbol{\Omega}_{\kappa\mu}(\hat{\boldsymbol{r}}) \\ B_{j-n}(r)\boldsymbol{\Omega}_{-\kappa\mu}(\hat{\boldsymbol{r}}) \end{pmatrix}. \tag{5.11}$$

Here $B_j(r)$ is the jth B-spline [75], $\boldsymbol{\Omega}_{\kappa\mu}(\hat{\boldsymbol{r}})$ is the spherical spinor [71]. This choice of basis functions is highly advantageous in the case of symmetric collisions, where the odd harmonics in the multipole expansion of the two-center potential (5.5) cancel out in the center-of-mass frame. Thus, the states with opposite spatial parity become decoupled, which reduces the size of matrices describing the discretized versions of the static and time-dependent Dirac equation (see below) by half, which significantly facilitates the computations.

Let us move from a multiindex $\kappa\mu j$ to a single index l by enumerating all the basis functions present in (5.9) from 1 to N. Then, substituting decomposition (5.9) into Eq. (5.1), multiplying by $u_l(\boldsymbol{r})$ from the left and performing spatial integration, one arrives at the following form of the discretized static Dirac equation

$$H\boldsymbol{c} = \varepsilon S\boldsymbol{c}, \tag{5.12}$$

where $H_{jk} = \langle u_j|H_0|u_k\rangle$, $S_{jk} = \langle u_j|u_k\rangle$ is the overlap matrix and $\boldsymbol{c} = \{c_1, \ldots, c_N\}$. Solving Eq. (5.12) yields a set of eigenvalues ε_i and eigenvectors $\boldsymbol{c}_i$ $(i = 1, \ldots, N)$ which represent a discretized version of the H_0 spectrum. When calculating the matrix H_{jk} it is convenient to split H_0 into two parts

$$H_0 = h^{\text{free}} + V, \tag{5.13}$$

where h^{free} is the Dirac Hamiltonian of a free electron

$$h^{\text{free}} = \boldsymbol{\alpha}\cdot\boldsymbol{p} + m\beta, \tag{5.14}$$

and V is the remaining two-center potential. The matrix elements of $h^{\rm free}$ are diagonal with respect to κ and have already been considered in the previous chapter (see, e.g., Eq. (4.16)). The matrix V_{jk} has a more complex structure. Its elements can be written as

$$V_{jk} = \sum_L g^{L0}(\kappa_j\mu, \kappa_k\mu) \int dr V_L(r, t_{\rm in}) \left[F_j(r)F_k(r) + G_j(r)G_k(r)\right], \tag{5.15}$$

where the functions $G_j(r)/F_j(r)$ are the upper/lower radial components of the basis functions $u_j(\boldsymbol{r})$ multiplied by r (see the definition in Eq. (4.13) and Eqs. (5.10)-(5.11)). The angular coefficients $g^{LM}(\kappa_j\mu_j, \kappa_k\mu_k)$ are defined as

$$\begin{aligned} g^{LM}(\kappa_j\mu_j, \kappa_k\mu_k) &= \int d\boldsymbol{n}\, \boldsymbol{\Omega}^\dagger_{\kappa_j,\mu_j}(\boldsymbol{n}) Y_{LM}(\boldsymbol{n}) \boldsymbol{\Omega}_{\kappa_k,\mu_k}(\boldsymbol{n}) \\ &= (-1)^{\frac{1}{2}+\mu_j} \sqrt{\frac{(2l_j+1)(2l_k+1)(2j_j+1)(2j_k+1)}{4\pi(2L+1)}} C^{L0}_{l_j0,l_k0} C^{LM}_{j_j\mu_j,j_k-\mu_k} \begin{Bmatrix} j_j & l_j & \frac{1}{2} \\ l_k & j_k & L \end{Bmatrix}. \end{aligned} \tag{5.16}$$

Here $C^{LM}_{j_1\mu_1,j_2\mu_2}$ are the Clebsch–Gordan coefficients and the quantum numbers l and j are related to κ via expression

$$l = \left|\kappa + \frac{1}{2}\right| - \frac{1}{2}, \tag{5.17}$$

$$j = |\kappa| - \frac{1}{2}. \tag{5.18}$$

Employing the relation

$$C^{L0}_{l_10,l_20} \begin{Bmatrix} j_1 & l_1 & \frac{1}{2} \\ l_2 & j_2 & L \end{Bmatrix} = \begin{cases} \frac{1}{\sqrt{(2l_1+1)(2l_2+1)}} C^{L0}_{j_1-\frac{1}{2},j_2\frac{1}{2}}, & \text{if } l_1+l_2+L \text{ is even}, \\ 0, & \text{otherwise}, \end{cases} \tag{5.19}$$

the expression (5.16) can be simplified and written as

$$g^{LM}(\kappa_j\mu_j, \kappa_k\mu_k) = (-1)^{\frac{1}{2}+\mu_j} \sqrt{\frac{(2j_j+1)(2j_k+1)}{4\pi(2L+1)}} C^{L0}_{j_j-\frac{1}{2},j_k\frac{1}{2}} C^{LM}_{j_j\mu_j,j_k-\mu_k}. \tag{5.20}$$

Due to the properties of the Clebsch-Gordan coefficients, $g^{LM}(\kappa_1\mu_1, \kappa_2\mu_2)$ have

nonzero values only for $L = |j_1 - j_2|,\ |j_1 - j_2| + 1,\ \ldots,\ j_1 + j_2$ with even $l_1 + l_2 + L$ and $M = \mu_1 - \mu_2$. Therefore, for any given pair of the basis functions $u_j(\boldsymbol{r})$ and $u_k(\boldsymbol{r})$ the sum over L in Eq. (5.15) will have a finite number of terms.

5.2 Time-dependent Dirac equation

The time-dependent wave function is represented by a sum similar to one displayed in Eq. (5.9) but with the coefficients depending on time

$$\varphi(\boldsymbol{r}, t) = \sum_{i=1}^{N} a_i(t) u_i(\boldsymbol{r}). \tag{5.21}$$

When using a static basis set comprised of non-orthogonal functions the time-dependent Dirac equation subject to certain initial conditions

$$\begin{cases} i\partial_t \varphi_i(\boldsymbol{r}, t) = H(t)\varphi_i(\boldsymbol{r}, t), \\ \varphi_i(\boldsymbol{r}, t_{\text{in}}) = \phi_i(\boldsymbol{r}), \end{cases} \tag{5.22}$$

is transformed into the following system of ordinary differential equations

$$\begin{cases} iS\dfrac{\partial \boldsymbol{a}_i(t)}{\partial t} = H(t)\boldsymbol{a}_i(t), \\ \boldsymbol{a}_i(t_{\text{in}}) = \boldsymbol{c}_i. \end{cases} \tag{5.23}$$

Here $\boldsymbol{a}_i = \{a_{1i}, \ldots, a_{Ni}\}$ denotes the array of expansion coefficients, $\boldsymbol{c}_i$ is the ith solution of the system (5.12) corresponding to the energy ε_i, $H_{jk}(t) = \langle u_j | H(t) | u_k \rangle$ is the Hamiltonian matrix, and $S_{jk} = \langle u_j | u_k \rangle$ is the overlap matrix. To solve this system we again turn to the Crank-Nicolson scheme [77]. This time, because of the non-orthogonality of the basis functions, the overlap matrix S makes appearance in the relation between the expansion coefficients $\boldsymbol{a}_i(t)$ at the neighboring time steps (cf. Eq. (4.36))

$$\left[S + \frac{i\Delta t}{2} H(t + \Delta t/2)\right] \boldsymbol{a}_i(t + \Delta t) = \left[S - \frac{i\Delta t}{2} H(t + \Delta t/2)\right] \boldsymbol{a}_i(t). \tag{5.24}$$

After the array of the expansion coefficients, corresponding to the wave func-

tion at the time $t_{\rm out}$, is found, the transition amplitudes $G(^{\zeta}|_{\xi})$ are evaluated as

$$G(^{\zeta}|_{\xi})_{ji} = \langle \phi_j | \varphi_i(t_{\rm out}) \rangle = \boldsymbol{c}_j^{\dagger} S \boldsymbol{a}_i(t_{\rm out}). \tag{5.25}$$

Here ζ and ξ correspond to the energy signs of the jth out-state and ith in-state. Finally, the mean number of electrons and positrons created from the vacuum in a certain state are evaluated according to Eqs. (2.45) and (2.46).

5.2.1 Approximation neglecting the internuclear axis rotation

In the monopole approximation we utilized the spherical symmetry of the problem which allowed us to greatly simplify the numerical calculations. It was achieved due to the fact that the time-dependent potential in that case coupled only basis functions with identical relativistic angular quantum numbers κ and angular momentum projections μ. This allowed us to perform calculations for any permitted combination of κ and μ separately with relatively small-sized matrices in the discretized version of the time-dependent Dirac equation (see Eq. (4.32)). When going beyond the monopole approximation in the time-dependent problem, we lose any symmetry, except for the case of the head-on collision. In collisions of this sort the inertial frame of reference can be chosen in such a way, that its z-axis is directed along the internuclear line. By doing so, we obtain axial symmetry and become able to deal with basis functions corresponding to different values of μ separately. The calculations for such collisions are considerably more complicated, compared to the monopole approximation. At the same time, they are substantially less time consuming than in the general case when functions with different μ get coupled. For collisions with non-zero impact parameters the axial symmetry can be regained if we move to the rotating reference frame with z-axis directed along the internuclear line. But for this we need to neglect the additional terms appearing in the Hamiltonian due to the transition to this noninertial reference frame [63, 64]. The exact Hamiltonian in this reference frame can be written with a good accuracy as

$$H(t) = h^{\rm free} + V(\boldsymbol{r}, t) - \hat{\boldsymbol{J}} \cdot \boldsymbol{\omega}. \tag{5.26}$$

Here $h^{\rm free}$ is the free-electron Hamiltonian defined in Eq. (5.14), $V(\boldsymbol{r}, t)$ is the time-dependent potential of the moving nuclei, $\hat{\boldsymbol{J}}$ is the operator of the total angular momentum of the electron, and $\boldsymbol{\omega}$ is the angular-velocity vector of the internuclear

axis. It is argued that the $-\hat{\boldsymbol{J}}\cdot\boldsymbol{\omega}$ term in the Hamiltonian (5.26) can not significantly affect the pair-creation process compared to the strong potential $V(\boldsymbol{r},t)$ (see, e.g., Refs. [33, 65, 66]) and thus is often ignored. By neglecting the rotational term, one obtains the axially symmetric Hamiltonian

$$H(t) = h^{\rm free} + V(\boldsymbol{r},t). \tag{5.27}$$

Calculating the contributions of each term on the right-hand side of Eq. (5.27) independently one can slightly optimise evaluation of the Hamiltonian matrix $H_{jk}(t)$. Since $h^{\rm free}$ does not depend on time, its matrix can be calculated only once at the start of the program, stored in the system memory and reused at need. The remaining $V(\boldsymbol{r},t)$ matrix, on the other hand, has to be evaluated at every internuclear distance $R(t_i + \Delta t_i/2)$, where i enumerates discrete time steps and $\Delta t_i = t_{i+1} - t_i$. The use of the spherical spinors to describe angular dependence of the basis functions allows us to take the angular part of the matrix elements analytically, see Eq. (5.15). The radial integration is performed numerically. Being independent of the angular variables, $h^{\rm free}$ couples only functions of the same angular symmetry. Therefore, the matrix $h^{\rm free}_{jk} = \langle u_j|h^{\rm free}|u_k\rangle$ is diagonal with respect to the quantum numbers κ and μ. The structure of the matrix $V_{jk}(t) = \langle u_j|V(\boldsymbol{r},t)|u_k\rangle$ is more complex. It is also diagonal with respect to μ, but if the number of the terms in the expansion (5.5) is not explicitly restricted, then functions with any values of κ get coupled, potentially by more than one term.

As it was stated above, an accurate description of a two-center wave function within one-center basis set requires the latter to contain a relatively large number of functions describing the angular motion. Thus, the dimensions of the matrices appearing in Eqs. (5.23) and (5.24) can reach substantial values. In our numerical procedure, the radial integrals used to construct the Hamiltonian matrix at a specific time instant are obtained by interpolation of the integrals precalculated for a number of points along the nuclear trajectory and stored in an array. Bearing this in mind, the actual calculations within sufficiently large basis sets could potentially demand a significant amount of the system memory. The use of B-splines to deal with the radial degree of freedom allows us to noticeably reduce the size of the needed memory. This is achieved due to strong localisation of the B-splines. Namely, a jth-order B-spline has non-zero values in at most $j+1$ contiguous grid intervals. Therefore, when the number of the nodes in the grid is large compared to the order of the

B-splines, only a small fraction of the splines overlaps allowing the radial integrals and the corresponding matrix elements to acquire non-zero values. Another benefit of having sparse matrices in Eq. (5.24) is the possibility to apply the algorithms designed specifically to work with matrices of this sort. Starting with a certain percentage of non-zero elements in the matrices these algorithms provide better performance compared to the regular dense-matrix counterparts. In our calculations we utilize the `PARDISO` [78, 79] code to solve systems of linear equations.

5.2.2 Accounting for the rotation of the internuclear axis

To find out to which extent rotation of the internuclear axis can affect the pair-creation probabilities we performed calculations with this rotation taken into account. We did this in two different ways. The first method is similar to the one described in the previous section. The problem is considered in the rotating reference frame, but this time the rotational term is retained in the Hamiltonian. In the second one the collision process is regarded in the inertial reference frame with the origin located at the center of mass. The Hamiltonian in this case becomes dependent on the angle between the internuclear line and z-axis. Let us begin with calculations in the rotating reference frame. As it was stated above in this case the Hamiltonian reads

$$H(t) = h^{\rm free} + V(\boldsymbol{r}, t) - \hat{\boldsymbol{J}} \cdot \boldsymbol{\omega}. \tag{5.28}$$

The first two terms have already been considered in detail in the previous section. Therefore, here we focus only on the last one. Let us assume that the collision takes place in the xz plane. Then, the angular-velocity vector is directed along the y-axis, that is $\boldsymbol{\omega} = (0, \omega, 0)$, and the scalar product is reduced to

$$-\hat{\boldsymbol{J}} \cdot \boldsymbol{\omega} = -\hat{J}_y \omega. \tag{5.29}$$

The operator $\hat{J}_y$ of the y-projection of the total electron angular momentum can be expressed in terms of the ladder operators $\hat{J}_+/\hat{J}_-$, which raise/lower the total angular momentum z-projection μ. These operators are defined as

$$\hat{J}_\pm = \hat{J}_x \pm i\hat{J}_y \tag{5.30}$$

and act on the eigenfunctions of the operators $\hat{J}^2$ and $\hat{J}_z$, i.e. spherical spinors $\mathbf{\Omega}_{\kappa,\mu}(\boldsymbol{n})$ in the case of electrons, according to

$$\hat{J}_{\pm}\mathbf{\Omega}_{\kappa,\mu}(\boldsymbol{n}) = \sqrt{(j \mp \mu)(j \pm \mu + 1)}\mathbf{\Omega}_{\kappa,\mu\pm1}(\boldsymbol{n}), \tag{5.31}$$

where j is total angular momentum quantum number related to κ via Eq. (5.18). Thus, the rotational term in (5.28) can be conveniently rewritten as

$$-\hat{\boldsymbol{J}} \cdot \boldsymbol{\omega} = \frac{i\omega}{2}\left(\hat{J}_+ - \hat{J}_-\right). \tag{5.32}$$

Then, for the matrix elements one readily obtains

$$\begin{aligned}\langle u_i^{\kappa_a\mu_a}| - \hat{\boldsymbol{J}} \cdot \boldsymbol{\omega}|u_j^{\kappa_b\mu_b}\rangle &= i\delta_{\kappa_a\kappa_b}\frac{\omega}{2}S_{ij}^{\kappa_a} \\ &\times \left(\delta_{\mu_a,\mu_b+1}\sqrt{(j_b - \mu_b)(j_b + \mu_b + 1)} - \delta_{\mu_a,\mu_b-1}\sqrt{(j_b + \mu_b)(j_b - \mu_b + 1)}\right),\end{aligned} \tag{5.33}$$

$$S_{ij}^{\kappa} = \int dr \left[G_i^{\kappa}(r)G_j^{\kappa}(r) + F_i^{\kappa}(r)F_j^{\kappa}(r)\right], \tag{5.34}$$

where $G_i^{\kappa}(r)/F_i^{\kappa}(r)$ are the upper/lower radial components of the basis functions $u_i^{\kappa\mu}(r)$ multiplied by r (see Eqs. (5.10)–(5.11)). As one can see from Eq. (5.33) the rotational term is diagonal with respect to κ and only couples functions with $\Delta\mu = \pm 1$.

On the other hand the internuclear axis rotation can be also taken into account in the inertial reference frame represented in Fig. 20. The origin of this reference frame is located at the center of mass and its z-axis is directed along the vector of initial velocity of the nucleus A. The Hamiltonian in this case acquires an explicit dependence on the angle $\theta_{AB}(t)$ between the z-axis and the internuclear axis (see Fig. 20). In the inertial reference frame the Hamiltonian has a simple form

$$H(t) = h^{\text{free}} + V(\boldsymbol{r}, t). \tag{5.35}$$

The two-center nuclear potential can be expressed in a form similar to Eq. (5.3)

$$V(\boldsymbol{r}, t) = \sum_{\alpha=A,B}\sum_{L=0}^{\infty} V_L^{\alpha}\left(r, R_{\alpha}(t)\right)\sqrt{\frac{2L+1}{4\pi}}P_L\left(\cos\left(\theta - \theta_{AB}(t)\right)\right), \tag{5.36}$$

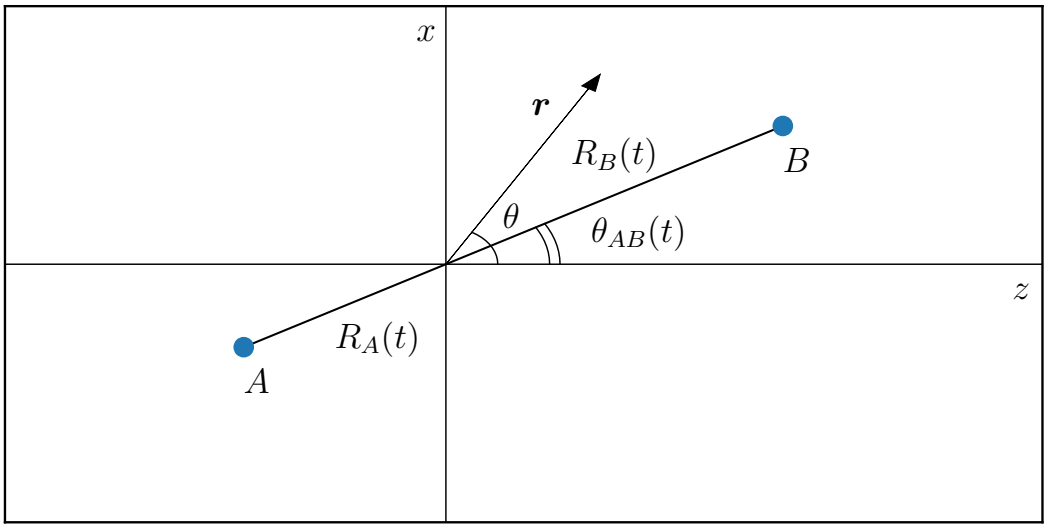

Figure 20: Inertial reference frame for the general case of nuclei with different masses.

where

$$V_L^{\alpha}\left(r, R_{\alpha}(t)\right) = \int_{\theta_{AB}(t)}^{\theta_{AB}(t)+\pi} d\theta \ \sin\left(\theta - \theta_{AB}(t)\right) P_L\left(\cos\left(\theta - \theta_{AB}(t)\right)\right) V_{\alpha}\left(|\boldsymbol{r} - \boldsymbol{R}_{\alpha}(t)|\right). \quad (5.37)$$

Employing again the property (5.7) of the Legendre polynomials, we arrive at the following expansion of the potential $V(\boldsymbol{r}, t)$ over the spherical harmonics:

$$V(\boldsymbol{r}, t) = \sum_{L=0}^{\infty} \sum_{M=-L}^{L} V_L(r, t) Y_{LM}(\hat{\boldsymbol{r}}) Y_{LM}^{*}\left(\hat{\boldsymbol{R}}_B(t)\right), \quad (5.38)$$

$$V_L(r, t) = V_L^A\left(r, R_A(t)\right) + V_L^B\left(r, R_B(t)\right). \quad (5.39)$$

In contrast to Eq. (5.5), all harmonics are present in the expansion (5.38), which means that functions with all possible pairs of κ and μ get coupled. All dependence of $V(\boldsymbol{r}, t)$ on the internuclear axis rotation angle is contained within the last factor in (5.38), that is $Y_{LM}^{*}\left(\hat{\boldsymbol{R}}_B(t)\right)$. The matrix elements of the two-center potential (5.38) are very similar to the ones given by Eq. (5.15). However, now in addition to the sum over L we also obtain sum over M, and each LM-term in the sum is

multiplied by the corresponding spherical harmonic $Y^*_{LM}\left(\hat{\boldsymbol{R}}_B(t)\right)$:

$$V_{jk} = \sum_{LM} g^{LM}(\kappa_j\mu_j, \kappa_k\mu_k) Y^*_{LM}\left(\hat{\boldsymbol{R}}_B(t)\right) \int dr V_L(r,t)\left[F_j(r)F_k(r) + G_j(r)G_k(r)\right]. \tag{5.40}$$

5.3 Results

Following the method described above, we examined how inclusion of the higher-order spherical harmonics in the potential affects the results obtained within the monopole approximation. To this end, we performed calculations of the ground-state energy, critical internuclear distances, pair-creation probabilities, and positron energy spectra for various numbers of multipoles taken into account in the decomposition of the two-center nuclear potential.

5.3.1 Ground-state energies and critical internuclear separations

Figure 21a demonstrates the ground-state energy of the U_2^{183+} quasimolecule as a function of the internuclear distance in the range from 30 to 80 fm. The figure contains the curves corresponding to the monopole approximation ($|\kappa|_{\max} = 1$), $|\kappa|_{\max} = 3$, and $|\kappa|_{\max} = 5$. For comparison we also included the result obtained in Ref. [80] using the Dirac-Sturm approach, in which the two-center basis set is constructed from the one-center Dirac-Sturm orbitals localised at the nuclei. The nuclear charge distribution in the work [80] was described with the Fermi model. It is seen from the figure that the most pronounced change of the ground-state energy is associated with the transition from the monopole approximation ($|\kappa|_{\max} = 1$) to the basis with $|\kappa|_{\max} = 3$. The line corresponding to $|\kappa|_{\max} = 5$ almost coincides with the one of [80], and with $|\kappa|_{\max} = 7$ the difference with the results of [80] becomes invisible in the considered region of internuclear separations. Within a wider scope of the internuclear distances, the dependence of the U_2^{183+} ground-state energy on $|\kappa|_{\max}$ is to be found in Fig. 21b. The figure illustrates the results obtained for $|\kappa|_{\max}$ up to 19 and internuclear distances in the range from 30 to 10000 fm. The curves are located strictly one under another, with the upper one corresponding to the monopole approximation and the lowest one was calculated in the basis with $|\kappa|_{\max} = 19$

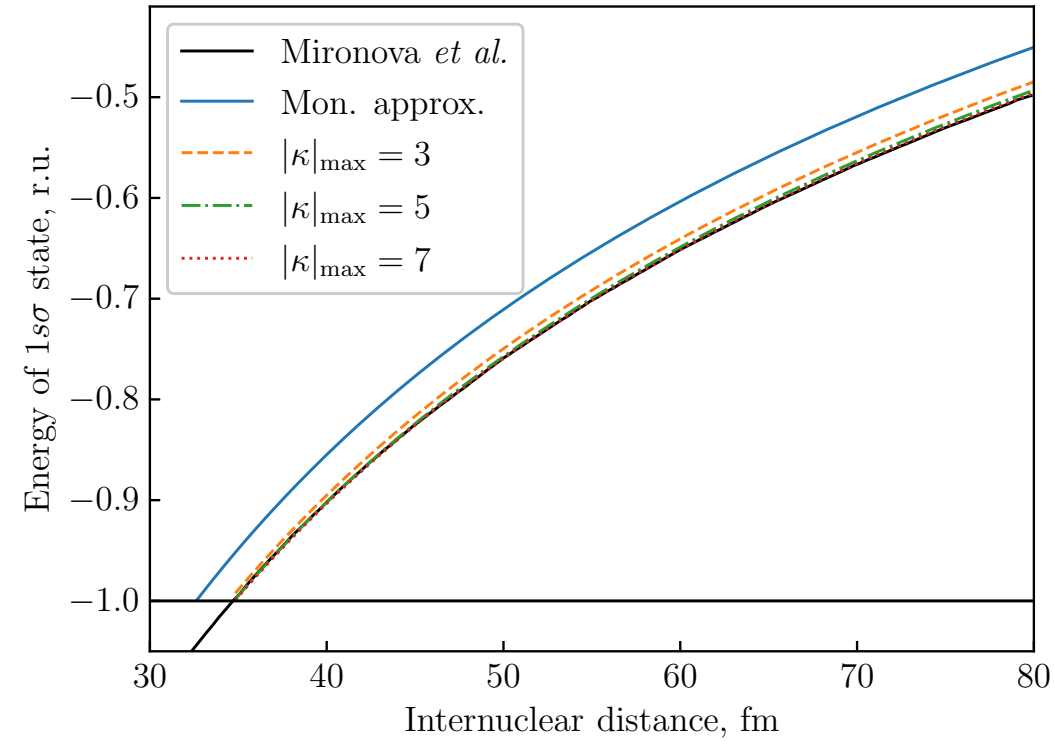

(a)

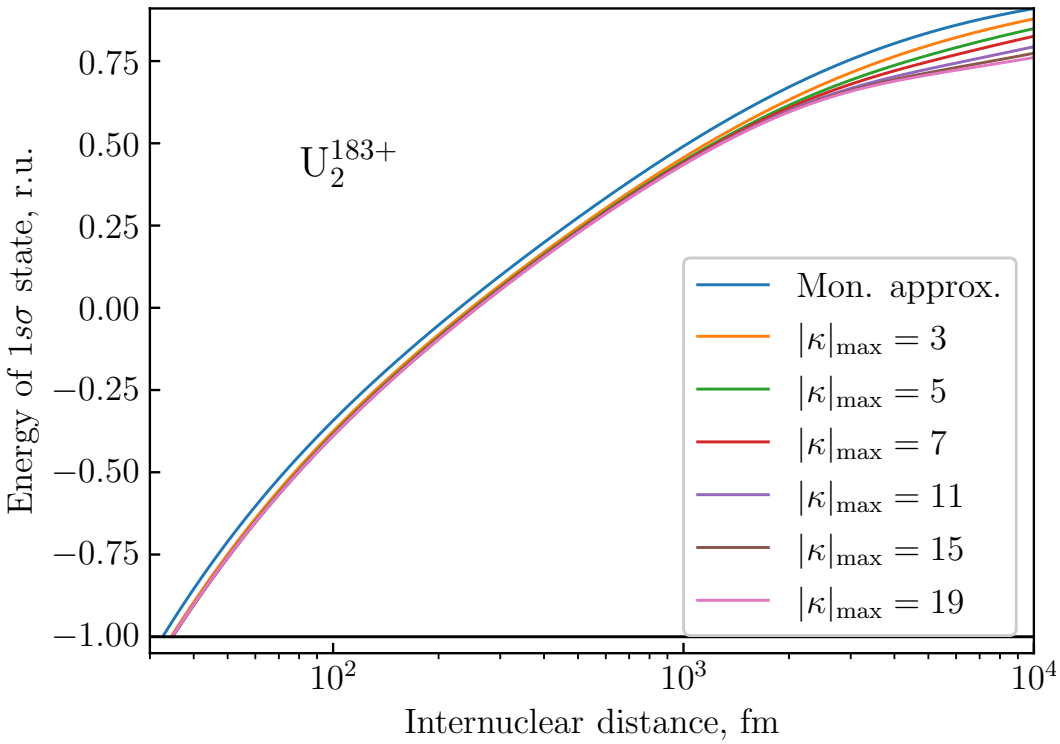

(b)

Figure 21: Energy of $1s\sigma$ state of the U_2^{183+} quasimolecule as a function of internuclear distance. Mironova *et al.* denotes the data from Ref. [80].

One of the most important characteristics pertaining to a given pair of nuclei when studying the spontaneous electron-positron pair creation is the critical internuclear distance $R_{\rm cr}$. Together with the trajectory parameters, such as the collision energy E and the impact parameter b or the minimal internuclear separation $R_{\rm min}$ and the parameter $\eta = E/E_0$, $R_{\rm cr}$ determines the duration of the supercritical regime $\tau_{\rm cr}$ (see, e.g., Fig. 4). The critical distance is defined as the distance between the nuclei at which a certain quasimolecular bound-state energy level reaches the border of the negative-energy continuum. It depends on the nuclear charge numbers and has different values for different energy levels, $R_{\rm cr} = R^n_{\rm cr}(Z_{\rm A}, Z_{\rm B})$, where n specifies a certain energy level. The function $R^n_{\rm cr}(Z_{\rm A}, Z_{\rm B})$ is defined only for such $Z_{\rm A}$, $Z_{\rm B}$ for which there exits a solution of the equation $\varepsilon_n(Z_{\rm A}, Z_{\rm B}, R) = -mc^2$. For the considered in this research nuclei, only the lowest-energy $1s\sigma$ state dives into the negative-energy continuum for a noticeable period of time. For this reason, bellow we constrain ourselves to consideration of $R_{\rm cr}$ corresponding to the $1s\sigma$ state only, and omit the superscript.

In Table 1 we present the dependence of the $R_{\rm cr}$ on the number of κ-channels included in the basis set. The table contains the results obtained for the homonuclear quasimolecules with the nuclear charge numbers $87 \leq Z \leq 100$. For comparison we also included the values calculated in Refs. [46, 80]. To make the table more readable we only show the values until $R_{\rm cr}$ is converged, i.e. the last value in each row corresponds to the converged result. Here the nuclear root-mean-square charge radii $\langle r_n^2 \rangle^{\frac{1}{2}}$ were taken from Ref. [81] if the data is available there, otherwise we used the values from Ref. [82]. As it can be seen from the table, our converged values of $R_{\rm cr}$ are in a very good agreement with the findings of Ref. [80]. Across the whole range of the considered nuclear charge numbers the deviation does not exceed 0.02 fm, with our results being systematically smaller. This discrepancy can be partially accounted for by different nuclear charge distribution models. We regarded the nuclei as homogeneously charged spheres, whereas in Ref. [80] the Fermi model was utilized. The convergence rate noticeably depends on the nuclear charge Z. The number of needed κ-channels is the smallest for lighter nuclei and almost linearly grows with increasing Z. For example, to get $R_{\rm cr}$ with the accuracy of four significant digits for $Z = 87$ it is enough to have a basis with $|\kappa|_{\rm max} = 5$, whereas for $Z = 100$ $|\kappa|_{\rm max} = 17$ is needed. Analogous calculations were also carried out for heteronuclear one-electron quasimolequles. The results are represented in the Table 2.

Table 1: Dependence of the critical internuclear distance $R_{\rm cr}$ for $1s\sigma$ state on $|\kappa|_{\max}$ for homonuclear one-electron quasi-molecules. The superscript a denotes the results of Ref. [46], b is the data of Ref. [80].

Z	$\langle r_n^2\rangle^{\frac{1}{2}}$ (fm)	$\lvert\kappa\rvert_{\max}$									
		1	3	5	7	9	11	13	15	17	
87	5.5915	15.93	16.38	16.40							16.42^b
88	5.6079	19.13	19.82	19.87							19.89^b
		19.0799^a	19.7593^a								
89	5.6700	22.35	23.38	23.37	23.37	23.38					23.38^b
90	5.7848	25.61	26.82	26.94	26.95						26.96^b
		25.6651^a	26.8973^a								
91	5.7000	29.12	30.65	30.86	30.88						30.90^b
92	5.8571	32.56	34.39	34.67	34.70	34.71					34.72^b
		32.6217^a	34.4668^a								
93	5.7440	36.28	38.47	38.85	38.92	38.94					38.93^b
94	5.8601	39.98	42.49	42.96	43.06	43.09					43.10^b
		40.0043^a	42.5210^a								
95	5.9048	43.82	46.68	47.27	47.41	47.45	47.46				47.47^b
96	5.8429	47.82	51.07	51.78	51.98	52.04	52.05	52.06			52.06^b
		47.8263^a	51.0716^a								
97	5.8160	51.90	55.54	56.38	56.64	56.72	56.75	56.76			56.77^b
98	5.8440	56.06	60.09	61.07	61.39	61.49	61.54	61.55	61.56		61.56^b
		56.0564^a	60.0818^a								
99	5.8650	60.32	64.76	65.89	66.27	66.41	66.46	66.48	66.49		66.50^b
100	5.8860	64.68	69.55	70.81	71.26	71.44	71.51	71.54	71.55	71.56	71.57^b

Table 2: Dependence of the critical internuclear distance $R_{\rm cr}$ for $1s\sigma$ state on $|\kappa|_{\max}$ for heteronuclear one-electron quasimolecules with $Z_{\rm A} = 92$. The superscript ^{a} denotes the results of Ref. [46].

$Z_{\rm B}$	MA	$\lvert\kappa\rvert_{\max}$							
		2	3	4	5	7	9	11	13
82	15.82	15.74	16.25	16.25	16.27				
83	17.44	17.32	17.98	17.98	18.01				
84	19.04	18.91	19.71	19.71	19.74				
85	20.69	20.54	21.49	21.49	21.55				
86	22.27	22.10	23.19	23.19	23.26				
87	23.93	23.74	25.00	25.00	25.10				
88	25.61	25.40	26.82	26.82	26.95	26.96			
89	27.34	27.10	28.71	28.70	28.87	28.88			
90	29.03	28.78	30.55	30.54	30.74	30.76			
91	30.82	30.54	32.50	32.49	32.74	32.77			
92	32.56		34.39		34.67		34.70		34.71
93	34.41	34.09	36.42	36.40	36.74	36.80	36.81		
94	36.22	35.88	38.38	38.37	38.75	38.82	38.83		
95	38.08	37.72	40.41	40.40	40.83	40.92	40.93		
96	39.99	39.62	42.51	42.50	42.99	43.10	43.12		
97	41.93	41.53	44.53	44.62	45.17	45.30	45.33	45.34	
98	43.88	43.47	46.77	46.75	47.36	47.52	47.55	47.56	47.57
	43.894[a]	43.483[a]	46.792[a]	46.787[a]					

5.3.2 Pair-creation probabilities

Having studied the relevant static properties of the one-electron quasimolecules, we moved to the dynamical problem of low-energy nuclear collisions. Within the framework of this task we investigated how going beyond the monopole approximation affects the signatures of the transition to the supercritical regime found in the previous chapter. To this end, we performed calculations of the pair-creation probabilities and positron energy spectra for collisions of heavy nuclei with various charge numbers. The nuclei were treated classically as homogeneously charged spheres of radius $R_{\rm n} = 1.2A^{1/3}$ fm, where $A = 2.5Z$ is the atomic mass number. Their motion was described by the hyperbolic trajectories. As was demonstrated

in Ref. [55], when the rotation of the internuclear axis is neglected, the dominant contribution to the probability comes from states with angular momentum projections $|\mu| = \frac{1}{2}$. Influence of the internuclear axis rotation will be considered in the next subsection, the calculations described here were performed with the rotation neglected. Therefore, only states with $\mu = \frac{1}{2}$ were included into the basis set and the results were doubled. The basis functions (5.10), (5.11) were constructed with B-splines of the 9th order generated on the grid of size $R_{\rm box} = 26400$ fm. The nodes were distributed polynomially with $r_i = R_{\rm box}\left(i/(N-1)\right)^4$. The initial and final internuclear distance was taken to be $R(t_{\rm in}) = R(t_{\rm out}) \equiv R_0 = 5000$ fm. The number of propagated electron states was reduced by introducing a cutoff energy $\varepsilon_{\rm c} = 6mc^2$ Only states with energy $\varepsilon \in (-mc^2,\ \varepsilon_c]$ were taken into account in Eq. (2.45), providing the relative inaccuracy of the sum on the level of 10^{-4}.

First, we studied the dependence of the pair-creation probability on the number of the κ channels included in the expansion (5.21) of the time-dependent wave function. For this purpose we considered collisions of uranium nuclei at the energy in the target rest frame of 6.218 MeV/u. Table 3 contains the total pair-creation probability $P_{\rm t}$ and the contributions of the ground ($P_{\rm g}$) and all bound states ($P_{\rm b}$) obtained for several impact parameters in the range from 0 to 30 fm. For comparison the values calculated in Ref. [55] are also presented. The table shows a rather fast convergence of the total probability with respect to the number of the κ channels. For example, the basis with $|\kappa|_{\rm max} = 3$ already provides a deviation from the converged results of less than 1%. Thus, in further calculation only functions with $|\kappa| \leq 3$ were included in the basis.

After that, we studied the behavior of the pair-creation probability as a function of η with fixed $R_{\rm min}$ and examined how inclusion of terms with $L > 0$ in the expansion (5.5) of the two-center potential affects the signatures of the transition to the supercritical regime found in the monopole approximation. Further, we consider the total pair-creation probability and denote it with P omitting the subscript. As it was shown in the previous chapter (see also Refs. [59,60]), in the monopole approximation the pair-creation probability as a function of η starts to increase as $\eta \to 1$, when $R_{\rm min}$ and $Z_{\rm t} = Z_{\rm A} + Z_{\rm B}$ enter deeply enough into the supercritical domain of collision parameters. As it is demonstrated in Fig. 22 this qualitative change of the $P(\eta)$ near the point $\eta = 1$ still takes place in calculations with the two-center nuclear potential. The figure depicts $P(\eta)$ obtained for symmetric collisions with

Table 3: Dependence of the pair-creation probability on $|\kappa|_{\max}$ for collisions of uranium nuclei at the energy in the target rest frame of 6.218 MeV/u. P_{t} is the total pair-creation probability, P_{g} and P_{b} are the contributions of the ground and all bound states, respectively. The entries with $|\kappa|_{\max} = 1$ correspond to the monopole approximation.

	$\lvert\kappa\rvert_{\max}$	Impact parameter (fm)						
		0	5	10	15	20	25	30
P_{g}	1	1.04×10^{-2}	8.80×10^{-3}	6.02×10^{-3}	3.84×10^{-3}	2.41×10^{-3}	1.51×10^{-3}	9.50×10^{-4}
	3	1.09×10^{-2}	9.24×10^{-3}	6.41×10^{-3}	4.15×10^{-3}	2.64×10^{-3}	1.68×10^{-3}	1.07×10^{-3}
	5	1.11×10^{-2}	9.46×10^{-3}	6.58×10^{-3}	4.27×10^{-3}	2.73×10^{-3}	1.74×10^{-3}	1.11×10^{-3}
	7	1.10×10^{-2}	9.34×10^{-3}	6.50×10^{-3}	4.23×10^{-3}	2.70×10^{-3}	1.73×10^{-3}	1.11×10^{-3}
	9	1.08×10^{-2}	9.24×10^{-3}	6.42×10^{-3}	4.18×10^{-3}	2.67×10^{-3}	1.71×10^{-3}	1.10×10^{-3}
	11	1.08×10^{-2}	9.19×10^{-3}	6.39×10^{-3}	4.16×10^{-3}	2.66×10^{-3}	1.70×10^{-3}	1.09×10^{-3}
	Ref. [55]	1.09×10^{-2}	9.30×10^{-3}	6.47×10^{-3}	4.21×10^{-3}	2.73×10^{-3}	1.72×10^{-3}	1.11×10^{-3}
P_{b}	1	1.25×10^{-2}	1.05×10^{-2}	7.03×10^{-3}	4.39×10^{-3}	2.70×10^{-3}	1.66×10^{-3}	1.03×10^{-3}
	3	1.32×10^{-2}	1.12×10^{-2}	7.63×10^{-3}	4.85×10^{-3}	3.03×10^{-3}	1.89×10^{-3}	1.19×10^{-3}
	5	1.32×10^{-2}	1.11×10^{-2}	7.62×10^{-3}	4.86×10^{-3}	3.05×10^{-3}	1.91×10^{-3}	1.21×10^{-3}
	7	1.31×10^{-2}	1.11×10^{-2}	7.59×10^{-3}	4.84×10^{-3}	3.04×10^{-3}	1.91×10^{-3}	1.21×10^{-3}
	9	1.31×10^{-2}	1.11×10^{-2}	7.58×10^{-3}	4.83×10^{-3}	3.03×10^{-3}	1.90×10^{-3}	1.21×10^{-3}
	11	1.31×10^{-2}	1.11×10^{-2}	7.58×10^{-3}	4.83×10^{-3}	3.03×10^{-3}	1.90×10^{-3}	1.20×10^{-3}
	Ref. [55]	1.32×10^{-2}	1.12×10^{-2}	7.64×10^{-3}	4.87×10^{-3}	3.07×10^{-3}	1.93×10^{-3}	1.23×10^{-3}
P_{t}	1	1.29×10^{-2}	1.08×10^{-2}	7.26×10^{-3}	4.51×10^{-3}	2.75×10^{-3}	1.69×10^{-3}	1.04×10^{-3}
	3	1.36×10^{-2}	1.15×10^{-2}	7.83×10^{-3}	4.95×10^{-3}	3.08×10^{-3}	1.92×10^{-3}	1.20×10^{-3}
	5	1.36×10^{-2}	1.15×10^{-2}	7.81×10^{-3}	4.96×10^{-3}	3.10×10^{-3}	1.94×10^{-3}	1.22×10^{-3}
	7	1.35×10^{-2}	1.14×10^{-2}	7.79×10^{-3}	4.95×10^{-3}	3.09×10^{-3}	1.94×10^{-3}	1.22×10^{-3}
	9	1.35×10^{-2}	1.14×10^{-2}	7.78×10^{-3}	4.94×10^{-3}	3.09×10^{-3}	1.93×10^{-3}	1.22×10^{-3}
	11	1.35×10^{-2}	1.14×10^{-2}	7.78×10^{-3}	4.94×10^{-3}	3.09×10^{-3}	1.93×10^{-3}	1.22×10^{-3}
	Ref. [55]	1.38×10^{-2}	1.16×10^{-2}	8.01×10^{-3}	5.15×10^{-3}	3.46×10^{-3}	2.14×10^{-3}	1.42×10^{-3}

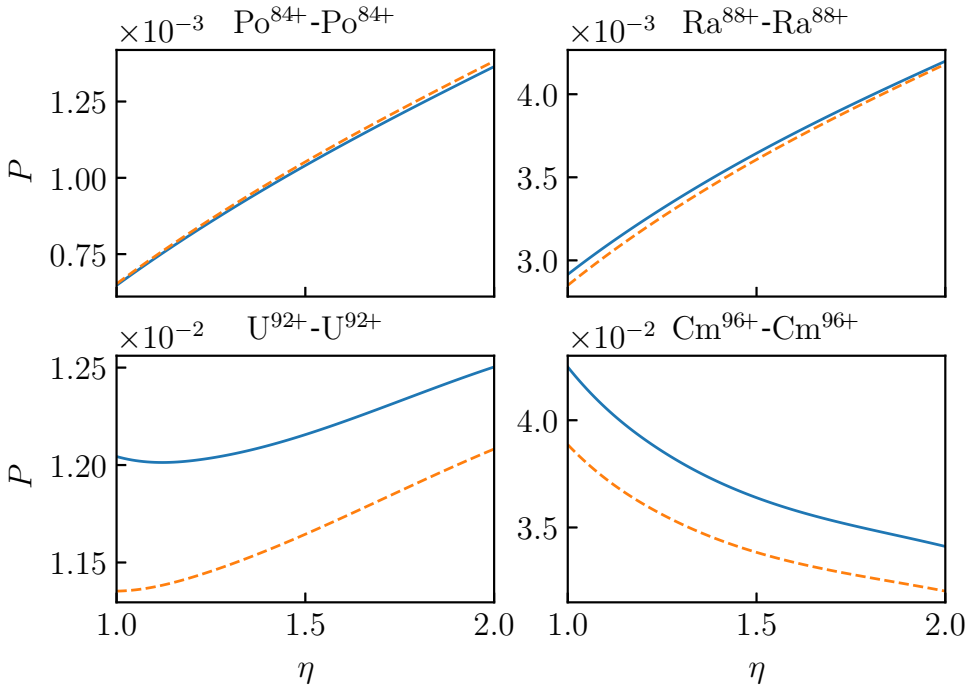

Figure 22: Total pair-creation probability as a function of η with $R_{\min} = 17.5$ fm. Solid blue lines depict results obtained with $|\kappa|_{\max} = 3$, dashed orange curves correspond to the monopole-approximation results ($|\kappa|_{\max} = 1$).

$R_{\min} = 17.5$ fm of nuclei with subcritical ($Z = 84$) and supercritical ($Z = 88$, 92, 96) charge numbers. For each Z there are two curves: the dashed orange one corresponds to the monopole approximation ($|\kappa|_{\max} = 1$) and the solid blue line was obtained in the basis with $|\kappa|_{\max} = 3$. Comparing the curves one can notice that the effects associated with higher-order terms somewhat enhance the manifestation of the increase of $P(\eta)$ as $\eta \to 1$ for supercritical charge numbers. For instance, in the case of the U^{92+}-U^{92+} collisions, the probability obtained with $|\kappa|_{\max} = 3$ exhibits a shallow minimum near $\eta = 1$, which is absent in the monopole approximation.

The influence of the nonmonopole terms becomes more apparent when considering the derivative of the pair-creation probability with respect to the parameter η, $dP/d\eta$, at $\eta = 1$. Figure 23 depicts this derivative and the individual contributions of odd ($\mathcal{P} = -1$) and even ($\mathcal{P} = 1$) states. Figure 23a represents $dP/d\eta$ as a function of Z with $R_{\min} = 17.5$ fm and Fig. 23b in turn represents this derivative as a function of $R_{\min}$ for $Z = 96$. As can be seen from the figures, the deviation from the monopole results is hardly visible until the corresponding channel becomes supercritical, which happens at $Z \approx 87.3$ for $\mathcal{P} = 1$ and $Z \approx 94.8$ for $\mathcal{P} = -1$. In the supercritical region the values of $dP/d\eta$ obtained with $|\kappa|_{\max} = 3$ lie lower than the monopole ones. This behavior of $dP/d\eta$ aligns with the findings of Refs. [46,47],

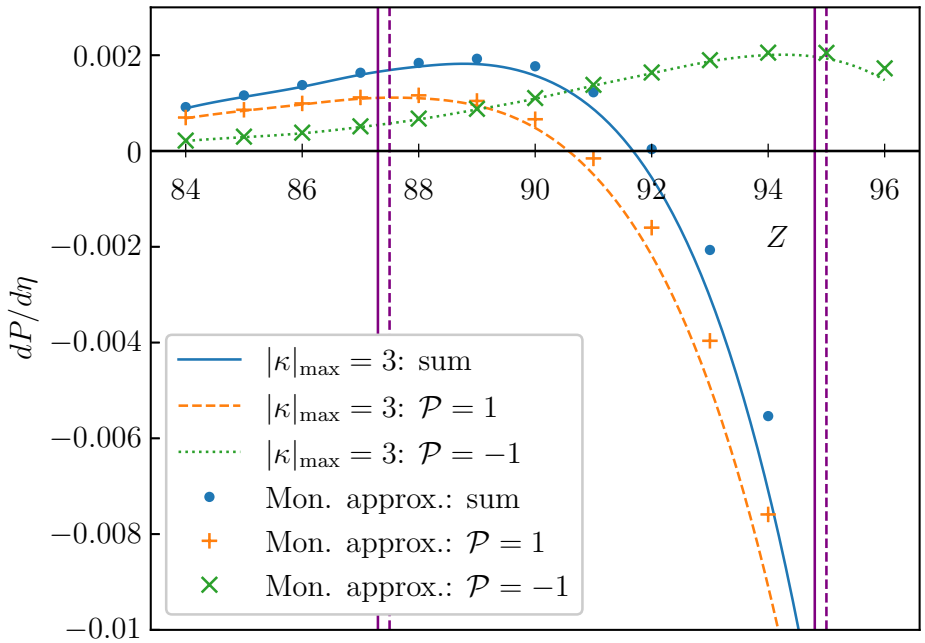

(a)

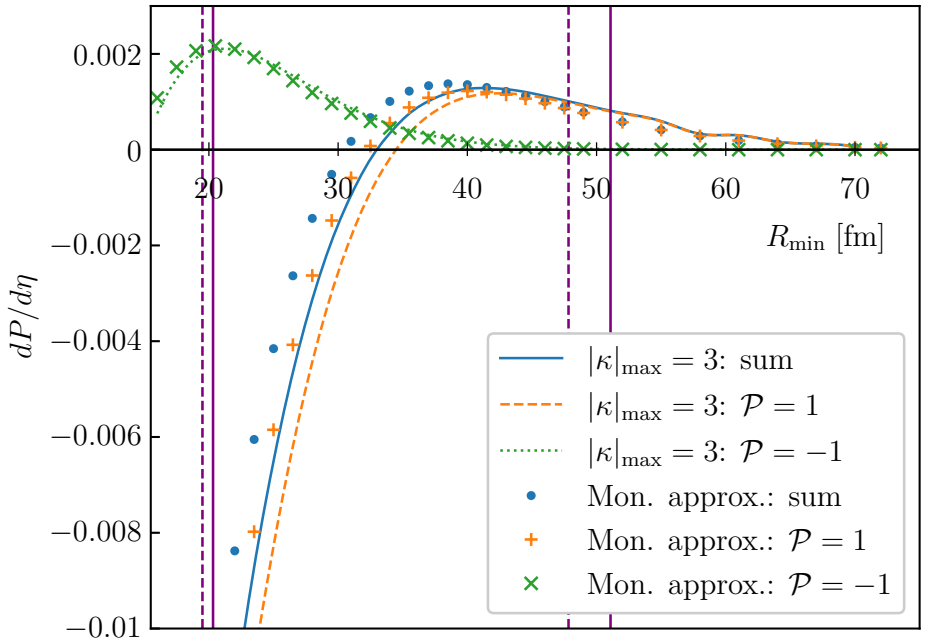

(b)

Figure 23: Derivative of the e^-e^+ pair-creation probability $dP/d\eta$ at $\eta = 1$ ($\theta = 180^\circ$) as a function of a) Z with $R_{\rm min} = 17.5$ fm, b) $R_{\rm min}$ for $Z = 96$. Vertical lines mark the values of the abscissa at which the energies of $1s\sigma$ and $2p_{1/2}\sigma$ states are equal to $-mc^2$. Dashed lines correspond to the monopole approximation ($|\kappa|_{\rm max} = 1$), solid lines to calculations with $|\kappa|_{\rm max} = 3$.

where the supercritical-resonance parameters were examined beyond the monopole approximation. According to Refs. [46,47], inclusion of higher-order terms in the potential decomposition results in about 20% increase in the resonance width of U_2^{183+}

quasimolecule at the internuclear distance of 16 fm. Furthermore, this increase in width turns out to be larger for larger internuclear separations. Note that supercritical resonance width is exclusively due to the spontaneous pair creation while in collisions of heavy nuclei both spontaneous and dynamic mechanisms contribute to the total pair-creation probability. As seen in Table 3, the overall increase in the pair-creation probability for head-on collisions of uranium nuclei at the energy of 6.218 MeV/u (which corresponds to the minimal internuclear distance $R_{\min} \approx 16.47$ fm) amounts to approximately 5%. This may indicate that the relative contribution of the spontaneous mechanism to the pair production became larger, although the electron-positron pairs are mostly created by the dynamic mechanism. As a result one may observe an enhancement of the signal indicating the transition to the supercritical regime found in $dP/d\eta$, namely the sign change from positive to negative. Another factor that can play a role is the extended duration of the supercritical regime, $\tau_{\rm cr}$, due to the increase in the critical internuclear distance $R_{\rm cr}$ (see Table 1).

5.3.3 Impact of the internuclear axis rotation on the pair-creation probability

Following the approach described in Section 5.2.2 we developed a numerical code implementing both procedures allowing one to take into account the rotation of the internuclear axis. Using this code we performed calculations of the pair-creation probabilities with electron captured into a bound state and the total pair-creation probabilities for symmetric collisions of uranium nuclei. The calculations were carried out in the basis of spatially even functions with $\kappa = -1, 2, -3$. The number of angular projections μ included in the basis varied for different methods. The calculations in the rotating reference frame neglecting the rotational coupling were independently conducted for $\mu = 1/2$ and $\mu = 3/2$. Then the results were summed and doubled. The calculations in the same reference frame but with enabled rotational coupling were performed within two basis sets. The first one included functions with $|\mu| \leq 3/2$. The second one contained functions with all possible angular momentum projections for the given set of κ, that is $|\mu| \leq 5/2$ in our case. Finally, the calculations in the inertial reference frame were carried out within the basis with $|\mu| \leq 5/2$. The results of the calculations for $R_{\min} = 17.5$ and 25 fm can be found in the Table 4. It is seen from the table that both methods of

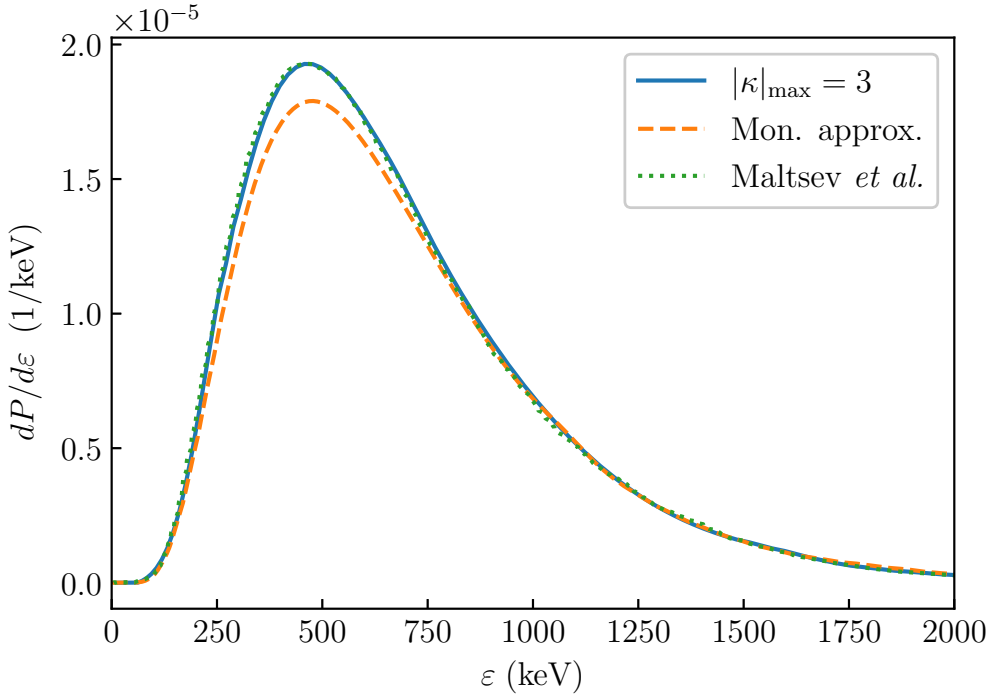

Figure 24: Energy spectra of the positrons emitted in head-on U^{92+}-U^{92+} collisions with energy $E = 6.218$ MeV/u. Maltsev *et al.* denotes the data from Ref. [55].

accounting for the rotational coupling yield identical results in the largest considered basis with $|\mu| \leq 5/2$. A small difference in the last significant digit of the results obtained in the rotating reference frame within the basis sets with $|\mu| \leq 3/2$ and $|\mu| \leq 5/2$ is found only for a large value of the parameter η, namely $\eta = 20$. This fact shows an advantage of calculations in the rotating reference frame compared to the inertial one. In addition to the greater sparsity of the matrices mentioned above, working in the rotating frame also allows one to operate with a smaller-size matrices, by using basis sets with fewer angular momentum projections. Bearing in mind the relation between the impact parameter and the new collision parameters $(R_{\min}, \eta)$ given by Eq. (3.3), one can clearly see that when considering pair-creation probability in low-energy collisions with small impact parameters rotational effects can be safely neglected. It is exactly this type of collisions that is used in search for the spontaneous pair-creation. For $R_{\min} = 17.5$ fm the influence of the rotational coupling starts to manifest only at $\eta = 5$. As it was expected, its impact increases with increasing impact parameter and collision energy.

5.3.4 Positron energy spectra

Another signature of the transition to the supercritical regime found in the previous chapter concerns the η-dependence of the maximum of the positron energy

Table 4: Pair-creation-probability obtained within the basis set with $\kappa = -1, 2, -3$. $P_{\rm b}$ – probability of pair creation with the electron in a bound state, $P_{\rm t}$ – total pair-creation probability, A — calculation neglecting the rotation of the internuclear axis, B — calculations taking into account the rotation of the internuclear axis: B1— in the rotating reference frame, B2 — in the inertial reference frame.

$R_{\rm min}$, fm		Method	$\eta = E/E_0$			
			1	5	10	20
17.5	$P_{\rm b}$	A: $\lvert\mu\rvert \le 3/2$	1.03×10^{-2}	7.95×10^{-3}	7.07×10^{-3}	5.94×10^{-3}
		B1: $\lvert\mu\rvert \le 3/2$	1.03×10^{-2}	7.96×10^{-3}	7.09×10^{-3}	5.96×10^{-3}
		B1: all μ	1.03×10^{-2}	7.96×10^{-3}	7.09×10^{-3}	5.96×10^{-3}
		B2: all μ	1.03×10^{-2}	7.96×10^{-3}	7.09×10^{-3}	5.96×10^{-3}
	$P_{\rm t}$	A: $\lvert\mu\rvert \le 3/2$	1.04×10^{-2}	1.04×10^{-2}	1.18×10^{-2}	1.44×10^{-2}
		B1: $\lvert\mu\rvert \le 3/2$	1.04×10^{-2}	1.05×10^{-2}	1.19×10^{-2}	1.46×10^{-2}
		B1: all μ	1.04×10^{-2}	1.05×10^{-2}	1.19×10^{-2}	1.47×10^{-2}
		B2: all μ	1.04×10^{-2}	1.05×10^{-2}	1.19×10^{-2}	1.47×10^{-2}
25	$P_{\rm b}$	A: $\lvert\mu\rvert \le 3/2$	4.19×10^{-3}	5.15×10^{-3}	5.25×10^{-3}	4.97×10^{-3}
		B1: $\lvert\mu\rvert \le 3/2$	4.19×10^{-3}	5.16×10^{-3}	5.27×10^{-3}	5.00×10^{-3}
		B1: all μ	4.19×10^{-3}	5.16×10^{-3}	5.27×10^{-3}	5.00×10^{-3}
		B2: all μ	4.19×10^{-3}	5.16×10^{-3}	5.27×10^{-3}	5.00×10^{-3}
	$P_{\rm t}$	A: $\lvert\mu\rvert \le 3/2$	4.20×10^{-3}	5.88×10^{-3}	7.11×10^{-3}	8.96×10^{-3}
		B1: $\lvert\mu\rvert \le 3/2$	4.20×10^{-3}	5.91×10^{-3}	7.18×10^{-3}	9.15×10^{-3}
		B1: all μ	4.20×10^{-3}	5.91×10^{-3}	7.18×10^{-3}	9.17×10^{-3}
		B2: all μ	4.20×10^{-3}	5.91×10^{-3}	7.18×10^{-3}	9.17×10^{-3}

spectra obtained in collisions with fixed $R_{\rm min}$. As it was shown in section 4.3.2 in the monopole approximation, in the case of subcritical collisions the spectra corresponding to larger η possess higher peak values, whereas for supercritical collisions the dependence is inverted and peak values decrease with increasing η. The layout of the tails of the spectra remains unchanged. In this section we will examine whether this behavior remains valid beyond the monopole approximation. At first, we regarded collisions of uranium nuclei at the energy of 6.218 MeV/u. The positron spectra calculated for the head-on collision in the framework of the monopole approximation and beyond it are depicted in Fig. 24. The spectrum obtained in the basis with $|\kappa|_{\rm max} = 3$ is in perfect agreement with the one given in Ref. [55]. Inclusion of spherical harmonics with $L > 0$ into the expansion of the two-center nuclear potential leads to a raise of the spectrum near the peak leaving the tail almost unchanged.

After that, we studied the dependence of the positron spectra on η for symmetric collisions with a fixed distance of the closest approach, $R_{\rm min}$. In Fig. 25 we

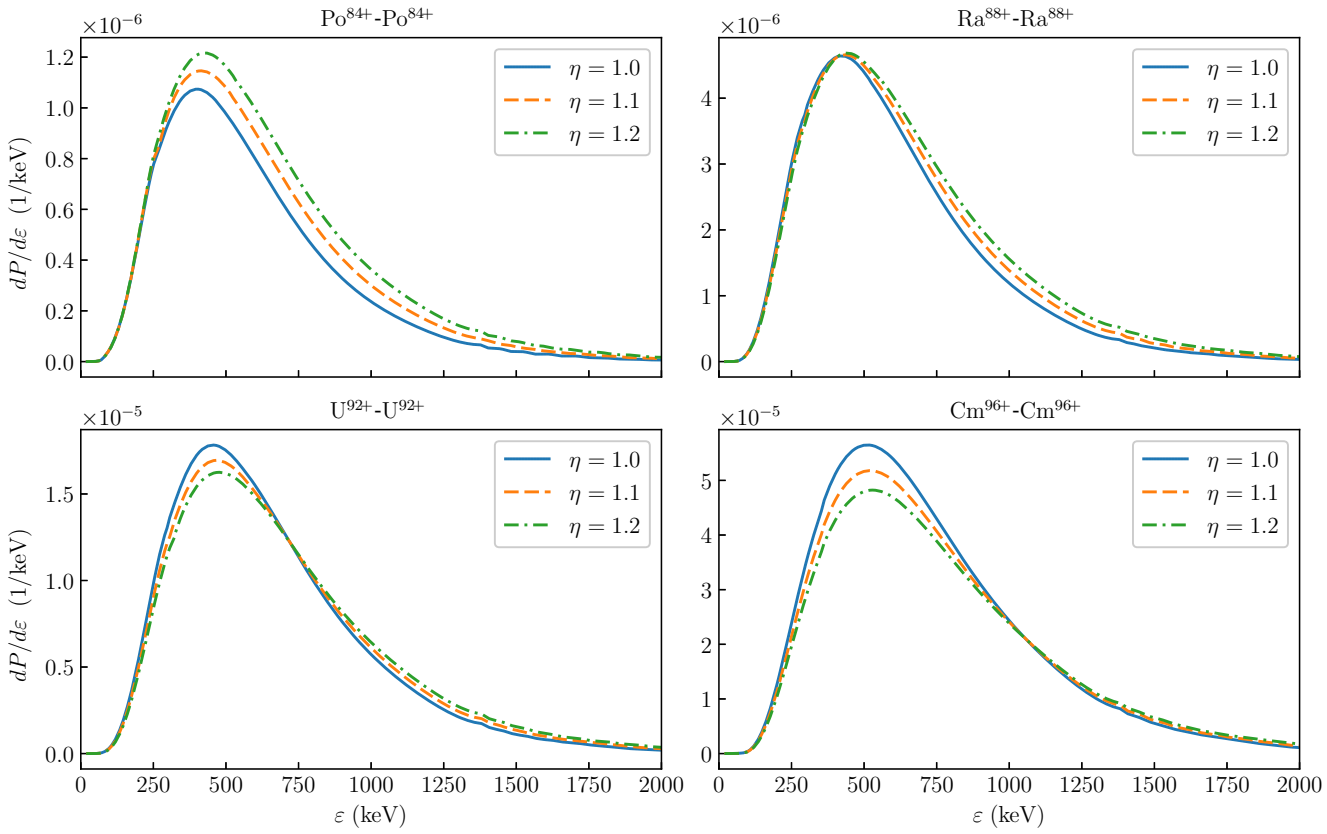

Figure 25: Positron spectra for the symmetric collisions with $Z = Z_{\mathrm{A}} = Z_{\mathrm{B}} = 84$–$96$ at $R_{\mathrm{min}} = 17.5$ fm and $\eta = E/E_0 = 1, 1.1, 1.2$.

present the spectra obtained for collisions of nuclei with charge numbers $Z = 84$, 88, 92, 96, $R_{\mathrm{min}} = 17.5$ fm, and $\eta = 1$, 1.1, 1.2. The results show that once the total charge number $2Z$ exceeds the critical value, the order of the curves near the peak gets reversed. In full accordance with the previous chapter, the subcritical collisions yield higher peak values of the positron spectrum for larger η, while in the case of the supercritical collisions the opposite relation between the peak height and η is established. The same behavior of the spectra with respect to η is found when the supercritical domain of the collision parameters is approached from a different direction, namely when Z is fixed and R_{min} is decreasing.

Conclusion

In this thesis we investigated a process of electron-positron pair creation in low-energy collisions of heavy nuclei. To this end, we implemented a numerical technique of solving the time-dependent Dirac equation using a finite static basis set. The basis set consists of bispinors characteristic to spherically symmetric fields. Their angular part is described by spherical spinors and radial components are constructed from B-splines in accordance the dual kinetic balance approach, designed to get rid of the unphysical spurious states. Using this code in the framework of the monopole approximation, we performed nonperturbative calculations of the pair-creation probabilities and the positron energy spectra for low energy collisions of heavy nuclei for a wide range of the collision parameters. To analyze the obtained results we introduced a pair of parameters $(R_{\min}, \eta)$, where $R_{\min}$ is the distance of the closest approach and $\eta = E/E_0$ is the ratio of the collision energy E to the energy E_0 of the head-on collision with the same $R_{\min}$. Alongside with the conventional collision energy E and the impact parameter, the pair $(R_{\min}, \eta)$ unambiguously specifies a collision trajectory. As a result of the analysis we found that the behavior of the pair-creation probability P on the parameter η with fixed $R_{\min}$ undergoes a qualitative change when the nuclei charge numbers Z_{A}, Z_{B} and the distance of the closest approach $R_{\min}$ get deeply enough in the supercritical domain with the border defined as the solution of the equation $\varepsilon_{1s\sigma}(Z_{\mathrm{A}}, Z_{\mathrm{B}}, R_{\min}) = -mc^2$. For subcritical collisions, that is with $\varepsilon_{1s\sigma}(Z_{\mathrm{A}}, Z_{\mathrm{B}}, R_{\min}) > -mc^2$, the pair-creation probability monotonously decreases at $\eta \to 1$. However, when Z_{A}, Z_{B} and $R_{\min}$ are inside the supercritical domain at a sufficient distance from the border, the decrease of $P(\eta)$ gives way to the increase at $\eta \to 1$, thus forming a minimum. The same change is observed in individual contribution of s and $p_{1/2}$ channels, when the corresponding lowest-energy bound state enters the lower continuum. The positron energy spectra also reveal a qualitative change for supercritical collisions. Namely, the increase of the peak values of the differential probability with increasing η, is replaced by the decrease in the supercritical domain. Consideration of the part of the produced pairs including only positrons in the energy range where the spontaneous mechanism can contribute allows one to enhance manifestation of these signatures of the transition to the supercritical regime.

The validity of the signatures found within the monopole approximation is

corroborated by calculations with the full two-center potential. Using the multipole expansion, we examined the influence of the higher-order spherical harmonics of the nuclear potential on the pair-creation probability, positron energy spectra and their dependence on η with fixed $R_{\min}$. The calculations were performed in the rotating quasimolecular reference frame, with the rotational term appearing in the Hamiltonian due to the transition to this noninertial reference frame neglected. The results of the calculations showed the same qualitative changes of $P(\eta)$ and the positron spectra as the ones found in the monopole approximation. Moreover, the derivative $dP/d\eta\big|_{\eta=1}$ becomes negative at smaller nuclear charges Z_{A}, Z_{B} and larger values of $R_{\min}$. Also we quantitatively investigated validity of the approximation neglecting the rotational coupling. To this end, we developed two calculation methods where the rotational effects are taken into account. The first one is based on calculation in the rotating quasimolecular reference frame but with the rotational term retained in the Hamiltonian. In the second one the calculations are performed in the inertial reference frame with the origin located at the center of mass. Both methods are in a perfect agreement with each other and demonstrate that the influence of the rotational coupling on the pair-creation probability is negligible for low-energy collisions with small impact parameters. It is exactly this type of collisions, that is employed for investigations of the spontaneous vacuum decay.

References

[1] Ehlotzky F., Krajewska K., Kamiński J. Z. Fundamental processes of quantum electrodynamics in laser fields of relativistic power // Rep. Prog. Phys. — 2009. — Vol. 72, no. 4. — P. 046401.

[2] Ruffini R., Vereshchagin G., Xue S.-S. Electron-positron pairs in physics and astrophysics: From heavy nuclei to black holes // Phys. Rep. — 2010. — Vol. 487, no. 1. — P. 1–140.

[3] Di Piazza A., Müller C., Hatsagortsyan K. Z., Keitel C. H. Extremely high-intensity laser interactions with fundamental quantum systems // Rev. Mod. Phys. — 2012. — Vol. 84. — P. 1177–1228.

[4] Fedotov A., Ilderton A., Karbstein F. et al. Advances in QED with intense background fields // Phys. Rep. — 2023. — Vol. 1010. — P. 1.

[5] Pomeranchuk I., Smorodinsky J. On the energy levels of systems with $Z > 137$ // J. Phys. USSR. — 1945. — Vol. 9. — P. 97.

[6] Gershtein S. S., Zeldovich Y. B. Positron production during the mutual approach of heavy nuclei and the polarization of the vacuum // Zh. Eksp. Teor. Fiz. — 1969. — Vol. 57. — P. 654.

[7] Pieper W., Greiner W. Interior electron shells in superheavy nuclei // Z. Physik A. — 1969. — Vol. 218. — P. 327.

[8] Popov V. S. Electron energy levels at $Z > 137$ // Pisma Zh. Eksp. Teor. Fiz. — 1970. — Vol. 11. — P. 254.

[9] Popov V. S. Positron production in a Coulomb field with $Z > 137$ // Zh. Eksp. Teor. Fiz. — 1970. — Vol. 59. — P. 965.

[10] Popov V. S. // Yad. Fiz. — 1970. — Vol. 12. — P. 429.

[11] Popov V. S. On the properties of the discrete spectrum for z close to 137 // Zh. Eksp. Teor. Fiz. — 1971. — Vol. 60. — P. 1228.

[12] Zeldovich Y. B., Popov V. S. Electronic structure of superheavy atoms // Usp. Fiz. Nauk. — 1971. — Vol. 105. — P. 403.

[13] Müller B., Peitz H., Rafelski J., Greiner W. Solution of the Dirac Equation for Strong External Fields // Phys. Rev. Lett. — 1972. — Vol. 28. — P. 1235.

[14] Müller B., Rafelski J., Greiner W. Electron shells in over-critical external fields // Z. Physik A. — 1972. — Vol. 257. — P. 62.

[15] Müller B., Rafelski J., Greiner W. Auto-ionization of positrons in heavy ion collisions // Z. Physik A. — 1972. — Vol. 257. — P. 183.

[16] Mur V. D., Popov V. S. Bound states near the limit of the lower continuum (fermion case) // Teor. Mat. Fiz. — 1976. — Vol. 27. — P. 204.

[17] Popov V. S., Eletsky V. L., Mur V. D. Properties of deep-lying levels in a strong electrostatic field // Zh. Eksp. Teor. Fiz. — 1976. — Vol. 71. — P. 856.

[18] Müller B. Positron creation in superheavy quasi-molequles // Ann. Rev. Nucl. Sci. — 1976. — Vol. 26. — P. 351.

[19] Reinhardt J., Greiner W. Quantum electrodynamics of strong fields // Rep. Prog. Phys. — 1977. — Vol. 40, no. 3. — P. 219.

[20] Soff G., Reinhardt J., Müller B., Greiner W. Shakeoff of the Vacuum Polarization in Quasimolecular Collisions of Very Heavy Ions // Phys. Rev. Lett. — 1977. — Vol. 38. — P. 592–595.

[21] Migdal A. B. Fermions and Bosons in Strong Fields. — Moscow : Nauka, 1978.

[22] Rafelski J., Fulcher L. P., Klein A. Fermions and bosons interacting with arbitrarily strong external fields // Phys. Rep. — 1978. — Vol. 38, no. 5. — P. 227–361.

[23] Greiner W., Müller B., Rafelski J. Quantum Electrodynamics of Strong Fields. — Berlin : Springer-Verlag, 1985.

[24] Bosch F., Müller B. Positron creation in heavy-ion collisions // Progress in Particle and Nuclear Physics. — 1986. — Vol. 16. — P. 195–241.

[25] Müller-Nehler U., Soff G. Electron excitations in superheavy quasimolecules // Physics Reports. — 1994. — Vol. 246, no. 3. — P. 101–250.

[26] Reinhardt J., Greiner W. Supercritical fields and the decay of the vacuum // Proceeding of the Memorial Symposium for Gerhard Soff / Ed. by W. Greiner, J. Reinhardt. — EP Systema, Budapest, 2005. — P. 181–192.

[27] Rafelski J., Kirsch J., Müller B. et al. Probing QED Vacuum with Heavy Ions // New Horizons in Fundamental Physics / Ed. by S. Schramm, M. Schäfer. — Cham : Springer, 2017. — P. 211–251.

[28] Popov V. S. Spontaneous positron production in collisions between heavy nuclei // Zh. Eksp. Teor. Fiz. — 1973. — Vol. 65. — P. 35.

[29] Peitz H., Müller B., Rafelski J., Greiner W. Autoionization spectra of positrons in heavy-ion collisions // Lett. Nuovo Cimento. — 1973. — Vol. 8. — P. 37–42.

[30] Popov V. S., Voskresensky D. N., Eletskii V. L., Mur V. D. WKB method at $Z > 137$ and its applications to the theory of supercritical atoms // Zh. Eksp. Teor. Fiz. — 1979. — Vol. 76. — P. 431.

[31] Smith K., Peitz H., Müller B., Greiner W. Induced Decay of the Neutral Vaccum in Overcritical Fields Occurring in Heavy-Ion Collisions // Phys. Rev. Lett. — 1974. — Vol. 32. — P. 554–556.

[32] Smith K., Müller B., Greiner W. Dynamical theory of intermediate molecular phenomena in heavy ion scattering // J. Phys. B: Atom. Mol. Phys. — 1975. — Vol. 8, no. 1. — P. 75.

[33] Reinhardt J., Soff G., Müller B., Greiner W. Dynamical aspects: Coherent production of positrons in heavy ion collisions // Prog. Part. Nucl. Phys. — 1980. — Vol. 4. — P. 547.

[34] Soff G., Reinhardt J., Müller B., Greiner W. Coupled Channel Analysis of Inner-Shell Vacancy Formation in Superheavy Quasimolecules // Z. Physik. A. — 1980. — Vol. 294. — P. 137.

[35] Reinhardt J., Müller B., Greiner W. Theory of positron production in heavy-ion collisions // Phys. Rev. A. — 1981. — Vol. 24. — P. 103–128.

[36] Müller U., de Reus T., Reinhardt J. et al. Positron production in crossed beams of bare uranium nuclei // Phys. Rev. A. — 1988. — Vol. 37. — P. 1449–1455.

[37] Gumberidze A., Stöhlker Th., Beyer H. F. et al. X-ray spectroscopy of highly-charged heavy ions at FAIR // Nucl. Instrum. Methods Phys. Res., Sect. B. — 2009. — Vol. 267, no. 2. — P. 248–250.

[38] Lestinsky M. *et al.* Physics book: CRYRING@ESR // Eur. Phys. J. Special Topics. — 2016. — Vol. 225. — P. 797.

[39] Ma X., Wen W. Q., Zhang S. F. et al. HIAF: New opportunities for atomic physics with highly charged heavy ions // Nucl. Instrum. Methods Phys. Res., Sect. B. — 2017. — Vol. 408. — P. 169–173.

[40] Ter-Akopian G. M., Greiner W., Meshkov I. N. et al. Layout of new experiments on the observation of spontaneous electron-positron pair creation in supercritical Coulomb fields // Int. J. Mod. Phys. E. — 2015. — Vol. 24, no. 03. — P. 1550016.

[41] Ackad E., Horbatsch M. Numerical calculation of supercritical Dirac resonance parameters by analytic continuation methods // Phys. Rev. A. — 2007. — Vol. 75. — P. 022508.

[42] Kuleshov V. M., Mur V. D., Narozhny N. B. et al. Coulomb problem for a $Z > Z_{\rm cr}$ nucleus // Phys. Usp. — 2015. — Vol. 58, no. 8. — P. 785.

[43] Godunov S. I., Machet B. M., Vysotsky M. I. Resonances in positron scattering on a supercritical nucleus and spontaneous production of e^+e^- pairs // Eur. Phys. J. C. — 2017. — Vol. 77. — P. 82.

[44] Krylov K. S., Mur V. D., Fedotov A. M. On the resonances near the continua boundaries of the Dirac equation with a short-range interaction // Eur. Phys. J. C. — 2020. — Vol. 80. — P. 270.

[45] Ackad E., Horbatsch M. Supercritical Dirac resonance parameters from extrapolated analytic continuation methods // Phys. Rev. A. — 2007. — Vol. 76. — P. 022503.

[46] Marsman A., Horbatsch M. Calculation of supercritical Dirac resonance parameters for heavy-ion systems from a coupled-differential-equation approach // Phys. Rev. A. — 2011. — Vol. 84. — P. 032517.

[47] Maltsev I. A., Shabaev V. M., Zaytsev V. A. et al. Calculation of the Energy and Width of Supercritical Resonance in a Uranium Quasimolecule // Opt. Spectrosc. — 2020. — Vol. 128. — P. 1100–1104.

[48] Grashin P., Sveshnikov K. Vacuum polarization energy decline and spontaneous positron emission in QED under Coulomb supercriticality // Phys. Rev. D. — 2022. — Vol. 106. — P. 013003.

[49] Krasnov A., Sveshnikov K. Non-perturbative effects in the QED-vacuum energy exposed to the supercritical Coulomb field // Mod. Phys. Lett. A. — 2022. — Vol. 37, no. 21. — P. 2250136. — https://doi.org/10.1142/S021773232250136X.

[50] Grashin P. A., Sveshnikov K. A. The Gershtein-Greiner-Zeldovich Effect: Vacuum Charge Density and Vacuum Energy // Lett. PEPAN. — 2024. — Vol. 21. — P. 95–123.

[51] Ackad E., Horbatsch M. Calculation of electron-positron production in supercritical uranium-uranium collisions near the Coulomb barrier // Phys. Rev. A. — 2008. — Vol. 78. — P. 062711.

[52] Bondarev A. I., Tupitsyn I. I., Maltsev I. A. et al. Positron creation probabilities in low-energy heavy-ion collisions // Eur. Phys. J. D. — 2015. — Vol. 69, no. 4. — P. 110.

[53] Maltsev I. A., Shabaev V. M., Tupitsyn I. I. et al. Electron-positron pair creation in low-energy collisions of heavy bare nuclei // Phys. Rev. A. — 2015. — Vol. 91. — P. 032708.

[54] Maltsev I.A., Shabaev V.M., Tupitsyn I.I. et al. Pair production in low-energy collisions of uranium nuclei beyond the monopole approximation // Nucl. Instrum. Methods Phys. Res., Sect. B. — 2017. — Vol. 408. — P. 97–99.

[55] Maltsev I. A., Shabaev V. M., Popov R. V. et al. Electron-positron pair production in slow collisions of heavy nuclei beyond the monopole approximation // Phys. Rev. A. — 2018. — Vol. 98. — P. 062709.

[56] Popov R. V., Bondarev A. I., Kozhedub Y. S. et al. One-center calculations of the electron-positron pair creation in low-energy collisions of heavy bare nuclei // Eur. Phys. J. D. — 2018. — Vol. 72. — P. 115.

[57] Dulaev N. K., Telnov D. A., Shabaev V. M. et al. Angular and energy distributions of positrons created in subcritical and supercritical slow collisions of heavy nuclei // Phys. Rev. D. — 2024. — Vol. 109. — P. 036008.

[58] Voskresensky D. N. Electron-Positron Vacuum Instability in Strong Electric Fields. Relativistic Semiclassical Approach // Universe. — 2021. — Vol. 7, no. 104.

[59] Maltsev I. A., Shabaev V. M., Popov R. V. et al. How to Observe the Vacuum Decay in Low-Energy Heavy-Ion Collisions // Phys. Rev. Lett. — 2019. — Vol. 123. — P. 113401.

[60] Popov R. V., Shabaev V. M., Telnov D. A. et al. How to access QED at a supercritical Coulomb field // Phys. Rev. D. — 2020. — Vol. 102. — P. 076005.

[61] de Reus T. Positron emission in elastic collisions of fully ionized high-Z heavy ions // arXiv. — 2022. — P. 2201.07324.

[62] Popov R. V., Shabaev V. M., Maltsev I. A. et al. Spontaneous vacuum decay in low-energy collisions of heavy nuclei beyond the monopole approximation // Phys. Rev. D. — 2023. — Vol. 107. — P. 116014.

[63] Müller B., Kent-Smith R., Greiner W. Induced radiative transitions of intermediate molecules in heavy ion collisions // Phys. Lett. B. — 1974. — Vol. 49, no. 3. — P. 219–223.

[64] Müller B., Greiner W. The Two Centre Dirac Equation // Z. Naturforsch A. — 1976. — Vol. 31, no. 1. — P. 1–30.

[65] Betz W., Soff G., Müller B., Greiner W. Direct Formation of Quasimolecular $1s\sigma$ Vacancies in Uranium-Uranium Collisions // Phys. Rev. Lett. — 1976. — Vol. 37. — P. 1046.

[66] Soff G., Greiner W., Betz W., Müller B. Electrons in superheavy quasimolecules // Phys. Rev. A. — 1979. — Vol. 20. — P. 169.

[67] Soff G., Reinhardt J. Positron creation in heavy ion collisions the influence of the magnetic field // Phys. Lett. B. — 1988. — Vol. 211, no. 1. — P. 179–182.

[68] Voronov B. L., Gitman D. M., Tyutin I. V. // Theor. Math. Phys. — 2007. — Vol. 150. — P. 34.

[69] Gitman D. M., Tyutin I. V., Voronov B. L. Self-adjoint Extensions in Quantum Mechanics: General Theory and Applications to Schrödinger and Dirac Equations with Singular Potentials. — Boston : Birkhäuser Boston, 2012.

[70] Gallone M., Michelangeli A. Self-Adjoint Extension Schemes and Modern Applications to Quantum Hamiltonians. — Cham : Springer, 2023.

[71] Varshalovich D A, Moskalev A N, Khersonskii V K. Quantum Theory of Angular Momentum. — World Scientific, 1988. — https://www.worldscientific.com/doi/pdf/10.1142/0270.

[72] Akhiezer A. I., Berestetskii V. B. Quantum electrodynamics. — Moskva : Nauka, 1981.

[73] Fradkin E. S., Gitman D. M., Shvartsman S. M. Quantum Electrodynamics with Unstable Vacuum. — Berlin : Springerl-Verlag, 1991.

[74] Langhoff P. W., Sims J., Corcoran C. T. Stieltjes-integral approximations to photoabsorption and dispersion profiles in atomic helium // Phys. Rev. A. — 1974. — Vol. 10. — P. 829–841.

[75] de Boor C. A Practical Guide to Splines. — New York : Springer-Verlag, 2001.

[76] Shabaev V. M., Tupitsyn I. I., Yerokhin V. A. et al. Dual Kinetic Balance Approach to Basis-Set Expansions for the Dirac Equation // Phys. Rev. Lett. — 2004. — Vol. 93. — P. 130405.

[77] Crank J., Nicolson P. A practical method for numerical evaluation of solutions of partial differential equations of the heat-conduction type // Proc. Cambridge Philos. Soc. — 1947. — Vol. 43. — P. 50.

[78] Schenk O., Gärtner K. PARDISO // Encyclopedia of Parallel Computing / Ed. by David Padua. — Boston : Springer US, 2011. — P. 1458–1464.

[79] Developer Reference for Intel® oneAPI Math Kernel Library for Fortran. — URL: https://www.intel.com/content/www/us/en/docs/onemkl/developer-reference-fortran/2024-1/onemkl-pardiso-parallel-direct-sparse-solver-iface.html.

[80] Mironova D. V., Tupitsyn I. I., Shabaev V. M., Plunien G. Relativistic calculations of the ground state energies and the critical distances for one-electron homonuclear quasi-molecules // Chem. Phys. — 2015. — Vol. 449. — P. 10.

[81] Angeli I., Marinova K. P. Table of experimental nuclear ground state charge radii: An update // At. Data Nucl. Data Tables. — 2013. — Vol. 88. — P. 69.

[82] Johnson W. R., Soff G. The lamb shift in hydrogen-like atoms, $1 \leq Z \leq 110$ // At. Data Nucl. Data Tables. — 1985. — Vol. 33. — P. 405.